

© Copyright 1995
Jason Eugene Fabritz

**A Two Dimensional Numerical Model for Simulating the Movement and
Biodegradation of Contaminants in a Saturated Aquifer**

by

Jason Eugene Fabritz

A thesis submitted in partial fulfillment
of the requirements for the degree of

Master of Science in Civil Engineering

University of Washington

1995

Master's Thesis

In presenting this thesis in partial fulfillment of the requirements for a Master's degree at the University of Washington, I agree that the Library shall make its copies freely available for inspection. I further agree that extensive copying of this thesis is allowable only for scholarly purposes, consistent with "fair use" as prescribed in the U.S. Copyright Law. Any other reproduction for any purposes or by any means shall not be allowed without my written permission.

Acknowledgments

I would like to thank advisor, Prof. Joel Massmann, for his support and guidance with this thesis, and for his sponsoring my return to graduate study at the University of Washington. I would also like to thank my committee members, Prof. David Stensel and Prof. John Ferguson for their help and guidance.

This material is based upon work supported under a National Science Foundation Graduate Fellowship. Any opinions, findings, conclusions or recommendations expressed in this publication are those of the author and do not necessarily reflect the views of the National Science Foundation.

Table of Contents

List of Figures.....	iii
List of Tables.....	vi
1. Introduction	1
2. Subsurface Processes.....	3
2.1 Introduction.....	3
2.2 Mass Transport.....	5
2.3 Mass Transfer.....	6
3. Model Implementation.....	15
3.1 Introduction.....	15
3.2 Numerical Method Overview.....	20
3.3 Aquifer Discretization.....	25
3.4 Estimating Groundwater Velocities.....	26
3.5 Estimating fluxes for Advection and Dispersion.....	27
3.6 Simulating Kinetic Reactions.....	29
3.7 Incorporating Equilibrium Reactions.....	30
3.8 Oscillations and Stability.....	31
4. Model Performance.....	35
4.1 Introduction.....	35
4.2 Measures of Performance.....	37
4.3 Use of Dimensionless Variables.....	38
4.4 One-Dimensional Conservative Solute with a Continuous Source.....	40
4.5 One-Dimensional Conservative Solute from a Pulse Injection.....	45
4.6 Two-Dimensional Conservative Solute Transport.....	50
4.7 One-Dimensional Solute with First Order Decay.....	54
4.8 Kinetic Reactions.....	59
4.9 Stratified Porous Media.....	65
4.10 One-Dimensional Biostimulation Experiment.....	68
5. Example Problem.....	74
5.1 Introduction.....	74
5.2 Problem Description.....	74

5.3 No-action.....	76
5.4 Pump and Treat	82
5.5 Pump and Treat with Biodegradation	85
5.6 Conclusions	92
6. Conclusions	94
7. References	96
Appendix A Monod Kinetics and Competitive Inhibition	100
Appendix B Integrated Operator-Splitting Method.....	105
Appendix C Solute Transport Equation	110
Appendix D Linear Integrated Method	117
Appendix E Global Timestep Calculation.....	121
Appendix F Additional Kinetic Reaction Verification Tests	129
Appendix G Bugs User’s Manual.....	140

List of Figures

Figure 2.1.1 Subsurface Processes	3
Figure 3.2.1 Standard Operator-Splitting Procedure	21
Figure 3.2.2 Operator-Splitting Procedure modified by Kinzelbach and Schäfer	22
Figure 3.2.3 Integrated Operator-Splitting Procedure	24
Figure 3.3.1 Illustration of a 5 x 4 Aquifer Mesh.....	25
Figure 3.5.1 Node layout for computing solute flux	27
Figure 3.8.1 Unstable Time Oscillations.....	31
Figure 3.8.2 Stable Space Oscillations.....	32
Figure 3.8.3 Maximum and Minimum Courant Number Criteria for one-dimensional Simulations	34
Figure 4.4.1 Log RSSE Contours as a Function of Pe and Co for One-Dimensional Conservative Solute Transport with Continuous Source.....	41
Figure 4.4.2 One-Dimensional Conservative Solute Transport with Continuous Source, $Pe = 2.5$, $Co = 0.36$, $RSSE = 1.0 \times 10^{-5}$	42
Figure 4.4.3 One-Dimensional Conservative Solute Transport with Continuous Source, $Pe = 250$, $Co = 0.36$, $RSSE = 1.2$	43
Figure 4.4.4 One-Dimensional Conservative Solute Transport with Continuous Source, $Pe = 250$, $Co = 0.995$, $RSSE = 1.1 \times 10^{-2}$	44
Figure 4.5.1 Log RSSE Contours as a Function of Pe and Co for One-Dimensional Conservative Solute Transport with a Pulse Source	46
Figure 4.5.2 One-Dimensional Conservative Solute Transport with a Pulse Source, $Pe = 2.5$, $Co = 0.36$, $RSSE = 2.6 \times 10^{-5}$	47
Figure 4.5.3 One-Dimensional Conservative Solute Transport with a Pulse Source, $Pe = 250$, $Co = 0.36$, $RSSE = 1.4$	48
Figure 4.5.4 One-Dimensional Conservative Solute Transport with a Pulse Source, $Pe = 250$, $Co = 0.995$, $RSSE = 7.3 \times 10^{-4}$	49
Figure 4.6.1 Two-Dimensional Conservative Solute Transport with a Pulse Source, Cross-sectional Profiles at a Relative Distance of $Y = 0.50$ $Pe = 0.5$, $Co = 0.082$, $\alpha_l/\alpha_t = 10$, Flow Angle = 30°	51
Figure 4.6.2 Two-Dimensional Conservative Solute Transport with a Pulse Source, Cross-sectional Profiles at a Relative Distance of $Y = 0.50$ $Pe = 0.5$, $Co = 0.082$, $\alpha_l/\alpha_t = 5$, Flow Angle = 30°	52
Figure 4.6.3 Two-Dimensional Conservative Solute Transport with a Pulse Source, Cross-sectional Profiles at a Relative Distance of $Y = 0.50$ $Pe = 0.1$, $Co = 0.049$, $\alpha_l/\alpha_t = 20.0$, Flow Angle = 30°	53

Figure 4.7.1 RSSE as a Function of Damkohler Number and Peclet Number (using the Maximum Allowable Courant Number) for One- Dimensional Reactive Solute Transport with a Continuous Source	55
Figure 4.7.2 One-Dimensional Reactive Solute Transport with Continuous Source, $Pe = 0.2$, $Co = 0.099$, $Da = 0.001$, $RSSE = 4.02 \times 10^{-4}$	56
Figure 4.7.3 One-Dimensional Reactive Solute Transport with Continuous Source, $Pe = 100$, $Co = 0.9905$, $Da = 1.0$, $RSSE = 1.14 \times 10^{-1}$	57
Figure 4.7.4 One-Dimensional Reactive Solute Transport with Continuous Source, $Pe = 2$, $Co = 0.618$, $Da = 0.1$, $RSSE = 5.7 \times 10^{-3}$	58
Figure 4.8.1 First Order Decay with Varying k	60
Figure 4.8.2 RSSE as a Function of First Order Decay Coefficient and Calculation Timestep.....	61
Figure 4.8.3 Competitive Monod Decay $k = 0.2$, $K_{sa} = 5.0$, $K_{sd} = 10.0$, $Y_x =$ 0.5 , $Y_A = 1.0$, $Y_D = 2.5$, $y_i = 0.2$	63
Figure 4.8.4 Squared Relative Residual as a Function of Global Timestep for Competitive Monod Decay.....	64
Figure 4.9.1 Laboratory Column.	65
Figure 4.9.2 Concentration at outflow boundary for Stratified System.	67
Figure 4.10.1 Schematic representation of the test zone used in biostimulation experiments.	68
Figure 4.10.2 Experimental (symbols) and modeled (lines, this model) breakthrough curves of methane and oxygen at observation well S2, 2.2 m from injection well SI, (Figure 4 in literature).	70
Figure 4.10.3 Modeled biomass profiles computed by Semprini and McCarty (symbols) and this model (lines), (Figure 5 in literature).....	71
Figure 4.10.4 Experimental (symbols) and modeled (lines, this model) breakthrough curves of methane and oxygen at observation at well S2 under alternative pulsing strategy (Figure 7 in literature).	72
Figure 4.10.5 Modeled biomass concentrations computed by Semprini and McCarty (symbols) and this model (lines) at well S2 (Figure 8 in literature).	73
Figure 5.2.1 TCE Spill Site.	74
Figure 5.3.1 No Action Aquifer System Layout.....	76
Figure 5.3.2 No Action TCE Border Concentration using Kinetic and Equilibrium Sorption.....	79
Figure 5.3.3 No Action TCE Border Concentration with different dissolution rates.....	80

Figure 5.3.4 No Action TCE Border Concentration using different grid spacing	81
Figure 5.3.5 No Action Distribution of Mass	82
Figure 5.4.1 Pump and Treat Aquifer System Layout.....	82
Figure 5.4.2 Pump and Treat vs. No-Action Aqueous TCE Boundary Concentration	84
Figure 5.4.3 Pump and Treat Mass Distribution	85
Figure 5.5.1 Pump and Treat with Biodegradation Aquifer System Layout.....	86
Figure 5.5.2 Pump and Treat boundary TCE concentration with and without Biodegradation	89
Figure 5.5.3 Pump and Treat with Biodegradation Mass Distribution.....	90
Figure 5.5.4 Distribution of Biomass and TCE _{aq} after 7.8 years.....	91
Figure 5.5.5 Distribution of Biomass, Oxygen, and Methane after 7.8 years.	92
Figure B.1 Comparison of IOS and OS Error as a Function of kDt	109
Figure F.1 Single Monod Decay with Varying k , and K_s	130
Figure F.2 Squared Relative Residual as a Function of Single Monod Decay Coefficients and Global Timestep.	131
Figure F.3 Double Monod Decay. $k = 0.2$, $K_{sd} = 5.0$, $K_{sd} = 10.0$, $Y_x = 0.5$, $Y_A = 1.0$, $Y_D = 2.5$	132
Figure F.4 Squared Relative Residual as a Function Global Timestep for Double Monod Reaction.....	133
Figure F.5 Kinetic Linear Sorption, $a = 0.1$, $K_d = 2.0$	134
Figure F.6 Squared Relative Residual as a Function of Global Timestep for Kinetic Linear Sorption.	135
Figure F.7 Kinetic Langmuir Sorption, $a = 0.1$, $k_1 = 8.0$, $k_2 = 1.0$	136
Figure F.8 Squared Relative Residual as a Function of Global Timestep for Kinetic Langmuir Sorption.....	137
Figure F.9 Kinetic Freundlich Sorption, $a = 0.2$, $k = 2.0$, $n = 0.8$	138
Figure F.10 Squared Relative Residual as a Function of Global Timestep for Kinetic Freundlich Sorption.	139

List of Tables

Table 2.3.1 Sample Values for Single Monod Kinetic Substrate Consumption Parameters	13
Table 2.3.2 Sample Values for Double Monod Kinetic Substrate Consumption Parameters	13
Table 2.3.3 Sample Values for Biomass Growth and Decay	13
Table 3.1.1 Comparison of Numerical Methods, Dimensions and Flow Type	16
Table 3.1.2 Comparison of Numerical Methods, Biological Reactions.....	17
Table 3.1.3 Comparison of Numerical Methods, Biomass Transport, and Sorption Kinetics	18
Table 3.1.4 Comparison of Numerical Methods, Numerical Techniques	19
Table 3.2.1 IOS Order of Calculation.....	23
Table 4.10.1 One-Dimensional Biostimulation Parameters	69
Table 5.2.1 Aquifer Material Properties.....	75
Table 5.2.2 TCE Sorption and Biodegradation Coefficients.....	75
Table 5.3.1 No-Action Simulation Parameters.....	76
Table 5.5.1 Pump-and-Treat with Biodegradation parameters.....	86
Table 5.6.1 Approximate Computation Times for Various Aquifer Simulations	93
Table B.1 IOS Order of Calculation.....	106

1. Introduction

Organic compounds, including hydrocarbons and chlorinated solvents, have become widespread contaminants in the soil and groundwater due to inadequate storage and disposal techniques. Considerable research has been conducted over the last two decades to develop ways of removing contamination and restoring the subsurface. Recent efforts have focused on in-situ techniques, primarily in the area of bioremediation.

In-situ bioremediation has advantages over traditional remediation such as pump-and-treat and excavation and disposal. It has the potential of destroying the contaminant in the subsurface, thereby eliminating the need to treat a waste stream. It reduces the potential of transferring contaminants to the atmosphere. Also, microbes may be able to degrade non-aqueous phase contaminant that traditional pump-and-treat systems cannot effectively move.

Many numerical models have been constructed to help evaluate relevant factors involved in the design of in-situ bioreactors. However, most of these models do not include multiple species and comprehensive collections of biological processes. There is a growing need for general purpose groundwater models that include biological processes.

This thesis presents a numerical model capable of simulating many of the important subsurface processes involved in bioremediation design. It simulates two-dimensional saturated steady-state flow aquifers with advection and dispersion of multiple reactive solutes. It includes kinetic and equilibrium Langmuir and Freundlich isotherms, as well as first-order and higher reactions. Single, double, and competitive Monod kinetic reactions are used to represent biological reactions. Certain combinations of reactions in this model can be used to simulate other processes such as intermediate toxicity and cometabolic degradation.

Construction of a new model was chosen over modification of an existing program for multiple reasons. First, it is easy to introduce programming errors while modifying existing code. Due to unfamiliarity with existing code, the programmer may be unaware of the assumptions made by it. This can lead to errors which are very difficult to locate and correct. In addition, existing programs are primarily written in FORTRAN. C++ is a better programming language to use for this type of groundwater model. The object-oriented language style lends well to dynamically including different types of reactions. Finally, a general purpose program should be easy to use. The computer program described in this thesis was written to take advantage of the Microsoft Windows™ interface for inputting data and viewing results.

The organization of this thesis is as follows: Chapter 2 presents a discussion of important subsurface processes. The numerical methodology is developed in Chapter 3. Chapter 4 evaluates model performance in a general sense. An example remedial design is presented in Chapter 5. Many of the detailed calculations are included in the appendices. The User's Manual to the model is included in the final appendix.

2. Subsurface Processes

2.1 Introduction

This chapter provides an overview of the common chemical, biochemical, and solute transport processes that can occur in a saturated aquifer. It includes values reported in literature for parameters and kinetic constants of natural, engineered, and modeled systems where applicable.

Figure 2.1.1 illustrates a conceptual view of the processes occurring in a saturated aquifer.

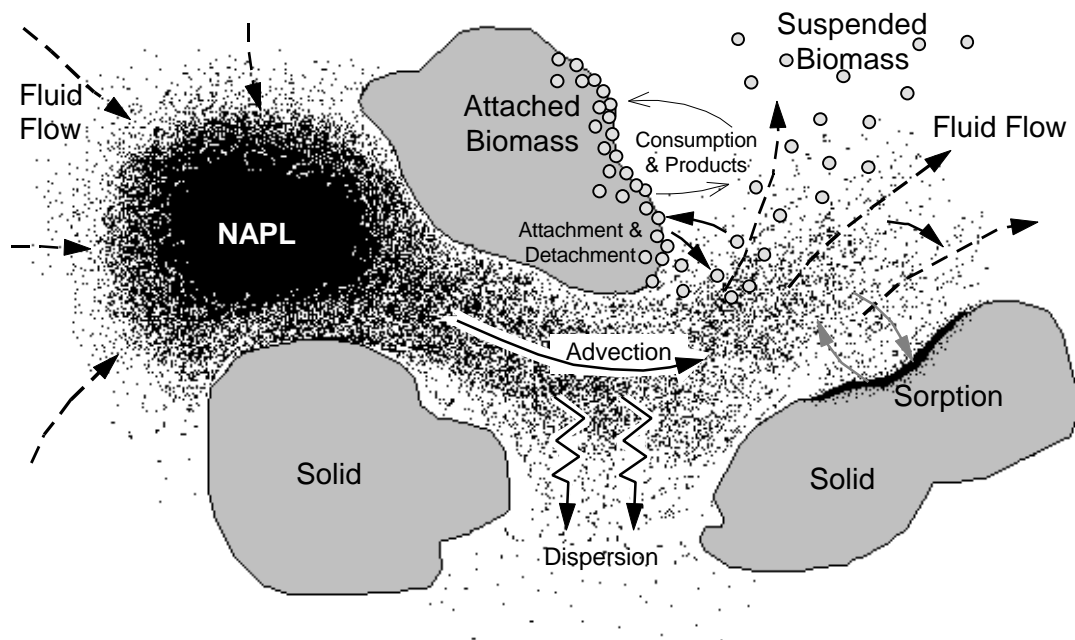


Figure 2.1.1 Subsurface Processes

A saturated aquifer consists of a porous media, saturating fluid, aqueous and sorbed chemicals and microbes, and sometimes non-aqueous phase liquids (NAPL's). Pressure gradients (measured as hydraulic head gradients) within the aquifer cause fluid to flow through the porous media. This results in advective transport of aqueous species. Dispersive mixing processes resulting from heterogeneity in the flow field cause solute profiles to “spread” as they move through the aquifer.

Many subsurface processes act as sinks and sources for aqueous species. These processes divide into two major groups: conservative and non-conservative mass transfer processes. Conservative processes transfer mass from one phase to another,

conserving total mass. Some examples include the dissolution of NAPL into the aqueous phase and sorption of aqueous species onto immobile porous media. Non-conservative processes transfer mass from one form to another. Some examples are radioactive decay and substrate metabolism by bacteria.

Many recent studies have focused on the role of these non-conservative biological processes in the subsurface. These processes include: substrate consumption, biomass growth, cometabolic transformations, intermediate toxicity, effects on material properties, biomass suspension into the aqueous phase, biomass transport, and biomass movement into the attached phase.

The three major conceptual models explaining the distribution of biomass in the attached phase are Monod, microcolony, and biofilm (Odenrantz, 1992). The Monod model assumes nothing about the distribution of bacteria in the pore space. The bulk concentration of substrates and contaminants drive the biokinetics. The microcolony model assumes microorganisms group themselves in colonies of 10-100 organisms. It assumes that the microcolony sizes are small enough that internal diffusion of substrate to the microorganisms is negligible, making the biokinetics a function of bulk concentration (Odenrantz, 1992). The biofilm model assumes microbes distribute themselves uniformly over the soil particles creating a film. Internal diffusion limits the transport of substrate and contaminants to the microbes in the film.

This thesis uses only Monod type reactions. Monod type reactions are easier to manipulate than the biofilm model and require less input parameters and calibration. Semprini and McCarty (1991, 1993) successfully used Monod kinetics to model in-situ biostimulation and bioremediation at a field site. In addition, Odenrantz (1992) determined that there is little difference in results between the use of Monod and biofilm models for many conditions common to groundwater modeling of natural and engineered systems.

The fundamental equation for advective-dispersive-reactive transport of chemicals and microbes is (Freeze and Cherry, 1979):

$$\frac{\mathbf{d}C}{\mathbf{d}t} = \nabla(\nabla DC - VC) + R(C, t) \quad (2.1)$$

Where: $\mathbf{d}C/\mathbf{d}t$ = time rate of change in concentration (M/L³·T)
 C = concentration (M/L³)
 D = dispersion coefficient (L²/T)
 V = pore water velocity (L/T)
 R = net rate of reaction (sink/source term) (M/L³·T)

Equation (2.1) consists of two major groups of processes: mass transport and mass transfer. Mass transport includes advective and dispersive transport of aqueous species caused by fluid flow and spatial concentration gradients. Mass transfer includes process such as sorption and biological degradation. The $R(C,t)$ term in Equation (2.1) represents the sum of these transfer processes.

2.2 Mass Transport

Mass transport is the process responsible for the movement of solutes and suspended biomass in the saturated aquifer. It consists of two major processes: advection and dispersion. Advective transport is a function of the average linear velocity (or pore water velocity):

$$V = \frac{q}{n} \quad (2.2)$$

Where: V = pore water velocity (L/T)
 q = darcy velocity (L/T)
 n = effective porosity

The pore water velocity is the specific discharge divided by porosity. In turn, the specific discharge is a function of hydraulic gradient and hydraulic conductivity:

$$q = K \frac{dh}{dl} \quad (2.3)$$

Where: q = specific discharge ($L^3/L^2 \cdot T$)
 K = hydraulic conductivity (L/T)
 dh = change in hydraulic head (L)
 dl = change in length (L)

Hydraulic conductivity values range from 1.0 to 10^{-13} m/s for gravel to unfractured metamorphic rocks respectively (Freeze and Cherry, 1979).

Dispersive transport is a mixing process that is a function of spatial concentration gradients. The dispersion coefficient in Equation (2.1) is a function of two processes: molecular diffusion and mixing due to pore water velocity variations. The equations calculating the longitudinal and transverse dispersion coefficients are:

$$D_l = \mathbf{a}_l |V| + D^* \quad (2.4)$$

$$D_t = \mathbf{a}_t |V| + D^* \quad (2.5)$$

- Where: D_l = dispersion coefficient in principal direction of flow
(longitudinal dispersion coefficient) (L^2/T)
 D_t = dispersion coefficient perpendicular to direction of flow
(transverse dispersion coefficient) (L^2/T)
 \mathbf{a}_l = longitudinal dispersivity coefficient (L)
 \mathbf{a}_t = transverse dispersivity coefficient (L)
 D^* = effective diffusion coefficient (L^2/T)
 V = pore water velocity (in principle direction) (L/T)

The effective diffusion coefficient, D^* , is the molecular diffusion coefficient in water adjusted for porous media effects. The dispersivity coefficients are a measure of mixing effects caused by heterogeneity in the hydraulic flow field and are typically a function of scale (Fetter, 1993).

2.3 Mass Transfer

Mass transfer is the process responsible for the conversion of one component species to another. This process, represented by the $R(C,t)$ term in Equation (2.1), can be the sum of sorption, desorption, decay, abiotic reaction, and metabolism by bacteria. It may also be a function of multiple solutes.

Rate functions typically kinetically limit mass transfer processes. However, in certain circumstances the process proceeds so rapidly relative to the time frame resolution, the process *appears* to be in *equilibrium* at all times. These processes are called equilibrium reactions and are mathematically simple compared to their counterparts, kinetic reactions.

Mass transfer processes in a saturated aquifer consist of two major groups: conservative phase transfer processes and non-conservative decay processes. Conservative phase transfer processes are reactions by which mass is transferred from one phase to another. For example, sorption processes move mass between the mobile aqueous phase and the immobile sorbed phase, total mass is always conserved.

The equation representing the rate of transfer between the aqueous phase and sorbed phase is:

$$\frac{dC_s}{dt} = a(C_s^* - C_s) \quad (2.6)$$

Where: dC_s/dt = change in sorbed species concentration (M/L³·T)
 C_s = solute concentration in sorbed phase (M/M)
 a = rate constant (T⁻¹)
 C_s^* = equilibrium concentration of solute in the solid phase as determined by partitioning equation (M/M)

Two major relationships describe the equilibrium partitioning of aqueous and sorbed species: Freundlich and Langmuir isotherms. Isotherm refers to the relationship holding true at a constant temperature. The Freundlich isotherm is:

$$C_s^* = kC^{1/n} \quad (2.7)$$

Where: C_s^* = equilibrium solute concentration in the solid phase (M/M)
 k = partitioning coefficient (L³/M)ⁿ
 n = exponential constant
 C = concentration of solute in the liquid phase (M/L³)

If n is 1.0, Equation (2.7) reduces to a linear relationship. The partitioning coefficient for the linear case can vary from 0 to 100,000 cm³/g. (See Fry and Istok (1994) for a comprehensive review of linear partitioning coefficients.)

The Langmuir partitioning relationship is:

$$C_s^* = \frac{Qk_L C}{1 + k_L C} \quad (2.8)$$

Where: C_s^* = equilibrium solute concentration in the solid phase (M/M)
 Q = partitioning constant (M/M)
 k_L = saturation constant (L³/M)
 C = concentration of the solute in the liquid phase (M/L³)

Alvarez-Cohen et al. (1993) found that TCE sorption onto a synthetic hydrophobic zeolite in a column study was best represented by the Langmuir relationship where $Q = 201$ mg/g and $k_L = 0.521$ l/mg.

However, the use of the Langmuir isotherm is not common in most groundwater applications. Many applications involve concentrations at low levels. At these levels, both the Freundlich and Langmuir isotherms approach a linear relationship. In many

cases, laboratory data only exists for these low concentrations, resulting in a linear relationship.

Non-conservative decay processes are reactions by which mass is transferred from one type to another. For example, organic substrates are transformed to carbon dioxide. These processes consist of two major sub-groups: abiotic and biological processes. Abiotic processes include chemical reactions not mediated by microbes. For example, radioactive decay is a reaction by which mass changes from one form to another. Total mass of the original species is not conserved. The equation representing the rate of radioactive decay is:

$$\frac{dC_1}{dt} = -F \frac{dP}{dt} = -kC_1 \quad (2.9)$$

Where: dC_1/dt = rate of change in decaying species concentration (M/L³·T)
 dP/dt = rate of change in product concentration (M/L³·T)
 C_1 = concentration of decaying species (M/L³)
 k = rate constant (T⁻¹)
 F = Stoichiometric ratio of reactant to product (M/M)

Biologically mediated processes include biomass growth, substrate consumption, products formation, cometabolism, and intermediate toxicity. Since microbes mediate these processes, the mathematical representation is more involved.

Typically two mathematical equations represent a biological process: the rate equation and the stoichiometry equation. The rate equation for a biological process usually yields the rate of primary substrate consumption. The three major rate equations representing primary substrate consumption are single Monod, double Monod, and competitive Monod. (See Appendix A for a discussion of the development of Monod kinetics.)

Single Monod kinetics assume the process is a function of only one limiting substrate. The equation for primary substrate consumption using single Monod kinetics is:

$$\frac{dC_1}{dt} = -kX \frac{C_1}{K_{s1} + C_1} \quad (2.10)$$

Where: k = maximum substrate utilization rate
(M substrate/M cells·T)
 X = biomass concentration (M/L³)
 C_1 = primary substrate concentration (M/L³)
 K_{s1} = substrate half-saturation constant (M/L³)

There are two special cases that derive from single Monod kinetics: zero order and first order kinetics. Zero-order kinetics assume the limiting substrate in single Monod kinetics is in such excess ($C_I \gg K_{SI}$) that the term drops from the equation. The resulting rate equation is:

$$\frac{dC_I}{dt} = -kX \quad (2.11)$$

Where: k = maximum substrate utilization rate (M primary/M cells·T)
 X = biomass concentration on a pore volume basis (M/L³)
 C_I = concentration of primary substrate (M/L³)

Zero-order kinetics are infrequently used because most bioremediation applications treat low concentrations of contaminants. A more common simplification of single Monod kinetics is first order kinetics.

First-order kinetics assume the concentration of the limiting substrate in the single Monod relationship is so small compared to the saturation constant ($C_I \ll K_{SI}$) that the concentration term in the denominator can be neglected. The resulting rate equation is:

$$\frac{dC_I}{dt} = -k'XC_I \quad (2.12)$$

Where: k' = maximum substrate utilization rate (M primary/M cells·T)
(equals k/K_{SI} of the single Monod Relationship)
 X = biomass concentration on a pore volume basis (M/L³)
 C_I = concentration of primary substrate (M/L³)

The use of single Monod or first-order kinetics does not address the situation where two limiting substrates are important (an electron donor and electron acceptor for example). For these cases, double Monod kinetics has been developed.

Double Monod kinetics add an additional limiting substrate to the rate equation. The primary substrate consumption rate is now a function of biomass concentration and two substrates:

$$\frac{dC_1}{dt} = -kX \frac{C_1}{K_{S1} + C_1} \cdot \frac{C_2}{K_{S2} + C_2} \quad (2.13)$$

- Where: k = maximum substrate utilization rate (M primary/M cells·T)
 X = biomass concentration on a pore volume basis (M/L³)
 C_1 = concentration of the primary substrate (M/L³)
 C_2 = concentration of the secondary substrate (M/L³)
 K_{S1} = primary substrate half saturation constant (M/L³)
 K_{S2} = secondary substrate half saturation constant (M/L³)

This relationship is generally used when the secondary substrate (C_2) is only available at very low concentrations. The value of the half saturation constant (K_{S2}) is small as a result.

In some instances, a non-growth substrate competes with the growth substrate for enzyme active sites. Competitive Monod kinetics represent this situation. The equation representing primary substrate consumption is:

$$\frac{dC_1}{dt} = -kX \frac{C_1}{K_{S1} + C_1 + K_{Si} C_i / K_{Si}} \cdot \frac{C_2}{K_{S2} + C_2} \quad (2.14)$$

- Where: k = maximum substrate utilization rate (M primary/M cells·T)
 X = biomass concentration on a pore volume basis (M/L³)
 C_1 = concentration of primary substrate (M/L³)
 C_2 = concentration of secondary substrate (M/L³)
 C_i = concentration of inhibitor (M/L³)
 K_{S1} = saturation constant for primary substrate (M/L³)
 K_{S2} = saturation constant for secondary substrate (M/L³)
 K_{Si} = saturation constant for inhibitor (M/L³)

The stoichiometry equation for a biological process represents the conversion of mass from one form to another. These equations group into three major biological processes: biomass growth, biomass decay, and cometabolic transformation.

The biomass growth process includes growth of biomass, substrate consumption, and product formation. A typical equation representing this process is:

$$-\frac{1}{Y} \frac{dX}{dt} \Big|_{growth} = \frac{1}{F} \frac{dC_2}{dt} \Big|_{growth} = \frac{dC_1}{dt} \Big|_{growth} \quad (2.15)$$

Where: X = biomass concentration on a pore volume basis (M/L^3)
 Y = yield coefficient (M cells/ M primary substrate)
 C_2 = concentration secondary substrate (M/L^3)
 C_1 = concentration primary substrate (M/L^3)
 F = stoichiometric ratio of secondary substrate to primary substrate for biomass synthesis (M secondary/ M primary)

The rate of Equation (2.15) can be described by any of the rate equations presented above (Equations (2.10) through (2.14)). For example, the double Monod rate equation can represent methanotrophic growth in the subsurface. Methane is the primary growth substrate while oxygen is the secondary growth substrate.

Biomass decay includes decay of biomass and the consumption of substrates needed to complete the process. A typical equation representing this process is:

$$\frac{dC_1}{dt} \Big|_{decay} = d_c f_d \frac{dX}{dt} \Big|_{decay} \quad (2.16)$$

Where: $\frac{dX}{dt} \Big|_{decay} = bX$ or $bX \frac{C_1}{C_1 + K_{S1}}$, decay rate of biomass ($M/L^3 \cdot T$)
 X = biomass concentration on a pore volume basis (M/L^3)
 C_1 = concentration primary substrate (M/L^3)
 d_c = primary substrate demand for decay (M primary/ M cells)
 f_d = biodegradable fraction of biomass (M/M)
 b = biomass decay rate (M biomass decayed / M biomass)

The biomass decay rate is typically a first-order or single Monod relationship. The above equation can include consumption of a substrate in the decay process; this is typically an electron acceptor. For example, decay of methanotrophic bacteria uses a single monod rate equation where oxygen is the electron acceptor (primary substrate).

Cometabolic transformation is the process mediated by microbes in which a non-growth substrate is converted from one form to another. Sometimes this transformation includes side-effects such as intermediate toxicity. Intermediate toxicity is a process that damages or inactivates microbes during the degradation of certain toxic contaminants. A typical equation representing the stoichiometry of this process is:

$$\frac{1}{T_C} \frac{dX}{d} \Big|_{\text{intermediate toxicity}} = \frac{dC_1}{d} \Big|_{\text{degradation}} \quad (2.17)$$

Where: X = biomass concentration on a pore volume basis (M/L^3)
 C_1 = concentration degraded substrate (M/L^3)
 T_C = transformation capacity coefficient
 (M cells destroyed /M substrate degraded)

Often this process is competitive with the growth process and uses the competitive Monod rate equation. For example, cometabolic transformation of TCE by methanotrophs uses Equation (2.14) for the rate equation where the primary substrate is TCE, the secondary substrate is oxygen, and the inhibitor is methane. In addition, TCE degradation creates a toxic intermediate product, TCE-Epoxyde, which destroys biomass.

Biological processes also play an indirect role in the mass transport processes by changing material properties. Studies by Taylor and Jaffé (1990b), Taylor et al. (1990d) and Rittmann (1993) indicate that biomass growth affects material porosity, permeability, and dispersivity values.

The following tables present biological parameter values found in literature for the processes described above.

Table 2.3.1 Sample Values for Single Monod Kinetic Substrate Consumption Parameters

Source	Substrate	k (d^{-1})	K_{SI} (mg/l)	Experiment
Alvarez-Cohen et al. (1993)	TCE	0.31	1.1	Laboratory
Strand et al. (1990)	Methane	1.13	0.67	Laboratory
Broholm et al. (1992)	Methane	1.72	0.2	Laboratory
Taylor and Jaffé (1990a)	Methanol	7.70	0.799	Column

For a comprehensive review of Single Monod kinetic parameters, see Fry and Istok, 1994.

Table 2.3.2 Sample Values for Double Monod Kinetic Substrate Consumption Parameters

Source	Primary	k (d^{-1})	K_{S1} (mg/l)	Secondary	K_{S2} (mg/l)	Study
Srinivasan et al. (1988)	Creosote	0.87	0.1	Oxygen	0.1	Model
Semprini & McCarty (1991)	Methane	1.2 - 2.0	1.0 - 2.0	Oxygen	1.0	Model
Semprini & McCarty (1991)	Methane	3.5 - 5.0	0.2 - 0.3	Oxygen	.01 - 0.1	Model
Lindstrom et al. (1992)	--	4.34	0.12	Oxygen	7.7×10^{-4}	Model
Dhawn et al. (1993)	--	4.8	1.0	Oxygen	1.0	Model
Chen, Y-M, et al. (1992)	Benzene	8.3	12.2	Oxygen	0.1	Column
Chen, Y-M, et al. (1992)	Toluene	9.9	17.4	Nitrate	2.6	Column
Chen, Y-M, et al. (1992)	Toluene	9.9	17.4×10^{-6}	Oxygen	0.1	Column

Table 2.3.3 shows some biomass growth parameters used both in single and double Monod studies.

Table 2.3.3 Sample Values for Biomass Growth and Decay

Source	Y (mg Cell/mg Sub)	b (day^{-1})	Study
Broholm et al. (1992)	0.2	0.12	Laboratory
Chen, Y-M, et al. (1992)	0.5	0.1	Column
Dhawn et al. (1993)	1.0 - 0.5	0.024	Model
Lindstrom et al. (1992)	0.278	0.02	Model
Semprini & McCarty (1991)	0.35 - 1.1	0.15 - 0.40	Literature
Semprini & McCarty (1991)	0.5	0.10 - 0.15	Model
Strand et al. (1989)	0.51	--	Laboratory
Taylor and Jaffé (1990a)	0.0975	0.0275	Column

The above tables represent only a small portion of the available literature on bioremediation parameters. These values were found in literature involving modeling

efforts. Even within this narrow scope, the values of these parameters still span over a large range. For example, the biomass yield coefficient varies from 0.1 to 1.0 mg cells/mg substrate and the biomass decay rate from 0.02 to 0.15 d⁻¹.

3. Model Implementation

3.1 Introduction

This chapter discusses the development of the numerical model. The model simulates two-dimensional saturated steady-state flow with advection and dispersion of multiple reactive solutes. It includes the processes of Langmuir and Freundlich isotherms, as well as first order and higher reactions. It uses single, double, and competitive Monod kinetics to represent biological processes. The model is also capable of representing other processes such as intermediate toxicity and cometabolic transformation by combinations of these reactions.

The fundamental equation that represents the sum of these processes is:

$$\frac{dC}{dt} = \nabla(\nabla DC - VC) + R(C, t) \quad (3.1)$$

Where: dC/dt = time rate of change in concentration (M/L³·T)
 C = concentration (M/L³)
 D = dispersion coefficient (L²/T)
 V = pore water velocity (L/T)
 R = net rate of reaction (sink/source term) (M/L³·T)

There are several options available when solving equation (3.1). Finite difference and finite element methods are very popular. Operator-splitting methods break down equation (3.1) into sub-problems and solve each sub-problem sequentially or simultaneously using the most appropriate method. A literature review was conducted to determine which methods have been employed by other researchers. Tables 3.1.1 through 3.1.4 summarize the results of a literature search of numerical models involving biodegradation.

The tables below illustrate that no single model includes all of the desired processes outlined above. Construction of a new model is necessary. Construction is chosen over modification of an existing program for multiple reasons. Modifying an existing model would require time and effort to learn how the existing code works. It would also be easy to introduce programming errors due to unfamiliarity with the existing code. In addition, most existing programs are written in FORTRAN. Inclusion of multiple different types of reactions is far easier to implement in C++.

Table 3.1.1 Comparison of Numerical Methods, Dimensions and Flow Type

Author(s)	Model	Dimensions	Flow Type & Kinetics	Advection & Dispersion	Number of Components
Chen & McTernan (1992)	MMGTM	Three	Steady-State Saturated	Transient	Two, Substrate and Oxygen
Chen et al. (1992)		One	Steady-State Saturated	Transient Coupled	Five
Dhawn (1993)	--	One	Steady-State Saturated	Diffusion Only [‡]	Two, Substrate and Oxygen
Kindred (1989)	--	One	Steady-State Saturated	Transient, Coupled	Three
Lindstrom (1992)	--	One	Steady-State Saturated	Transient, Decoupled	Two
Mills (1991)	COMET [°]	Two	Steady-State Saturated	Transient, Coupled	One
Odencrantz (1992)	--	Two	Steady-State Saturated	Transient, Decoupled	Two, Electron Donor & Acceptor
Rifai (1988)	Bioplume II	Two	Steady-State Saturated	Transient Decoupled	Two, Hydrocarbon and Oxygen
Semprini & McCarty (1991b)	--	One	Steady-State Saturated	Transient, Coupled	Two, Electron Donor & Acceptor
Sleep, Sykes (1993)	--	Three	Variably Saturated, Transient	Transient, Coupled	Arbitrary
Srinivasan, Mercer (1988)	Bio1D	One	Steady-State Saturated	Transient Coupled	1° and 2° Substrates and Oxygen
Taylor & Jaffé (1990b)	--	One	Transient, Saturated	Transient, Coupled	Two, Substrate & Biomass
Tim & Mostaghmi (1991)	VIROTRANS ^ª	One	Variably Saturated, Transient	Transient, Coupled	One, Virus
Zheng (1993)	--	Three	Steady-State Saturated	Transient, Decoupled	One
What is Desired		At Least Two	Steady-State or Transient		Four or greater

[†]This study was for biological stimulation only, not a biodegradation study.

[‡]Macropores

[°]Colloids-Metal Transport Model incorporates EPA's CML model, movement of contaminants on moving colloids.

^ªVirus Transport Model

Table 3.1.2 Comparison of Numerical Methods, Biological Reactions

Author(s)	Model	Biological Kinetics	Cometabolism	Competitive Inhibition	Contaminant Availability
Chen & McTernan (1992)	MMGTM	Single, Double Monod & First-Order	No	No	Soluble and Sorbed
Chen et al. (1992)		No	Yes	No	Soluble Only
Dhawn (1993)	--	Double Monod	--	No	Soluble Only
Kindred (1989)	--	Double Monod	Yes	No	Soluble Only
Lindstrom (1992)	--	Double Monod	No	No	Soluble Only
Mills (1991)	COMET	--	--	--	--
Odenrantz (1992)	--	Single, Double Monod & Biofilm	--	--	Soluble Only
Rifai (1988)	Bioplume II	Instantaneous	No	No	Soluble Only
Semprini & McCarty (1991b)	--	Double Monod & Biofilm	--	--	Soluble Only
Sleep, Sykes (1993)	--	--	--	--	--
Srinivasan, Mercer (1988)	Bio1D	Double Monod [†]	No	No	Soluble Only
Taylor & Jaffé (1990b)	--	Biofilm, (effectiveness factor)	--	--	Soluble Only
Tim & Mostaghmi (1991)	VIROTRANS	First-Order Decay	--	--	--
Zheng (1993)	--	--	--	--	--
What is Desired		Monod and First Order	Yes	Yes	Soluble and Sorbed

[†]Double Monod Kinetics were modified by including a term that accounts for the minimum substrate value below which nothing happens.

Table 3.1.3 Comparison of Numerical Methods, Biomass Transport, and Sorption Kinetics

Author(s)	Model	Biomass Transport	Biomass Growth	Sorption Partitioning	Sorption Kinetics
Chen & McTernan (1992)	MMGTM	No	Yes, Decoupled [†]	Linear, Langmuir & Freundlich	Equilibrium & Non-Equilibrium
Chen et al. (1992)		No	Yes	Linear	Equilibrium
Dhawn (1993)	--	No	Yes, Decoupled [†]	Linear	Equilibrium
Kindred (1989)	--	No	Yes	Linear	Equilibrium
Lindstrom (1992)	--	No	Yes	Linear	Equilibrium
Mills (1991)	COMET	Colloid Transport	--	Linear for Soil and Colloids	Equilibrium
Odenchantz (1992)	--	No	Yes, Decoupled [†]	Linear	Equilibrium
Rifai (1988)	Bioplume II	No	No	Linear	Equilibrium (inferred)
Semprini & McCarty (1991b)	--	No	Yes, Decoupled [†]	Linear	Equilibrium & Non-Equilibrium
Sleep, Sykes (1993)	--	--	--	none	none
Srinivasan, Mercer (1988)	Bio1D	No	No	Linear, Langmuir & Freundlich	Equilibrium
Taylor & Jaffé (1990b)	--	Yes	Yes	--	--
Tim & Mostaghmi (1991)	VIROTRANS	Yes	No	Linear for Virus	Equilibrium
Zheng (1993)	--	--	--	Linear	Equilibrium
What is Desired		Desired for Completeness	Yes	Linear, Langmuir & Freundlich	Equilibrium and Non-Equilibrium

[†]Decoupled from the fluid flow equation, does not effect fluid flow.

Table 3.1.4 Comparison of Numerical Methods, Numerical Techniques

Author(s)	Model	Hard Coded for Acceptor	Numerical Technique	Abiotic Reactions
Chen & McTernan (1992)	MMGTM	Yes	Crank-Nicholson Finite-Difference, Newton-Raphson	No
Chen et al. (1992)		Yes	Galerkin F.E. Picard Iteration	No
Dhawn (1993)	--	Yes	ISML [†]	No
Kindred (1989)	`	Yes	Optimal Test Function	No
Lindstrom (1992)	--	Yes	Eulerian-Lagrangian	No
Mills (1991)	COMET	--	--	--
Odenrantz (1992)	--	No	Operator-splitting	No
Rifai (1988)	Bioplume II	Yes	Method of Characteristics	No
Semprini & McCarty (1991b)	--	No	Finite Difference, Runge-Kutta	No
Sleep, Sykes (1993)	--	--	Finite Difference, IMPESC	No
Srinivasan, Mercer (1988)	Bio1D	Yes	Finite-Difference Crank Nicholson Newton-Raphson	No
Taylor & Jaffé (1990b)	--	--	Galerkin Finite Element, Weighted Finite-Difference	No
Tim & Mostaghmi (1991)	VIROTRANS	--	Galerkin Finite Element, Newton- Raphson, Picard Iteration	No
Zheng (1993)	--	--	MOC block-Centered, Finite-Difference, Forward Particles	No
What is Desired		No		Desired for Completeness

[†]The coupled set of ODE's were integrated using the International Mathematical & Scientific Library subroutine LGEAR and DPDES.

3.2 Numerical Method Overview

The numerical model developed in this thesis uses a method similar in nature to operator-splitting (OS) called integrated operator-splitting (IOS). Integrated operator-splitting was chosen because it allows different reactions to be easily included. This section describes the IOS method used in this model and how it relates to standard OS.

Standard operator-splitting divides equation (3.1) into two parts.

$$\left. \frac{d\mathbf{C}}{dt} \right|_{A\&D} = \nabla(\nabla DC - VC) \quad (3.2)$$

$$\left. \frac{d\mathbf{C}}{dt} \right|_{Rxn} = R(C, t) \quad (3.3)$$

The method integrates these equations separately and then recombines them to form equation (3.4) below:

$$\Delta C = C_f - C_o = \Delta C_{A\&D} + \Delta C_R \quad (3.4)$$

- Where: ΔC = change in control volume concentration over a timestep
 C_f = concentration at end of timestep
 C_o = concentration at beginning of timestep
 $\Delta C_{A\&D}$ = change in concentration due to advection and dispersion
 ΔC_R = change in concentration due to reactions

Operator-splitting solves the non-reactive solute transport term ($\Delta C_{A\&D}$) first. The result is an intermediate solution (C^*) that includes only the effects of advection and dispersion over the time interval Δt . It then uses this intermediate solution as the initial concentration to solve the reaction term (ΔC_R) for the concentration at the end of the timestep. Figure 3.2.1 graphically illustrates this process.

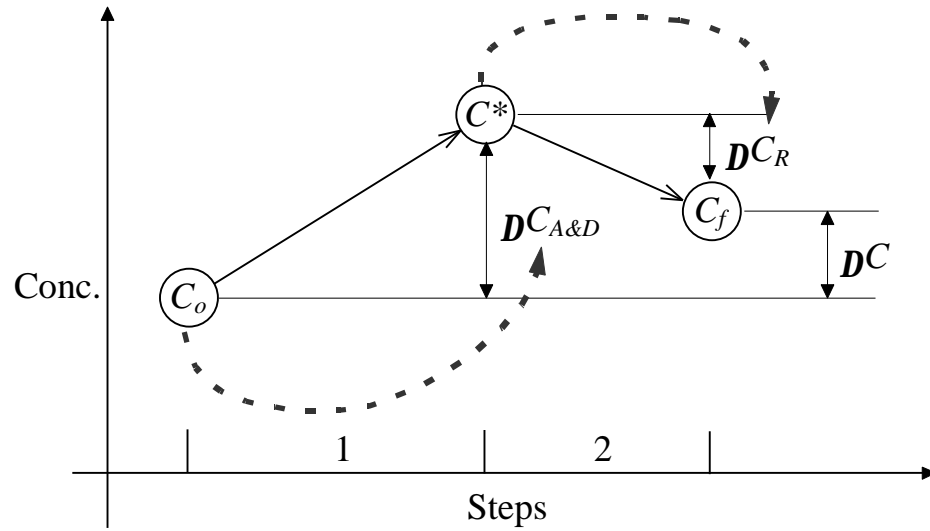


Figure 3.2.1 Standard Operator-Splitting Procedure

The dashed arrows in Figure 3.2.1 illustrate dependencies. In OS $\Delta C_{A\&D}$ is a function of the initial concentration, C_o . The reaction term, ΔC_R , is a function of the intermediate solution, C^* .

Other researchers have used methods similar to the Operator-Splitting method. Kinzelbach and Schäfer (1991) modified the standard OS method to partially re-couple equations (3.2) and (3.3). The value of ΔC_R enters into the solution of the $\Delta C_{A\&D}$ term as an added sink/source term in equation (3.2). In turn, $\Delta C_{A\&D}$ enters into the solution of ΔC_R as an extra constant sink/source reaction in equation (3.3). Figure 3.2.2 illustrates the dependencies associated with this method of solution.

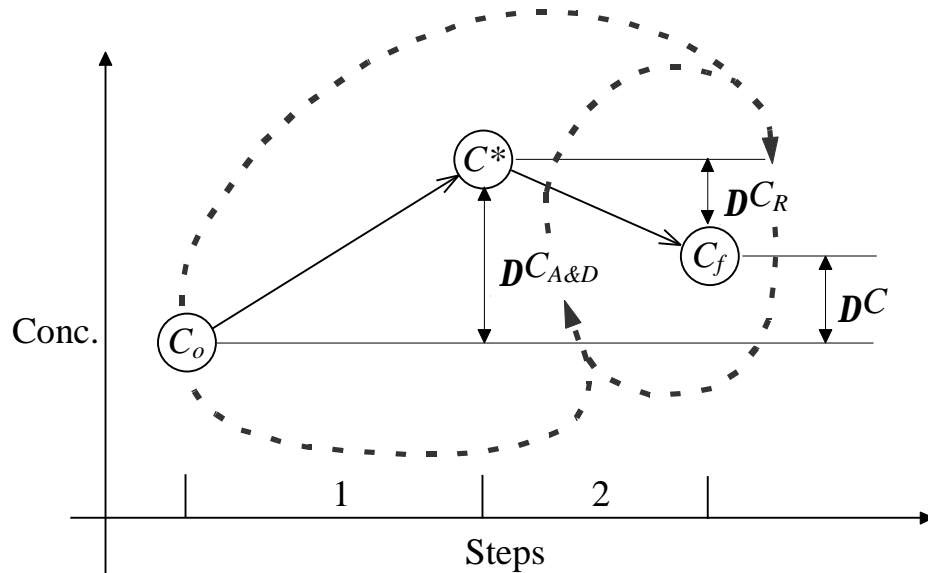


Figure 3.2.2 Operator-Splitting Procedure modified by Kinzelbach and Schäfer.

Kinzelbach and Schäfer iterate steps 1 and 2 until the final concentration, C_f , converges.

Integrated Operator-Splitting borrows from each of these ideas. The difference between this method and the others is that IOS only re-couples equation (3.3). (See Figure 3.2.3.) The calculation of $\Delta C_{A\&D}$ is independent of kinetic reactions. However, $\Delta C_{A\&D}$ still enters into the calculation of ΔC_R . In addition, this method makes a distinction between kinetic and equilibrium reactions. ΔC_R is split into two components, kinetic reactions (ΔC_K) and equilibrium reactions (ΔC_E). Also, the model simulates simultaneous movement and reaction of multiple species. Equation (3.5) rewrites equation (3.4) in a form used by IOS.

$$\Delta \mathbf{C} = \mathbf{C}_f - \mathbf{C}_o = \Delta \mathbf{C}_{A\&D} + \Delta \mathbf{C}_K + \Delta \mathbf{C}_E \quad (3.5)$$

Where: $\Delta \mathbf{C}$ = change array of concentration values over a time interval
 \mathbf{C}_f = array of concentration values at end of timestep
 \mathbf{C}_o = array of concentration values at beginning of timestep
 $\Delta \mathbf{C}_{A\&D}$ = change in concentration array due to solute flux
or advection-dispersion
 $\Delta \mathbf{C}_K$ = change in array due to kinetic reactions
 $\Delta \mathbf{C}_E$ = change in array due to equilibrium reactions

Vector notation is appropriate due to the simulation of multiple species. These species react with each other via kinetic or equilibrium equations. It would be inappropriate to

write a separate version of equation (3.5) for each solute since these solutes can be interdependent.

Similar to Kinzelbach and Schäfer's method, IOS uses an iterative procedure to calculate the concentration at the end of a timestep. Table 3.2.1 and Figure 3.2.3 present this iterative procedure.

Table 3.2.1 IOS Order of Calculation

Step	Compute	Equation	Comment
1	$\Delta C_{A\&D}$	(3.7)	This is computed first, it is only a function of initial concentration and length of time period. Its value will not change between iterations.
2	C_f	$C_f = C_o + \Delta C_{A\&D}$	Compute a trial final concentration, it is needed for the calculation of kinetic reactions.
3	ΔC_K	(3.9)	Compute the change in concentration due to kinetic reactions, which is a function of initial and final concentrations, and the length of time period.
4	ΔC_E	(3.10)	Compute the change in concentration due to equilibrium conditions, which is a function of initial concentrations and change in concentration due to flux and kinetic reaction.
5	ΔC	(3.5)	Compute the trial change in concentration at the node
6	C_f	$C_f = C_o + \Delta C$	Compute new trial final concentration. If the change in C_f from the last iteration is not sufficiently small, go back to step 3 and continue iteration.

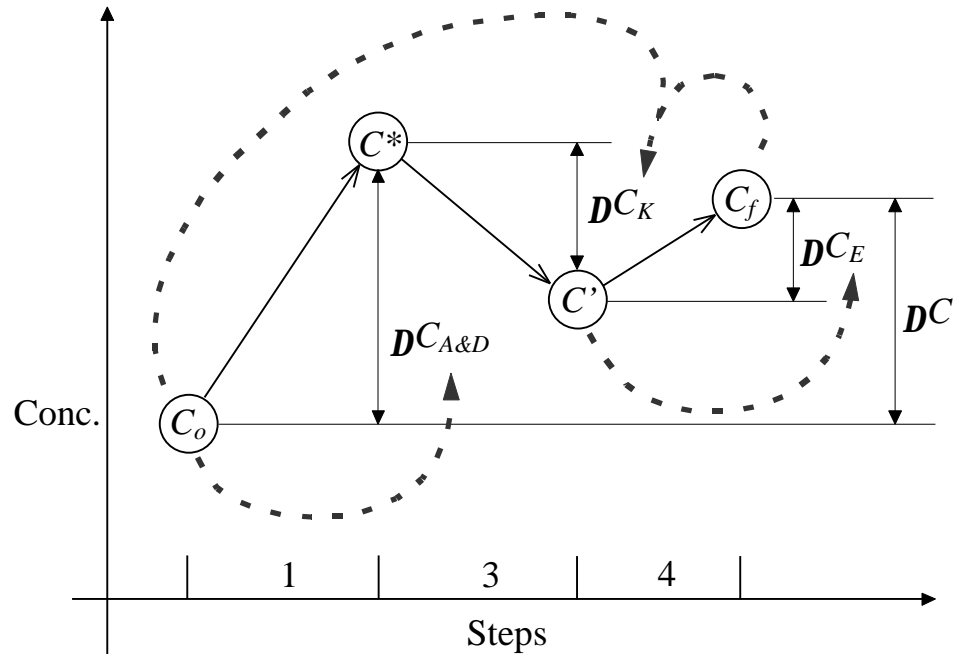


Figure 3.2.3 Integrated Operator-Splitting Procedure

The solution to each term on the right hand side of equation (3.5) uses a different set of underlying assumptions and methods of solution. The change in concentration due to advection and dispersion ($\Delta C_{A\&D}$) is a function of the length of the time step and the concentration at the beginning of the timestep. The model uses a finite difference method corrected for numerical dispersion developed by Poulsen (1994) to solve this term. The solution to the $\Delta C_{A\&D}$ term requires the calculation of fluid velocities. The model estimates these velocities using a finite difference technique described later in this section. The change in concentration due to kinetic reactions (ΔC_K) is a function of the time interval length and the concentration at both the beginning and end of the time interval. The linear integrated method described below is used to calculate this term. The change in concentration due to equilibrium reactions is solely a function of the initial concentrations and changes in concentration due to kinetic and flux components (C').

The following sections describe how the IOS method calculates the components of equation (3.5). The first section describes how the aquifer is discretized. The following section discusses how the model estimates groundwater velocities. A discussion of how the model calculates advective and dispersive fluxes follows in the next section. The subsequent section presents the Linear Integrated method and how it works. Equilibrium calculations appear in the following section. The final section discusses stability criteria. For additional information on the IOS method, see Appendix B.

3.3 Aquifer Discretization

The aquifer is divided into discrete elements using the Cartesian coordinate system. The material properties and solute concentrations are assumed to be constant throughout the element, but are allowed to differ between different elements. In this way a non-homogeneous aquifer is approximated as a collection of different homogeneous regions.

Figure 3.3.1 illustrates a “5 x 4” aquifer mesh.

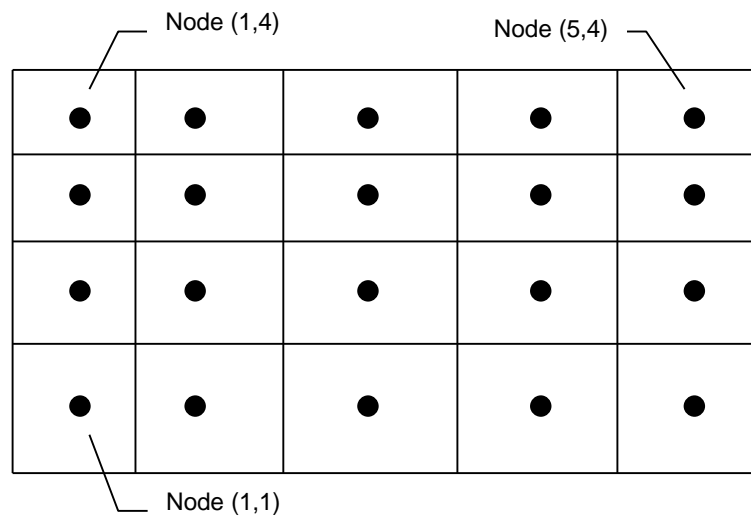


Figure 3.3.1 Illustration of a 5 x 4 Aquifer Mesh

Elements are node centered. Boundaries separating elements are located at an equal distance from each node. For boundary nodes, the exterior boundary is located the same distance from the node as its opposite boundary. Unless otherwise specified, boundary nodes are assumed to be a no-flow no-flux boundary.

3.4 Estimating Groundwater Velocities

The model estimates groundwater velocities using a finite difference method. The fundamental equation for flow in a saturated porous media is Darcy's Law (equation (2.3)). The model uses this equation to calculate groundwater velocities given the hydraulic head at each node. The finite difference solution to the hydraulic head at a given node is:

$$h_o = \frac{\Delta Y_w \left(\frac{K_{x-1}^{eq} h_{x-1}}{\Delta X_{x-1}} + \frac{K_{x+1}^{eq} h_{x+1}}{\Delta X_{x+1}} \right) + \Delta X_w \left(\frac{K_{y-1}^{eq} h_{y-1}}{\Delta Y_{y-1}} + \frac{K_{y+1}^{eq} h_{y+1}}{\Delta Y_{y+1}} \right) - Q}{\Delta Y_w \left(\frac{K_{x-1}^{eq}}{\Delta X_{x-1}} + \frac{K_{x+1}^{eq}}{\Delta X_{x+1}} \right) + \Delta X_w \left(\frac{K_{y-1}^{eq}}{\Delta Y_{y-1}} + \frac{K_{y+1}^{eq}}{\Delta Y_{y+1}} \right)} \quad (3.6)$$

$$\text{Where: } K_{x-1}^{eq} = \frac{2K_{x-1}K_o}{K_{x-1} + K_o}$$

$$K_{x+1}^{eq} = \frac{2K_{x+1}K_o}{K_{x+1} + K_o}$$

$$K_{y-1}^{eq} = \frac{2K_{y-1}K_o}{K_{y-1} + K_o}$$

$$K_{y+1}^{eq} = \frac{2K_{y+1}K_o}{K_{y+1} + K_o}$$

h_o = hydraulic head at center node

h_{x-1} = hydraulic head at node $x-1$

h_{x+1} = hydraulic head at node $x+1$

h_{y-1} = hydraulic head at node $y-1$

h_{y+1} = hydraulic head at node $y+1$

ΔX = distance between nodes in x direction

ΔY = distance between nodes in y direction

ΔX_w = node width in x direction

ΔY_w = node width in y direction

Q = external fluid flow into the node

To compute the hydraulic head surface, equation (3.6) is written for each node in the aquifer. The model solves the set of equations by inverting the resulting banded matrix.

3.5 Estimating fluxes for Advection and Dispersion

Figure 3.5.1 illustrates the spatial layout of nodes and notation used by this section to describe how the model calculates advection and dispersion.

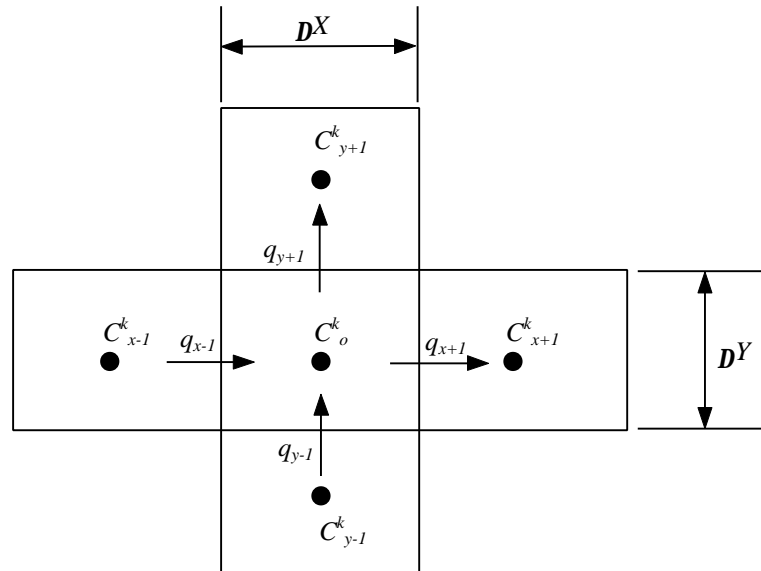


Figure 3.5.1 Node layout for computing solute flux

In the above figure, $x-1$ refers to the upstream node in the X direction, $x+1$ refers to the downstream node in the X direction. The same applies in the Y direction. C and q refer to the concentration of the k^{th} species and the specific discharge across element boundaries, respectively.

The continuity equation calculates the change in concentration due to flux, ΔC_f^k , by drawing a control volume around the center node:

$$\Delta C_F^k = \frac{(J_{x-1}^{x,k} - J_{x+1}^{x,k})\Delta t}{n\Delta x} + \frac{(J_{y-1}^{y,k} - J_{y+1}^{y,k})\Delta t}{n\Delta y} \quad (3.7)$$

Where: ΔC_F^k = change in concentration of k^{th} species due to advection-dispersion

$J_{x+1}^{x,k}$ = flux of solute k from node $x-1$ to center node

n = element porosity

Δt = time step

ΔX = grid spacing in x direction

ΔY = grid spacing in y direction

The MCS method (Poulsen, 1994) is used to compute the flux between two nodes. It is an explicit finite difference method corrected for numerical dispersion. Equation (3.8) gives the equation used to calculate the flux between the two nodes. See Appendix C for a detailed discussion of the MCS method.

$$J_{x-1}^k = \left(\frac{q_{x-1}}{2} - \frac{q_{x-1}^2 \Delta t}{2n\Delta x} - \frac{nD_{xx}}{\Delta x} \right) (C_x^k - C_{x-1}^k) - \frac{nD_{xy}}{\Delta y} (C_{x-1}^k - C_{x-1,y-1}^k) + qC_{x-1}^k \quad (3.8)$$

Where: q_{x-1} = specific discharge from node $x-1$ to node center node

$J_{x-1}^{x,k}$ = mass flux from node $x-1$ to center node

C_x^k = concentration of k^{th} species in node x

C_{x-1}^k = concentration of k^{th} species in node $x-1$

Δt = timestep

n = porosity

D_x = dispersion in X direction

Δx = node spacing in X direction

D_{xy} = cross dispersion coefficient

3.6 Simulating Kinetic Reactions

The model uses the linear integrated (LI) method to calculate the change in concentration due to kinetic reactions. The LI method assumes that the rate of change in concentration over a time period remains constant, but allows it to change between time intervals. This linearization simplifies the calculation of changes in concentration, especially when reaction rates are dependent upon multiple species. Appendix D presents a detailed discussion of the LI method. The equation for change in nodal concentration due to kinetic reactions is:

$$\Delta \mathbf{C}_K = \sum_i^n \mathbf{A}_i \int_0^{\Delta t} R_i \left(\frac{\mathbf{C}_f - \mathbf{C}_o}{\Delta t} t + \mathbf{C}_o \right) dt \quad (3.9)$$

Where: $\Delta \mathbf{C}_K$ = change in concentration array due to kinetic reactions
 \mathbf{C}_f = concentration array at beginning of timestep
 \mathbf{C}_o = concentration array at end of timestep
 \mathbf{A}_i = stoichiometric array of the i^{th} reaction
 R_i = rate function of the i^{th} reaction
 Δt = time step
 n = number of kinetic reactions

Equation (3.9) uses vector notation because some reaction rates can be a function of multiple species, and may change more than one species at a time.

Equation (3.9) also shows that $\Delta \mathbf{C}_K$ is a function of both the initial and final concentrations and the length of the timestep. This is one of the reasons for the iterative nature of the solution of equation (3.5). The other is due to the nature of the equilibrium reactions.

The model uses the timestep calculated for the stability of the advection and dispersion calculation (Equation (3.8)). However, on certain occasions when reaction rates are rapid compared to the chosen timestep, the iterative method used to solve equation (3.9) will not converge. The model responds to this problem by cutting the timestep used in equation (3.9) in half and calculating the final concentration (\mathbf{C}_f) for each sub-timestep.

3.7 Incorporating Equilibrium Reactions

The inclusion of equilibrium reactions complicates the system of equations represented by equation (3.5). Concentrations at the beginning of the time interval satisfy equilibrium conditions by definition. After advection and dispersion and kinetic reactions, the model adjusts the concentrations to satisfy equilibrium. The equilibrium term in equation (3.5) is a function of initial concentration, change in concentration due to advection and dispersion, and change in concentration due to kinetic reaction. Equation (3.10) depicts the calculation of changes due to equilibrium reactions:

$$\Delta \mathbf{C}_E = \sum_j^m \mathbf{A}_j E_j (\mathbf{C}_o + \Delta \mathbf{C}_F + \Delta \mathbf{C}_K) \quad (3.10)$$

- Where: $\Delta \mathbf{C}_E$ = change in concentration array due to equilibrium reactions
 $\Delta \mathbf{C}_F$ = change in concentration array due to solute flux
 $\Delta \mathbf{C}_K$ = change in concentration array due to kinetic reactions
 \mathbf{C}_o = concentration array at beginning of timestep
 \mathbf{A}_j = stoichiometric array of the j^{th} equilibrium reaction
 E_j = equilibrium function of the j^{th} equilibrium reaction
 m = number of equilibrium reactions

3.8 Oscillations and Stability

Like most explicit finite difference schemes, the numerical method outlined above is only conditionally stable (Poulsen, 1994). Under certain conditions, the numerical model is prone to oscillations in space or time. The use of too large of a timestep results in unstable time oscillations. Figure 3.8.1 illustrates time oscillations.

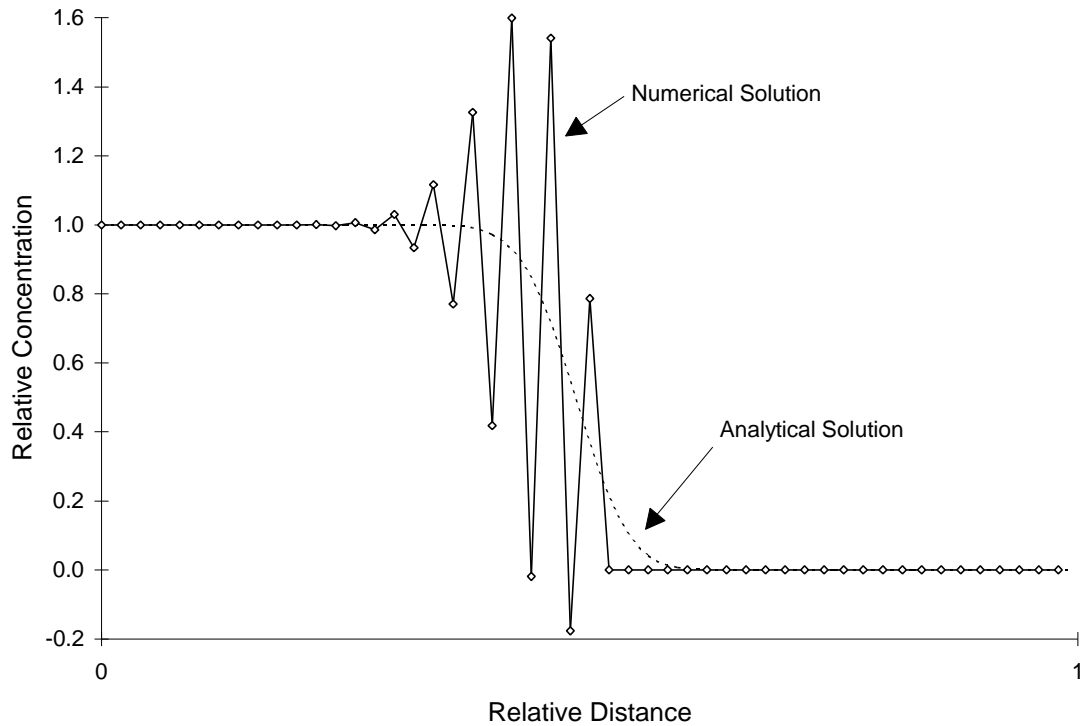


Figure 3.8.1 Unstable Time Oscillations

These oscillations grow larger as the simulation progresses in time, causing the simulation to eventually fail.

Use of too small of a timestep results in stable space oscillations. Unlike time oscillations, space oscillations do not grow as the simulation progresses in time. Figure 3.8.2 illustrates these oscillations.

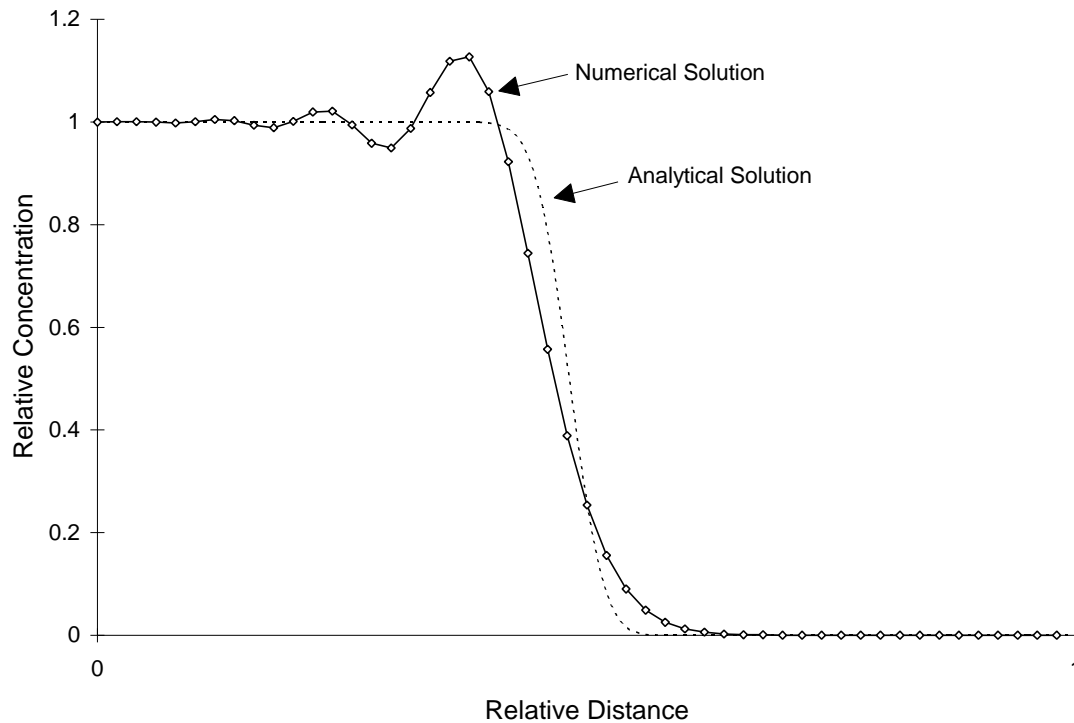


Figure 3.8.2 Stable Space Oscillations

Proper selection of the time step can control both time and space oscillations. This thesis uses the method of Wind and Van Doorne (1975) to determine the maximum allowable timestep to avoid numerical oscillations in time. This method assumes isotropic conditions without sink/source reactions. For space oscillations, this thesis uses a method based on maximum allowable fluxes to determine the minimum allowable timestep. These timestep criteria are a function of advective-dispersive properties; additional adjustment of the timestep may be necessary for the stability of sink/source reactions. Appendix E discusses the details of the timestep calculations.

The maximum and minimum allowable time steps (calculated in Appendix E) to avoid oscillations in a two-dimensional simulation are:

$$\Delta t \leq \frac{-B + \sqrt{B^2 + A}}{A} \quad (3.11)$$

$$\Delta t \geq \frac{\sqrt{A} - 2B}{A} \quad (3.12)$$

Where: $A = \left(\frac{q_x}{n\Delta x}\right)^2 + \left(\frac{q_y}{n\Delta y}\right)^2$
 $B = \frac{D_{xx}}{\Delta x^2} + \frac{D_{yy}}{\Delta y^2} - \frac{D_{xy}}{\Delta x\Delta y}$
 $q =$ darcy velocity (L/T)
 $\Delta t =$ timestep (T)
 $\Delta x =$ grid spacing (L)
 $n =$ material porosity

For the case of a one-dimensional simulation, equations (3.11) and (3.12) simplify to functions of the Courant and Peclet numbers. The criteria in one dimension as a function of Courant and Peclet numbers are:

$$Co \leq \sqrt{\frac{1}{Pe^2} + 1} - \frac{1}{Pe} \quad (3.13)$$

$$Co \geq 1 - \frac{2}{Pe} \quad (3.14)$$

Where: $Co = \frac{q\Delta t}{n\Delta x}$, courant number
 $Pe = \frac{q\Delta x}{nD}$, peclet number
 $q =$ darcy velocity (L/T)
 $\Delta t =$ timestep (T)
 $\Delta x =$ grid spacing (L)
 $n =$ material porosity

Figure 3.8.3 illustrates these equations for the one-dimensional case.

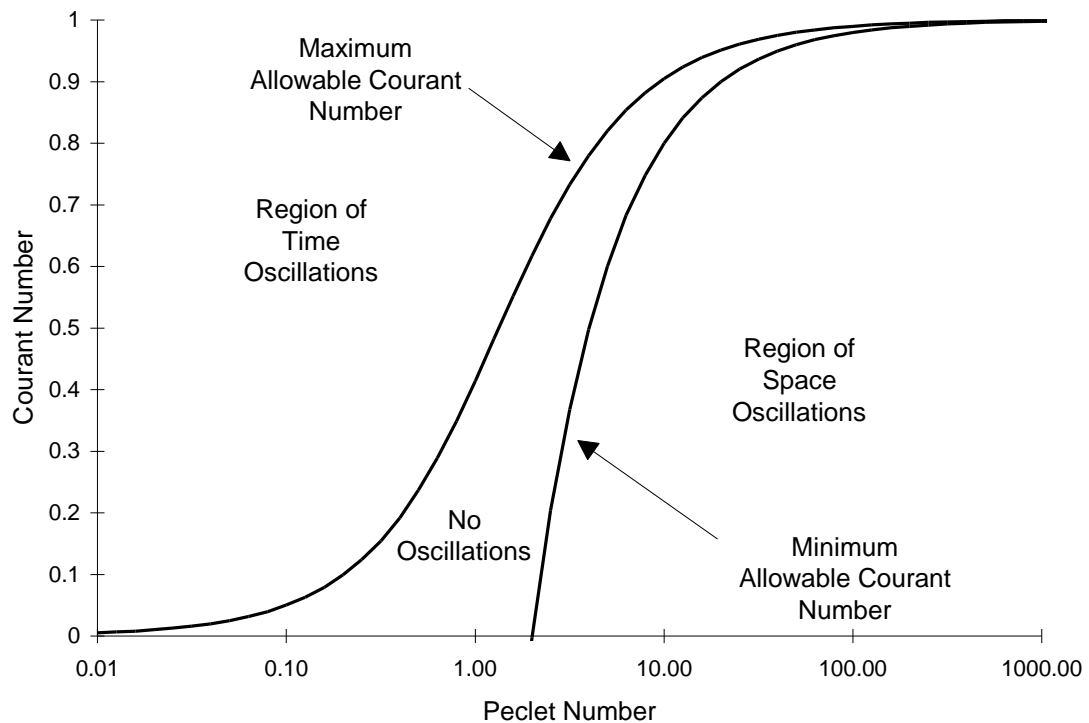


Figure 3.8.3 Maximum and Minimum Courant Number Criteria for one-dimensional Simulations

Using a time step in the region of no oscillations does not guarantee a perfect solution. There will still be errors associated with the numerical procedure, however they will not be oscillations associated with the time step.

In addition, the timestep criteria was developed under a unique set of assumptions. The timestep criteria assumes uniform aquifer properties; it may not apply to heterogeneous systems. In addition, it does not take sink/source reactions into account. In some cases, it may be necessary to use trial and error to find a suitable time step.

4. Model Performance

4.1 Introduction

This chapter evaluates model performance based on the accuracy of the numerical solution. Two major types of tests contribute to this process: verification and validation. Verification compares analytical and numerical solutions. For this process to be legitimate, the analytical and numerical solutions must start with the same assumptions, such as initial and boundary conditions. Validation compares numerical solutions with data from real world systems such as laboratory column and field studies.

Few simple analytical solutions describing solute transport coupled with reactions exist. Poulsen (1991) used an analytical solution of the advective-dispersive equation coupled with first order degradation. Fry et al. (1993) developed an analytical solution to the solute transport equation with rate-limited desorption and first order decay. However, like most analytical solutions incorporating kinetic equations of higher order, the method of solution ultimately requires numerical methods. This chapter only compares numerical solutions with simple analytical solutions.

Because of these limitations described above, verification tests will separate the advective-dispersive processes from the reaction processes and evaluate each individually. An exception is one-dimensional solute transport with first order decay. It is the only coupled case possessing a simple analytical solution. The following list presents the verification tests included in this chapter and Appendix F:

- Conservative Solute Tests
 - One-Dimensional Continuous Source
 - One-Dimensional Pulse Source
 - Two-Dimensional Pulse Source
- Non-Conservative Solute Tests
 - One-Dimensional Continuous Source with First-Order Decay
- Kinetic Reaction Tests
 - Linear Sorption (Appendix F)
 - Langmuir Sorption (Appendix F)
 - Freundlich Sorption (Appendix F)
 - First Order
 - Single Monod (Appendix F)
 - Double Monod (Appendix F)
 - Competitive Monod

In addition to verification tests, this chapter includes two validation-type tests. This chapter tests model performance in simulating conservative solute transport in stratified porous media (Sudicky et al., 1985). It also uses the model to reproduce biostimulation modeling studies conducted by Semprini et al. (1991).

Criteria defining acceptable and unacceptable error quantities do not exist. This is a function of model application. Some simulations may require high accuracy, while others may not. This chapter does not make decisions on the acceptability of performance. It simply presents the sensitivity of errors to various input parameters.

4.2 Measures of Performance

This chapter compares numerical and analytical solutions both qualitatively and quantitatively. Qualitative analysis involves a visual comparison of numerical and analytical solutions. Quantitative analysis uses mathematical means to measure the difference between numerical and analytical solutions. There are many ways to quantitatively measure the error in a numerical simulation. Some of these methods include: maximum absolute error, sum of absolute error, sum of squared error, relative sum of square error, and mass balance error.

Choice of a proper quantitative measurement of error is an important task. Sometimes the use of certain methods is inappropriate for the numerical model. For example, the numerical described in this thesis is mass conservative by definition, computing the mass balance error would be meaningless. Also, other methods may yield identical results. Numerical experimentation with this model has shown that error calculations using absolute and relative measurement yield qualitatively similar results.

This thesis uses the Relative Sum of Square Error (RSSE) to quantify the difference between numerical and analytical solutions. The definition of RSSE for this thesis is:

$$RSSE = \sum_{i=1}^{N_x} \sum_{j=1}^{N_t} \left(\frac{C_{Aij} - C_{Nij}}{m_j} \right)^2 \quad (4.1)$$

Where: $RSSE$ = relative sum of square error
 N_x = number of nodes in the aquifer
 N_t = number of time intervals in the simulation
 C_{Aij} = analytical concentration at node i , time j
 C_{Nij} = numerical concentration at node i , time j
 m_j = maximum analytical concentration in aquifer at time j

This method yields the sum of squared errors at every node in the aquifer for every timestep in the simulation. The errors are normalized by the maximum analytical concentration at each timestep. Numerical experimentation has shown that this computation yields similar results as other methods such as the maximum absolute error and sum of squared errors.

4.3 Use of Dimensionless Variables

The use of dimensionless variables for representing and calculating stability criteria is common in groundwater modeling. Dimensionless variables have the advantage of remaining independent of time and space scales. This chapter presents results as a function of three dimensionless variables; the Peclet number (Pe), the Courant number (Co), and the Damkohler number (Da).

The Peclet number relates the strength of advective forces relative to dispersive forces in the simulation. The Peclet number for a two-dimensional simulation is:

$$Pe = \frac{\sqrt{\left(\frac{V_x}{\Delta x}\right)^2 + \left(\frac{V_y}{\Delta y}\right)^2}}{\frac{D_{xx}}{\Delta x^2} + \frac{D_{yy}}{\Delta y^2} - \frac{D_{xy}}{\Delta x \Delta y}} \quad (4.2)$$

Where: V_x, V_y = pore water velocity in X and Y directions (L/T)
 Δx = grid spacing in the X direction (L)
 Δy = grid spacing in the Y direction (L)
 D_{xx} = principal dispersion coefficient in the X direction (L²/T)
 D_{yy} = principal dispersion coefficient in the Y direction (L²/T)
 D_{xy} = cross dispersion coefficient (L²/T)

The Courant number relates to amount of advection relative to the grid mesh size. The Courant number for a two-dimensional simulation is:

$$Co = \Delta t \sqrt{\left(\frac{V_x}{\Delta x}\right)^2 + \left(\frac{V_y}{\Delta y}\right)^2} \quad (4.3)$$

Where: Δt = time step (T)
 V_x, V_y = pore water velocity in X and Y directions (L/T)
 Δx = grid spacing in the X direction (L)
 Δy = grid spacing in the Y direction (L)

The Damkohler number relates the rate of solute decay to advection. The Damkohler number in one dimension is:

$$Da = \frac{k\Delta x}{V} \quad (4.4)$$

Where: k = first order decay rate (T^{-1})
 Δx = grid spacing (L)
 V = pore water velocity (L/T)

4.4 One-Dimensional Conservative Solute with a Continuous Source

This section evaluates model performance in simulating one-dimensional transport of a conservative solute with a continuous source. It reports RSSE as a function of Peclet (Pe) and Courant (Co) numbers. The analytical equation representing solute flow in the aquifer is (Fetter, 1994):

$$C(x,t) = \frac{C_o}{2} \left[\operatorname{erfc} \left(\frac{x-Vt}{2\sqrt{D_l t}} \right) + \exp \left(\frac{Vx}{D_l} \right) \operatorname{erfc} \left(\frac{x+Vt}{2\sqrt{D_l t}} \right) \right] \quad (4.5)$$

Where: t = time (T)
 x = distance from inlet (L)
 C_o = concentration at inlet (M/L^3)
 V = pore water velocity (L/T)
 D_l = dispersion coefficient (L^2/T)

Equation (4.5) makes the following assumptions about initial and boundary conditions:

- $C(x,0) = 0.0$ for $0 < x < \infty$
- $C(0,t) = C_o$ for $t > 0$
- Infinite Aquifer Length
- Homogeneous Material Properties

The model is incapable of simulating an aquifer of infinite length. This should not be a problem if the performance tests use simulation times short enough to prevent concentration profiles from reaching the aquifer outlet boundary.

Figure 4.4.1 illustrates log RSSE contours as a function of Peclet (Pe) and Courant (Co) numbers:

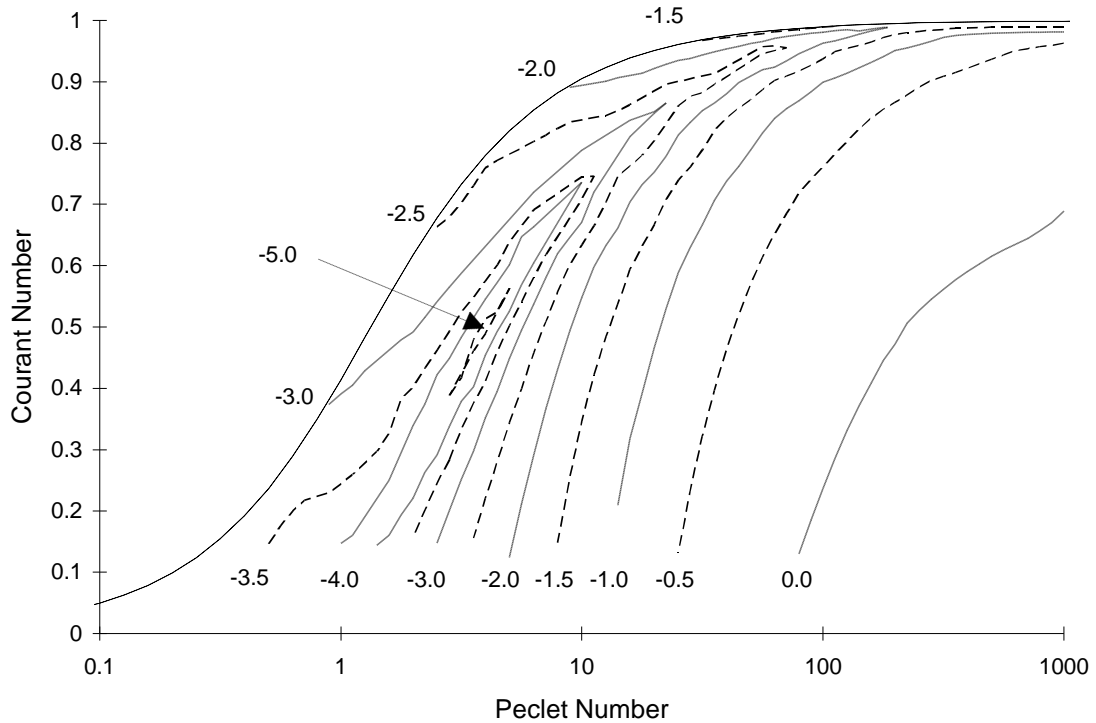


Figure 4.4.1 Log RSSE Contours as a Function of Pe and Co for One-Dimensional Conservative Solute Transport with Continuous Source

Figure 4.4.1 shows that the RSSE is highly sensitive to the choice of the Peclet and Courant number. In addition, it shows that the region around $Pe \approx 4.0$ and $Co \approx 0.5$ contains the lowest RSSE values and falls within the region of no oscillations in Figure 3.8.3.

Figure 4.4.1 also shows that selection of the appropriate Courant number has implications on model performance when simulating multiple solutes or heterogeneous systems. A Courant and Peclet number may be appropriate for one of the solutes and inappropriate for the others. For simulations with heterogeneous flow systems, different Courant and Peclet numbers will occur in different areas of the flow field.

Figure 4.4.2 through Figure 4.4.4 illustrate concentration profiles for various combinations of Peclet and Courant numbers. The three figures illustrate choices of: low Courant and Peclet number; low Courant number and High Peclet number; and

high Courant and Peclet number. Circles and lines represent numerical and analytical values respectively.

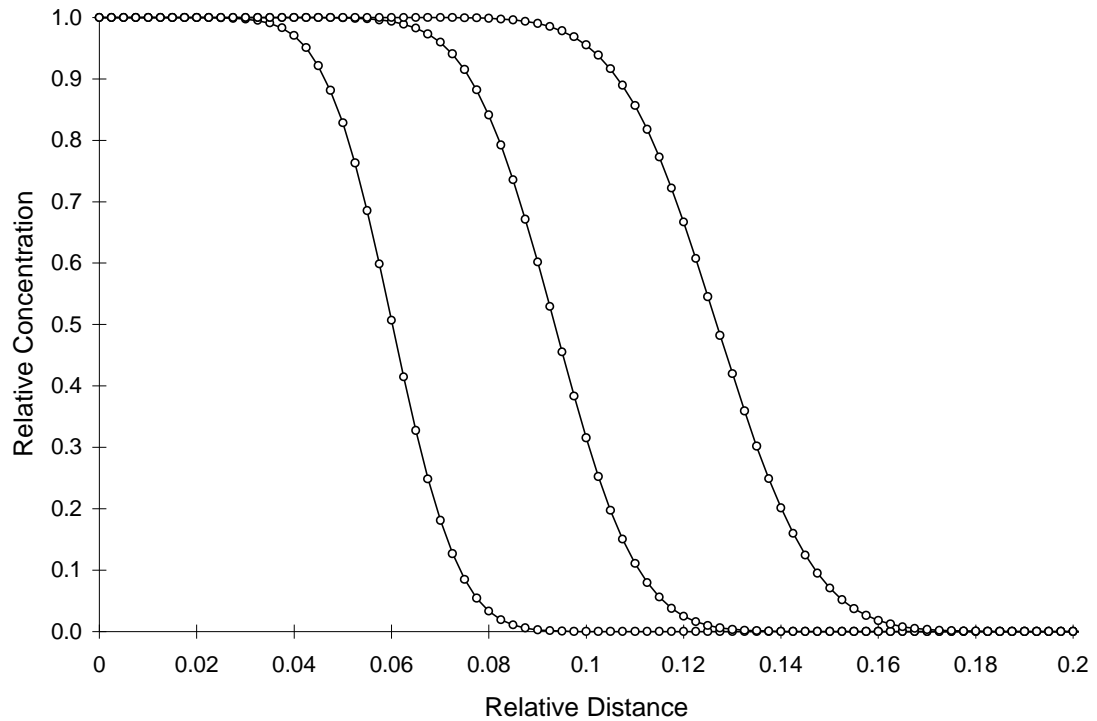


Figure 4.4.2 One-Dimensional Conservative Solute Transport
with Continuous Source, $Pe = 2.5$, $Co = 0.36$, $RSSE = 1.0 \times 10^{-5}$

Figure 4.4.2 illustrates the choice of a low Courant and Peclet number. This combination of Courant and Peclet numbers falls in the region of no oscillations in Figure 3.8.3.

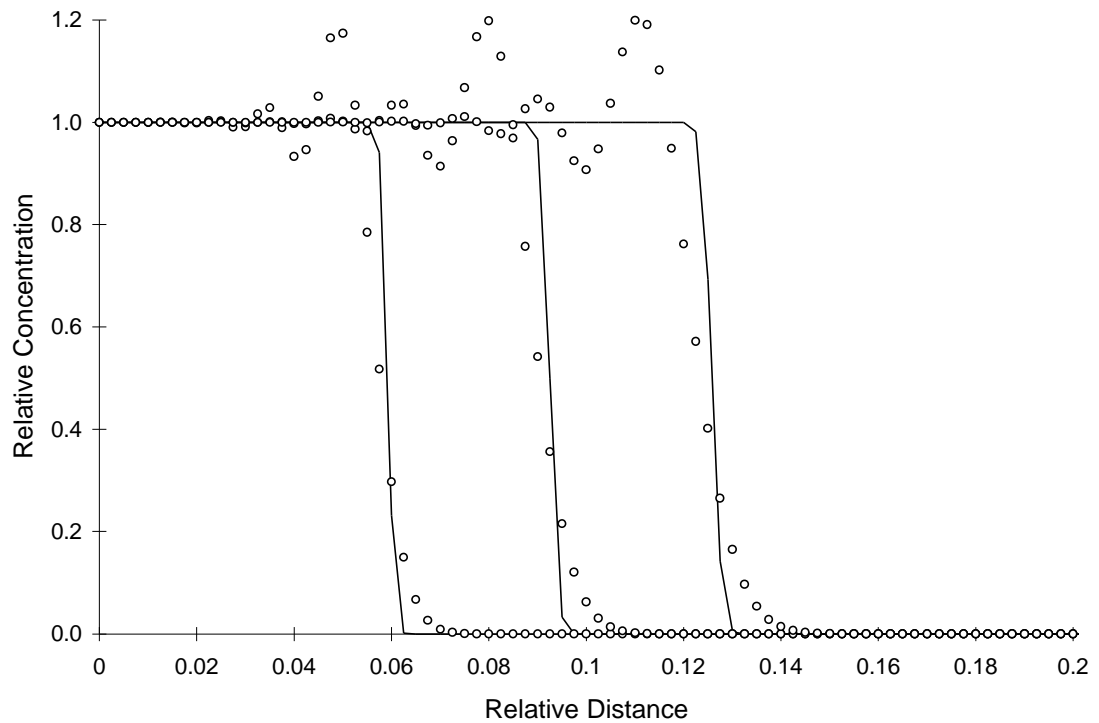


Figure 4.4.3 One-Dimensional Conservative Solute Transport
with Continuous Source, $Pe = 250$, $Co = 0.36$, $RSSE = 1.2$

Figure 4.4.3 illustrates a simulation with space oscillations. The choice of the Courant number is too low for the choice of Peclet number. This combination of Courant and Peclet number falls in the region of space oscillations in Figure 3.8.3.

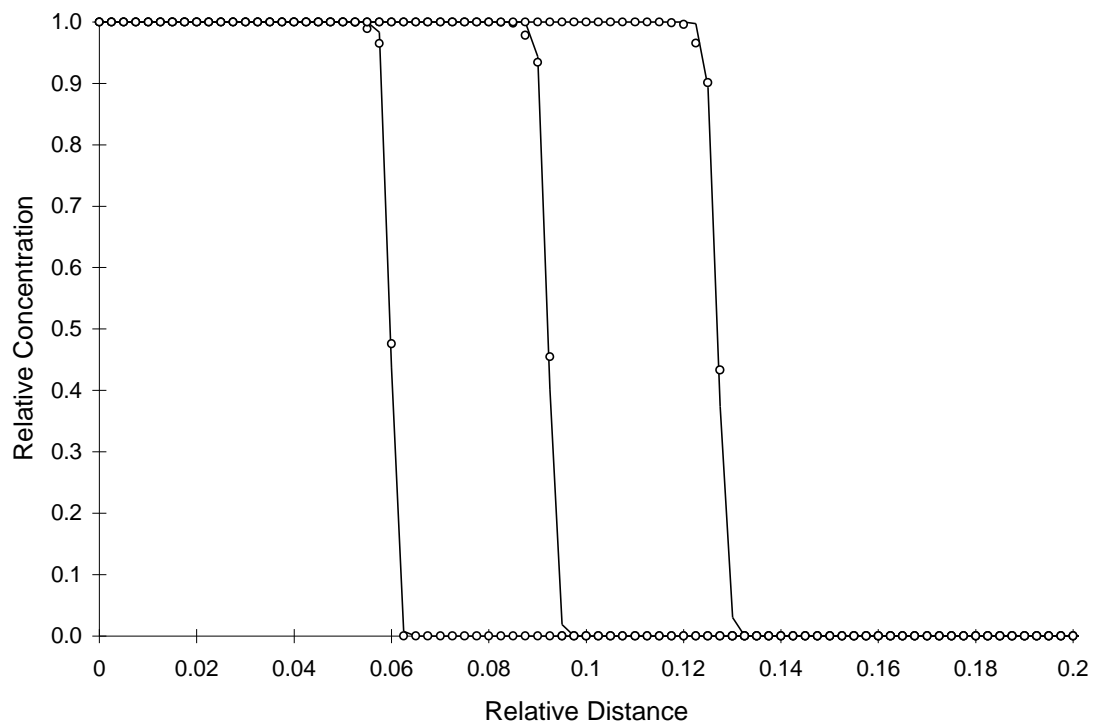


Figure 4.4.4 One-Dimensional Conservative Solute Transport
with Continuous Source, $Pe = 250$, $Co = 0.995$, $RSSE = 1.1 \times 10^{-2}$

Figure 4.4.4 illustrates the simulation of highly advective system. The combination of Courant and Peclet number falls in the region of no oscillations.

4.5 One-Dimensional Conservative Solute from a Pulse Injection

This section evaluates model performance in simulating one-dimensional transport of a conservative solute resulting from an instantaneous source. It reports RSSE as a function of Peclet (Pe) and Courant (Co) numbers. The analytical equation representing solute transport in the aquifer is (Fetter, 1994):

$$C(x,t) = \frac{C_o L}{2\sqrt{ptD_l}} \exp\left(-\frac{(x-Vt)^2}{4D_l t}\right) \quad (4.6)$$

Where: t = time (T)
 x = distance from inlet (L)
 C_o = initial concentration of pulse (M/L³)
 L = length of pulse application (L)
 V = pore water velocity (L/T)
 D_l = dispersion coefficient (L²/T)

Equation (4.6) makes the following assumptions about initial and boundary conditions:

- $C(x,0) = 0.0$ for $x \neq 0$
- $C(0,0) =$ Instantaneous Point Source
of Infinite Concentration
- Infinite Aquifer Length
- Homogeneous Material Properties

Figure 4.5.1 illustrates log RSSE contours as a function of Peclet (Pe) and Courant (Co) numbers:

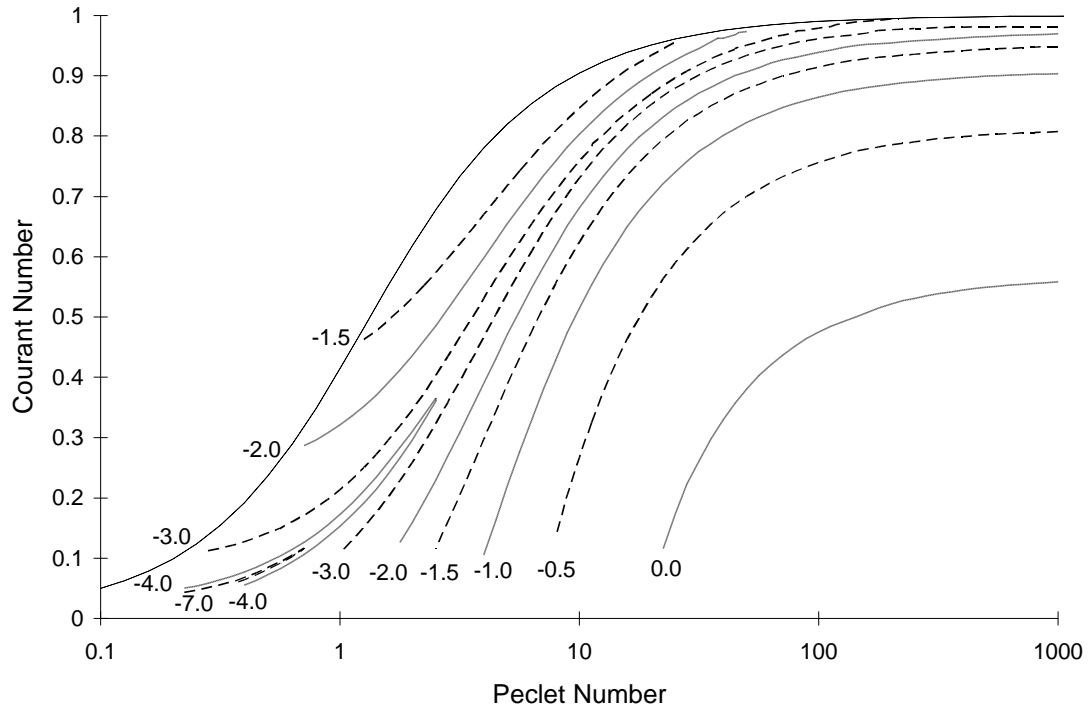


Figure 4.5.1 Log RSSE Contours as a Function of Pe and Co for One-Dimensional Conservative Solute Transport with a Pulse Source

Once again, Figure 4.5.1 shows that the RSSE is highly sensitive to the choice of Peclet and Courant number. It also shows that the region containing the lowest RSSE values corresponds to the region of no oscillations in Figure 3.8.3.

Figure 4.5.2 through Figure 4.5.4 illustrate concentration profiles for various combinations of Peclet and Courant numbers. The three figures illustrate choices of: low Courant and Peclet number; low Courant number and High Peclet number; and high Courant and Peclet number. Circles and lines represent numerical and analytical values respectively.

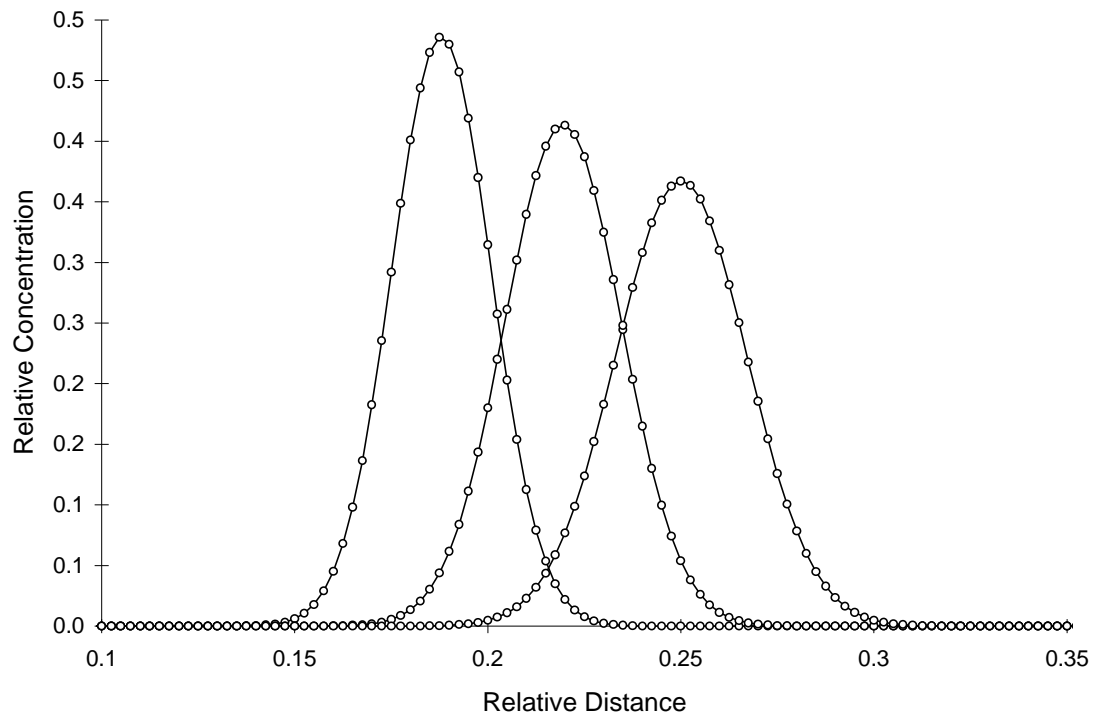


Figure 4.5.2 One-Dimensional Conservative Solute Transport
with a Pulse Source, $Pe = 2.5$, $Co = 0.36$, $RSSE = 2.6 \times 10^{-5}$

Figure 4.5.2 illustrates the choice of a low Courant and Peclet number. This combination of Courant and Peclet numbers falls in the region of no oscillations in Figure 3.8.3.

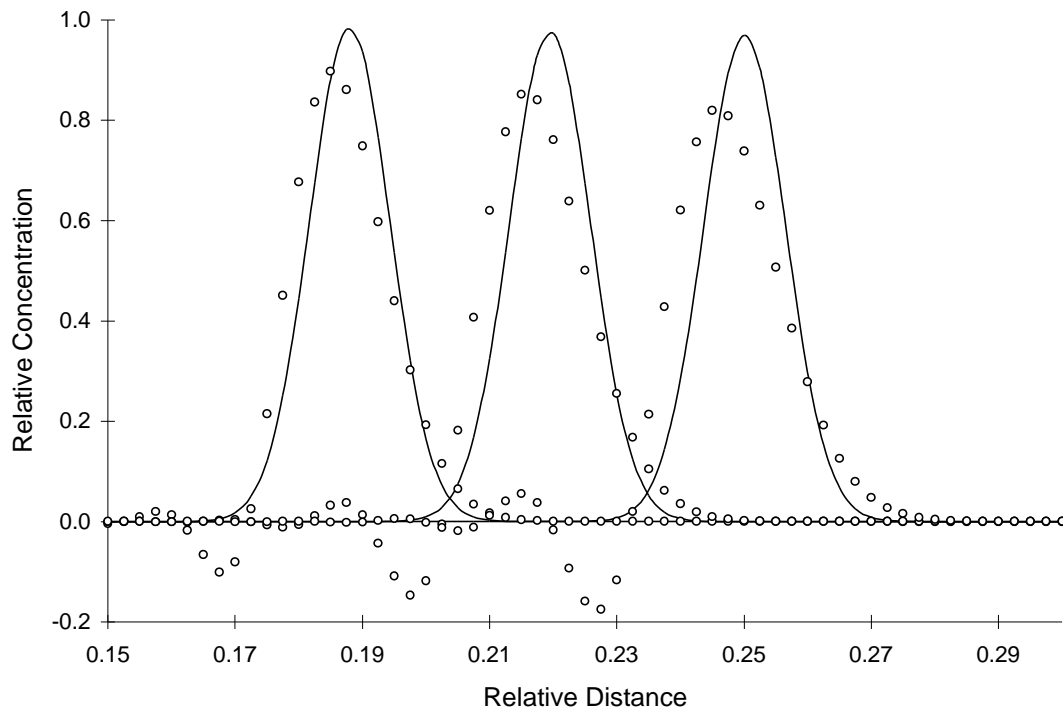


Figure 4.5.3 One-Dimensional Conservative Solute Transport
with a Pulse Source, $Pe = 250$, $Co = 0.36$, $RSSE = 1.4$

Figure 4.5.3 illustrates a simulation with space oscillations. The choice of the Courant number is too low for the choice of Peclet number. This combination of Courant and Peclet number falls in the region of space oscillations in Figure 3.8.3.

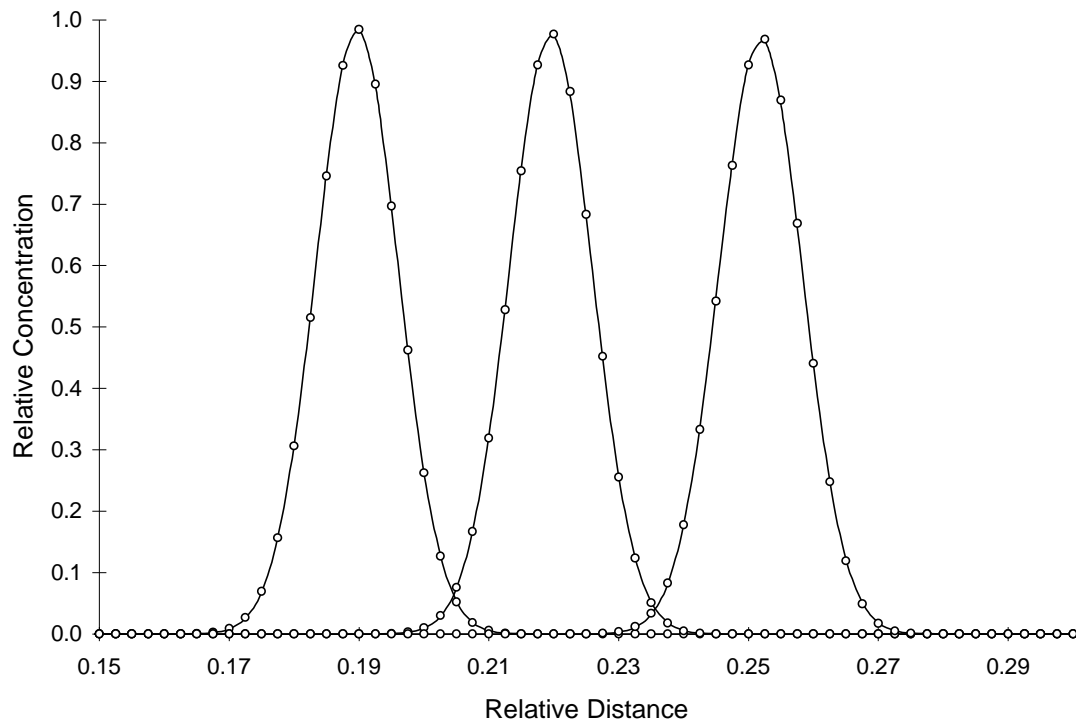


Figure 4.5.4 One-Dimensional Conservative Solute Transport
with a Pulse Source, $Pe = 250$, $Co = 0.995$, $RSSE = 7.3 \times 10^{-4}$

Figure 4.5.4 illustrates the simulation of highly advective system. The combination of Courant and Peclet number falls in the region of no oscillations.

4.6 Two-Dimensional Conservative Solute Transport

This section evaluates model performance in simulating the transport of a conservative solute in two dimensions. It uses the analytical solution to the case of a solute pulse injection. The analytical solution to two-dimensional solute transport is (Fetter, 1994):

$$C(x, y, t) = \frac{C_o A}{4pt\sqrt{D_l D_t}} \exp\left(-\frac{(x-Vt)^2}{4D_l t} - \frac{y^2}{4D_t t}\right) \quad (4.7)$$

Where: t = time (T)
 x = distance in X direction (L)
 y = distance in Y direction (from centerline of flow) (L)
 C_o = initial concentration of pulse (M/L³)
 A = area of pulse application (L²)
 V = pore water velocity (L/T)
 (in X direction, no flow in Y direction)
 D_l = longitudinal (X direction) dispersion coefficient (L²/T)
 D_t = transverse (Y direction) dispersion coefficient (L²/T)

Equation (4.7) makes the following assumptions about the initial and boundary conditions:

- $C(x, y, 0) = 0.0$ for $x \neq 0$ and $y \neq 0$
- $C(0, 0, 0) =$ Instantaneous Point Source
of Infinite Concentration
- Infinite Aquifer Length
- Homogeneous Material Properties

Figure 4.6.1 illustrates cross-sectional profiles of numerical and analytical solutions. This test used a dispersivity ratio (α_l/α_t) of 10. The angle of flow in the aquifer is at 30° from the X axis. Circles and lines represent numerical and analytical values, respectively.

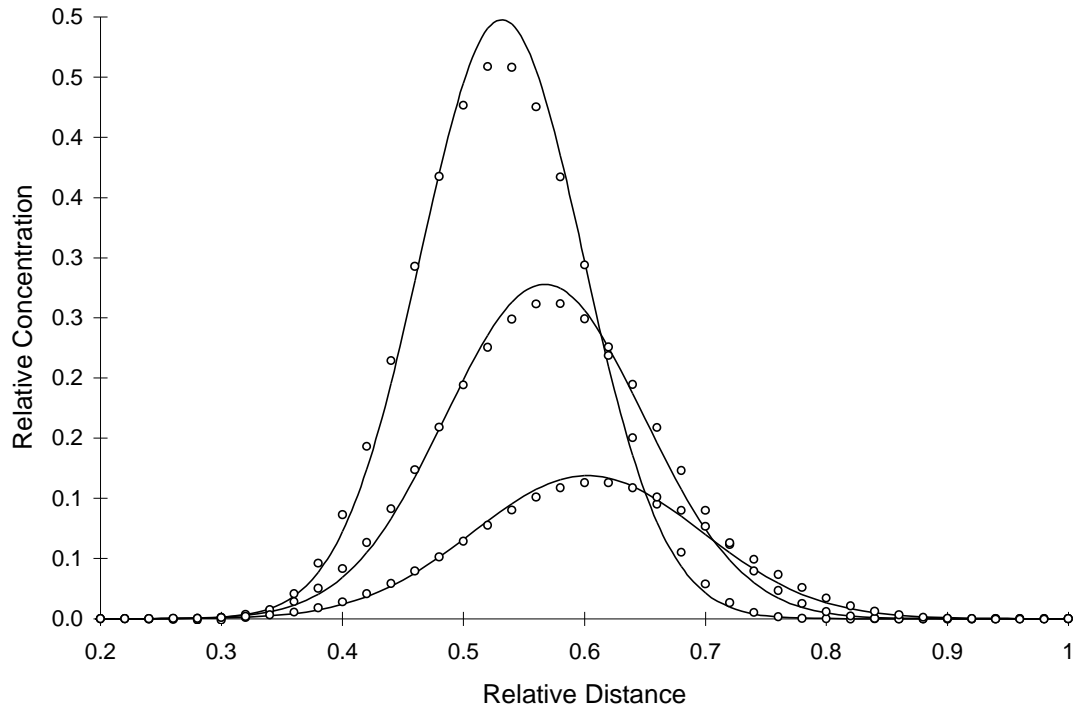


Figure 4.6.1 Two-Dimensional Conservative Solute Transport with a Pulse Source,
Cross-sectional Profiles at a Relative Distance of $Y = 0.50$
 $Pe = 0.5$, $Co = 0.082$, $\alpha_l/\alpha_t = 10$, Flow Angle = 30°

Figure 4.6.1 illustrates a simulation with low Peclet and Courant numbers. This combination of Courant and Peclet numbers falls inside the region of no oscillations in Figure 3.8.1.

Figure 4.6.2 illustrates a simulation using a dispersivity ratio of 5.0.

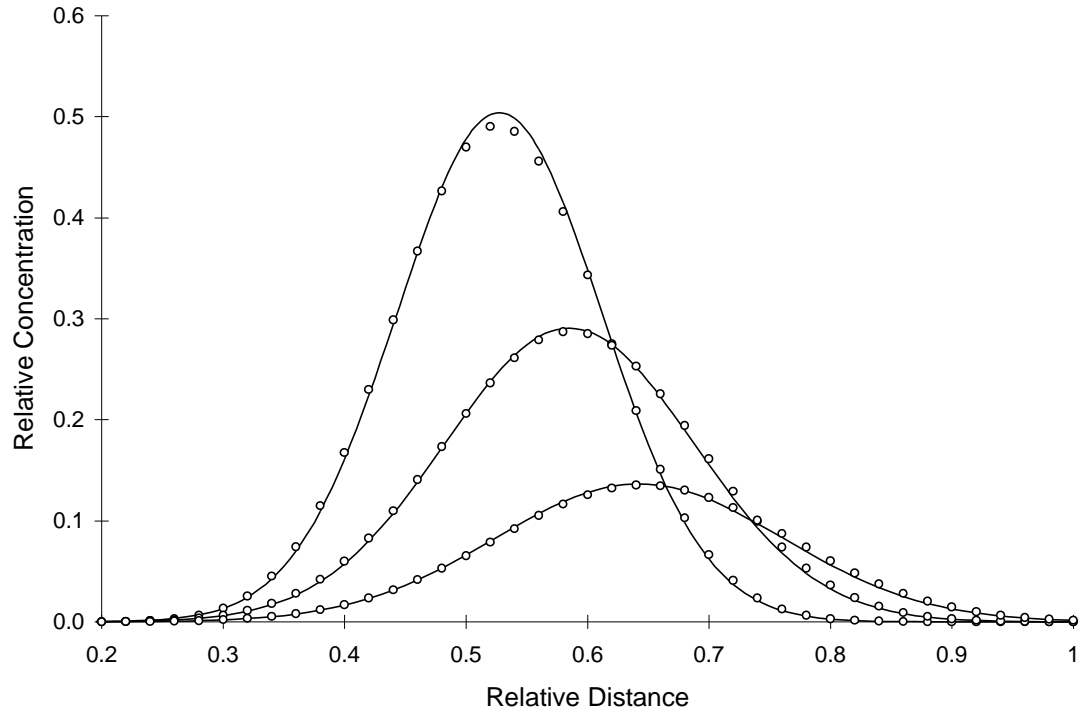


Figure 4.6.2 Two-Dimensional Conservative Solute Transport with a Pulse Source,
Cross-sectional Profiles at a Relative Distance of $Y = 0.50$
 $Pe = 0.5$, $Co = 0.082$, $\alpha_l/\alpha_t = 5$, Flow Angle = 30°

A comparison of Figure 4.6.1 and Figure 4.6.2 illustrates that decreasing the dispersivity ratio improves model performance. Numerical experimentation has shown this to be the case in general.

Figure 4.6.3 illustrates a simulation using a dispersivity ratio of 20.0.

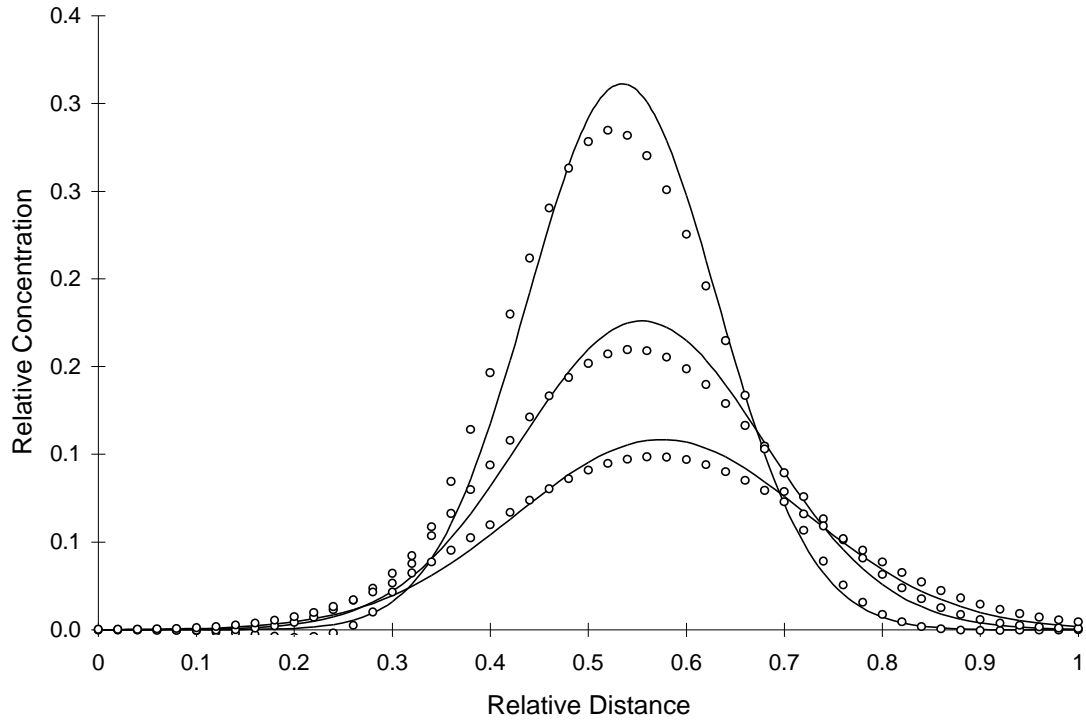


Figure 4.6.3 Two-Dimensional Conservative Solute Transport with a Pulse Source,
Cross-sectional Profiles at a Relative Distance of $Y = 0.50$
 $Pe = 0.1$, $Co = 0.049$, $\alpha_l/\alpha_t = 20.0$, Flow Angle = 30°

Once again, Figure 4.6.3 shows that performance deteriorates as the dispersivity ratio increases.

This analysis assumes that if model performance is satisfactory at a 30° angle, it will in turn be satisfactory at all flow angles. Numerical experimentation has confirmed this assumption.

4.7 One-Dimensional Solute with First Order Decay

This section evaluates model performance in simulating one-dimensional solute transport with first order decay. It reports RSSE as a function of Peclet, Courant, and Damkohler numbers. The analytical equation representing solute flow in the aquifer is (Poulsen, 1991):

$$C(x,t) = \frac{C_o}{2} \left[\exp\left(\frac{(1-A)Vx}{2D_l}\right) \operatorname{erfc}\left(\frac{(x-AVt)}{\sqrt{4D_l t}}\right) + \exp\left(\frac{(1+A)Vx}{2D_l}\right) \operatorname{erfc}\left(\frac{(x+AVt)}{\sqrt{4D_l t}}\right) \right] + \frac{C_i}{2} \exp(-Kt) \left[\operatorname{erfc}\left(\frac{Vt-x}{\sqrt{4D_l t}}\right) - \exp\left(\frac{Vx}{D_l}\right) \operatorname{erfc}\left(\frac{Vt+x}{\sqrt{4D_l t}}\right) \right] \quad (4.8)$$

$$\text{Where: } A = \sqrt{1 + \frac{4D_l K}{V^2}}$$

t = time (T)

x = distance in X direction (L)

C_o = concentration at inflow boundary (M/L^3)

C_i = initial concentration in aquifer (M/L^3)

K = first order degradation coefficient (T^{-1})

V = pore water velocity (L/T)

D_l = longitudinal dispersion coefficient (L^2/T)

Equation (4.8) makes the following assumptions:

- $C(x,0) = C_i$ for $x > 0$
- $C(0,t) = C_o$ for $t \geq 0$
- Infinite Aquifer Length
- Homogeneous Material Properties

Figure 4.7.1 illustrates RSSE as a function of Pe and Da . The Courant number is calculated as a function of Peclet number using equation (3.13). This test uses an initial aquifer concentration of 0.0.

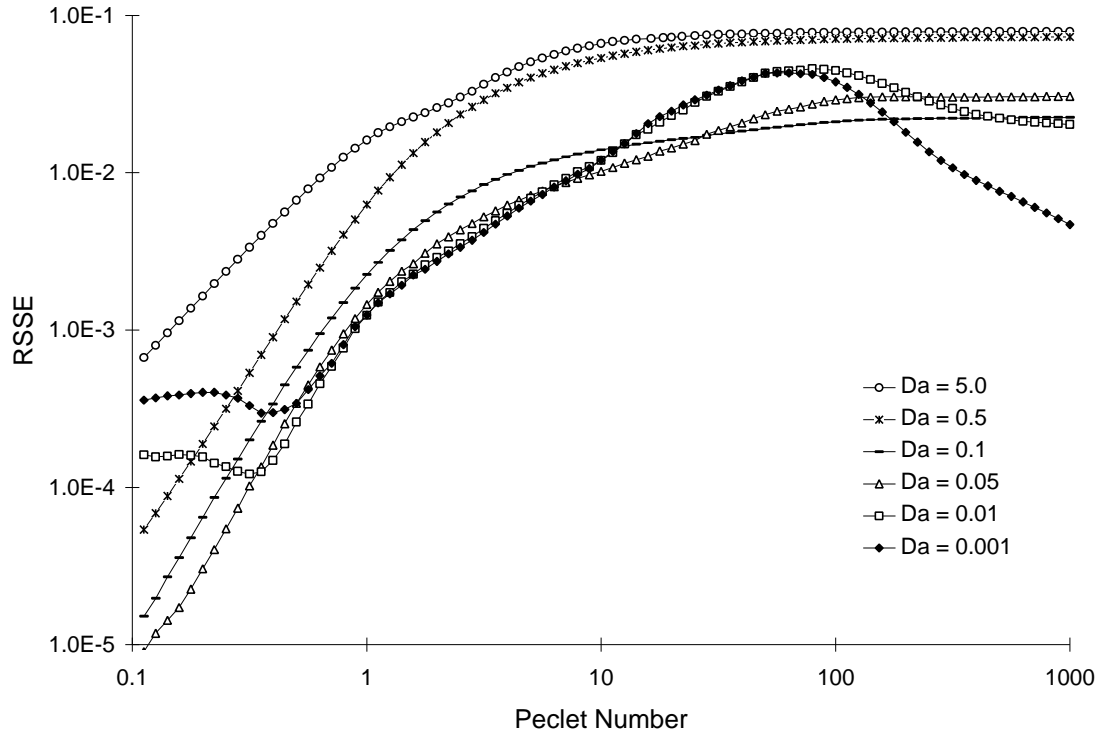


Figure 4.7.1 RSSE as a Function of Damkohler Number and Peclet Number (using the Maximum Allowable Courant Number) for One-Dimensional Reactive Solute Transport with a Continuous Source

Figure 4.7.2 illustrates the interaction of advective-dispersive and decay processes and how they effect model performance. Intuitively, it makes sense that increasing the Damkohler number will decrease model performance. This is the case in highly advective systems (high Peclet numbers). However, for highly dispersive systems (small Peclet numbers) it appears that there is an optimal Damkohler number. For conservative systems with a continuous source, the optimal Peclet number appears to be around 3.0 (see Figure 4.4.1). Decreasing pecelet numbers below 3.0 results in higher RSSE values. However, the addition of first order decay appears to counteract the processes responsible for increasing the RSSE value as Peclet number decreases.

Figure 4.7.2 through Figure 4.7.4 illustrate solute profiles at various combinations of dimensionless parameters.

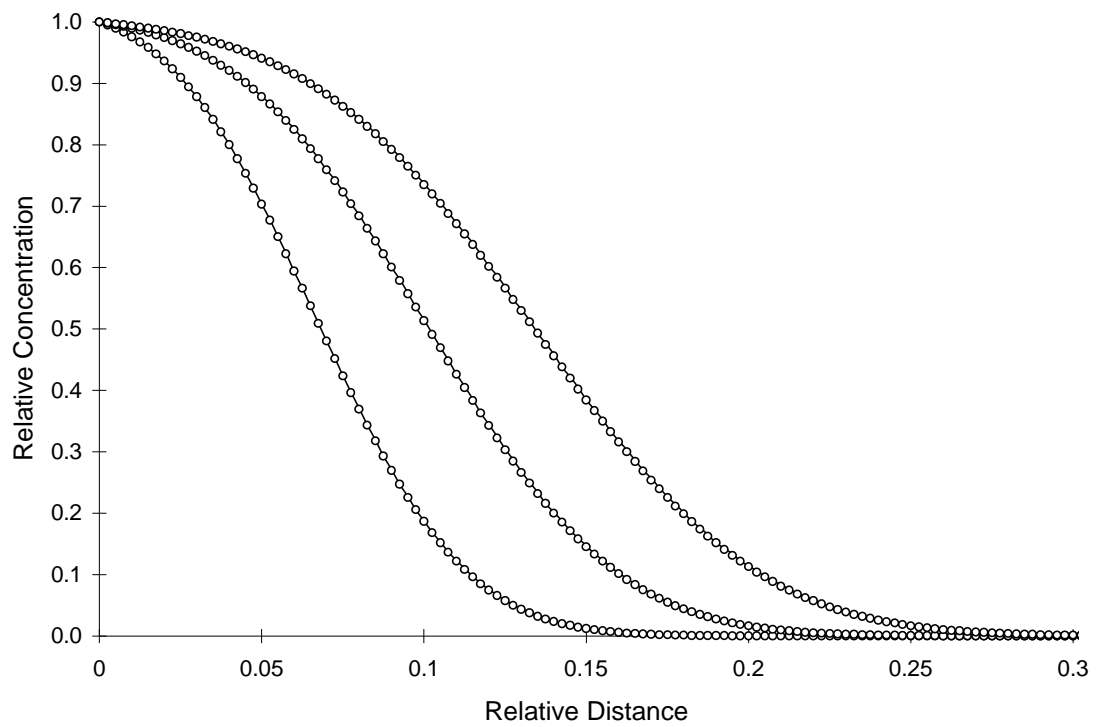


Figure 4.7.2 One-Dimensional Reactive Solute Transport with Continuous Source, $Pe = 0.2$, $Co = 0.099$, $Da = 0.001$, $RSSE = 4.02 \times 10^{-4}$

Figure 4.7.2 illustrates a highly dispersive system with a low decay rate.

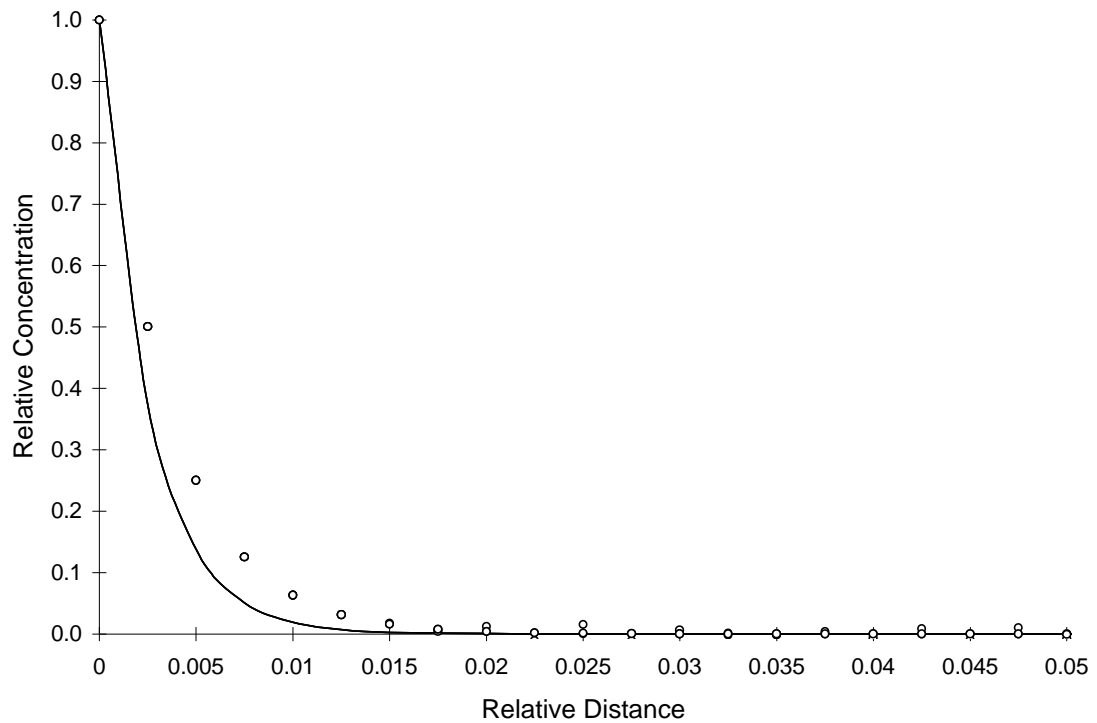


Figure 4.7.3 One-Dimensional Reactive Solute Transport with Continuous Source, $Pe = 100$, $Co = 0.9905$, $Da = 1.0$, $RSSE = 1.14 \times 10^{-1}$

Figure 4.7.3 illustrates a highly advective system with a moderately high decay rate. It appears that numerical solution leads the analytical solution. However the scale representing the relative distance in this simulation is small compared to Figure 4.7.2.

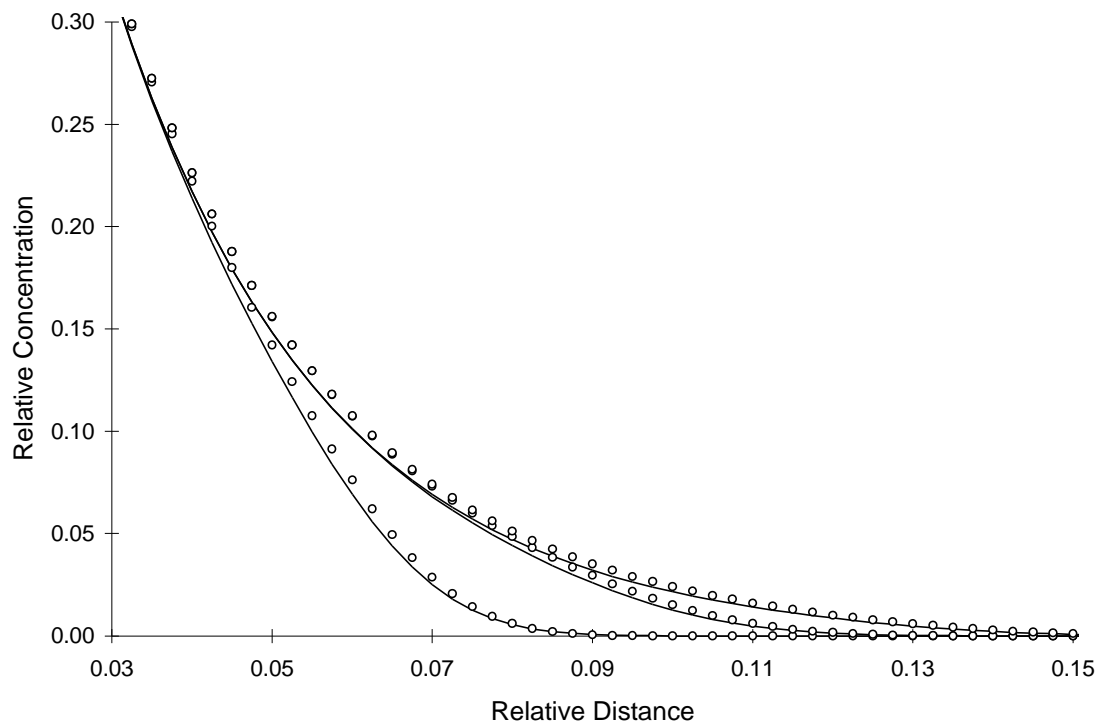


Figure 4.7.4 One-Dimensional Reactive Solute Transport with Continuous Source, $Pe = 2$, $Co = 0.618$, $Da = 0.1$, $RSSE = 5.7 \times 10^{-3}$

Figure 4.7.4 illustrates a moderately dispersive system with a moderate decay rate. It appears the numerical solution leads the analytical solution as in Figure 4.7.3.

4.8 Kinetic Reactions

This section evaluates model performance in simulating kinetic reactions. The tests do not include advection and dispersion. The aquifer systems in this section are similar to what one would expect under completely mixed conditions.

This section presents two figures for each type of kinetic reaction. The first figure illustrates model solution as a function of time compared to the true solution. The second figure plots RSSE (for one node) as a function of calculation time step. The calculation timestep is analogous to the timestep used to compute advection and dispersion fluxes. Some of the kinetic systems evaluated in this section are highly non-linear and require numerical methods to solve. The “true” solution used in these tests is calculated using the Mathematica™ software package (Wolfram Research Inc., 1988). The initial conditions in both figures are the same.

The following tests represent a small subset of the possible combinations of input parameters. It is not possible to anticipate all combinations and systems possible. The examples in this section include first order decay and competitive Monod reactions. Appendix F contains additional examples.

The equation representing first order decay is:

$$\frac{dC}{dt} = -kC \quad (4.9)$$

Where: dC/dt = time rate of change of concentration (M/L³·T)
 C = concentration of solute species (M/L³)
 k = decay coefficient (T⁻¹)

Figure 4.8.1 illustrates the model solution compared to the true solution using a calculation timestep of 2.0 and varying decay coefficients. Symbols and lines represent numerical and true values, respectively.

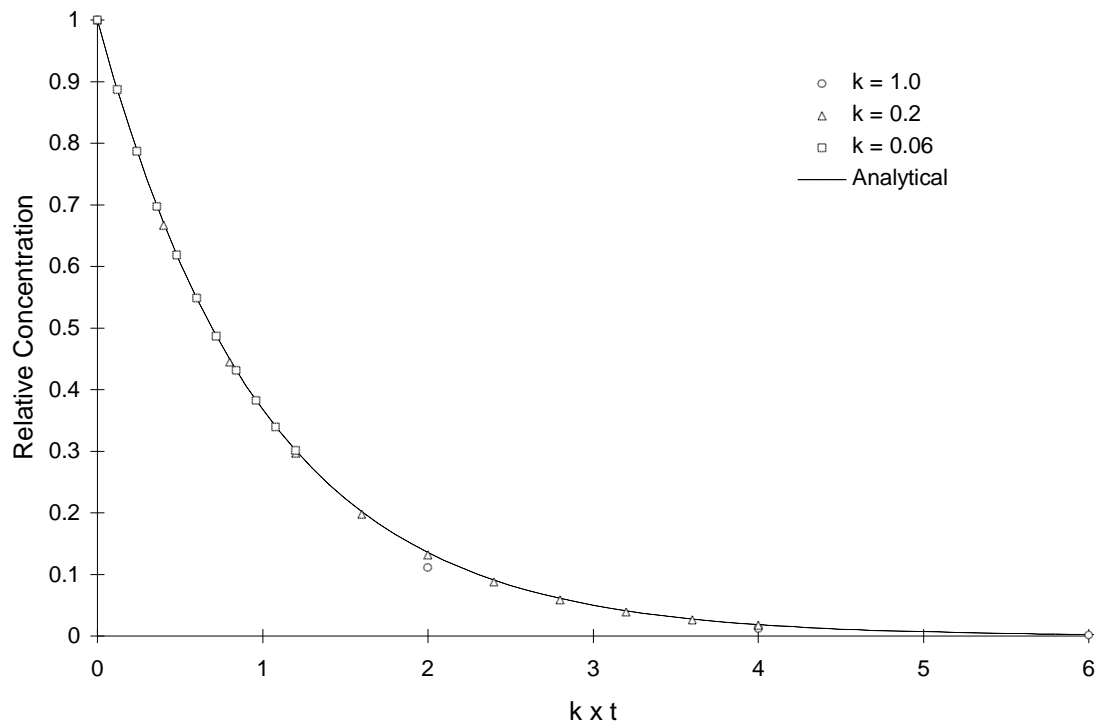


Figure 4.8.1 First Order Decay with Varying k .

Figure 4.8.2 illustrates the numerical solution errors at the time step of 20.0 for various decay coefficients.

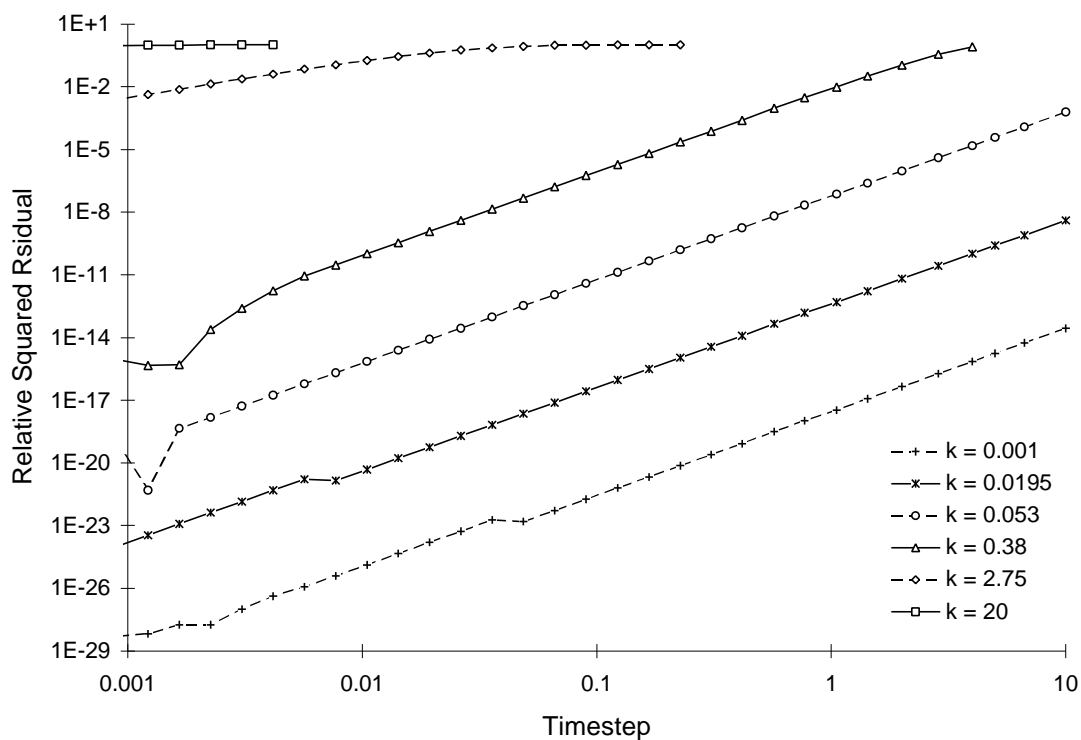


Figure 4.8.2 RSSE as a Function of First Order Decay Coefficient and Calculation Timestep

Figure 4.8.2 shows that increasing the rate coefficient and timestep increases the simulation RSSE value.

A simplified version of the competitive inhibition equation is:



$$\text{rate} = kX \frac{C_a}{K_{sa} + C_a} \cdot \frac{C_d}{K_{sd} + C_d + K_i C_i} \quad (4.11)$$

- Where:
- C_a = concentration of electron acceptor (M/L³)
 - C_d = concentration of electron donor (M/L³)
 - C_i = concentration of inhibitor (M/L³)
 - X = biomass concentration (M/L³)
 - k = maximum rate constant (L⁶/M³·T)
 - K_{sa} = half saturation constant for electron acceptor (M/L³)
 - K_{sd} = half saturation constant for electron donor (M/L³)
 - Y_a = stoichiometry coefficient for electron acceptor
 - Y_d = stoichiometry coefficient for electron donor
 - Y_x = stoichiometry coefficient for biomass
 - Y_i = stoichiometry coefficient inhibitor

Figure 4.8.3 compares the model and true solutions using a global calculation timestep of 2.0. For this test $k = 0.2$, $K_{sa} = 5.0$, $K_{sd} = 10.0$, $Y_x = 0.5$, $Y_A = 1.0$, $Y_D = 2.5$ and $Y_i = 0.2$. Circles and lines denote numerical and true values, respectively.

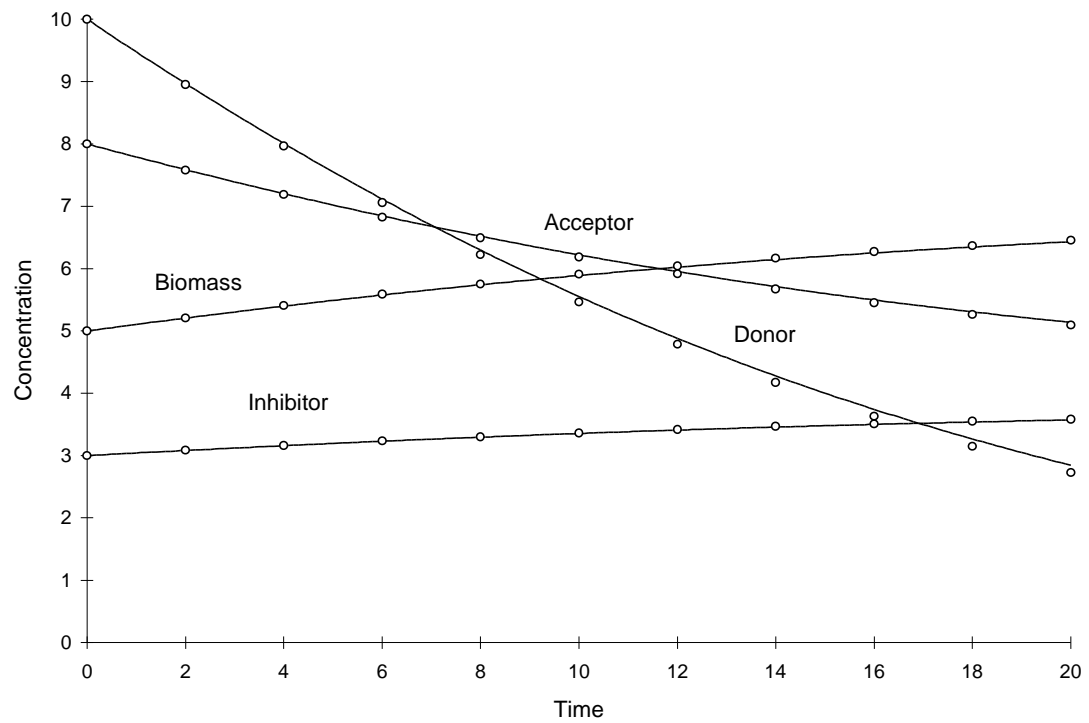


Figure 4.8.3 Competitive Monod Decay

$$k = 0.2, K_{sa} = 5.0, K_{sd} = 10.0, Y_x = 0.5, Y_A = 1.0, Y_D = 2.5, y_i = 0.2.$$

Figure 4.8.4 illustrates the Relative Squared Residual as a function of calculation time step:

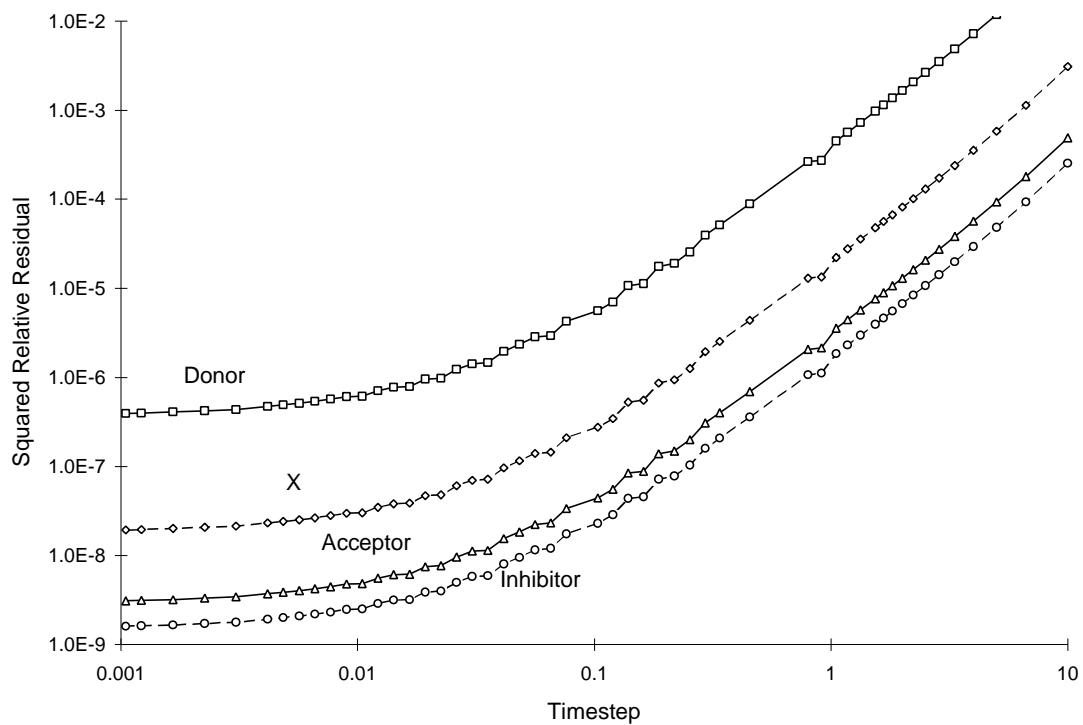


Figure 4.8.4 Squared Relative Residual as a Function of Global Timestep for Competitive Monod Decay.

See Appendix F for analysis of other kinetic reactions.

4.9 Stratified Porous Media

In 1985, Sudicky, Gillham, and Frind conducted multiple tracer tests with a column containing stratified porous media. The purpose of these experiments was to “examine the diffusion of a non-reactive tracer in layered media under controlled laboratory conditions.” They compared three theoretical equations using different assumptions to laboratory results. The theoretical model termed the “Thick-Layer solution” best fit the experimental results.

This section evaluates model performance in simulating an aquifer of moderate complexity. It uses the model to simulate the column used by Sudicky et al. The model is parameterized with the same material properties and boundary conditions which existed in the column. The results compare favorably with the “Thick-Layer” analytical solution.

The following figure illustrates the basic configuration of the column used by Sudicky et al.

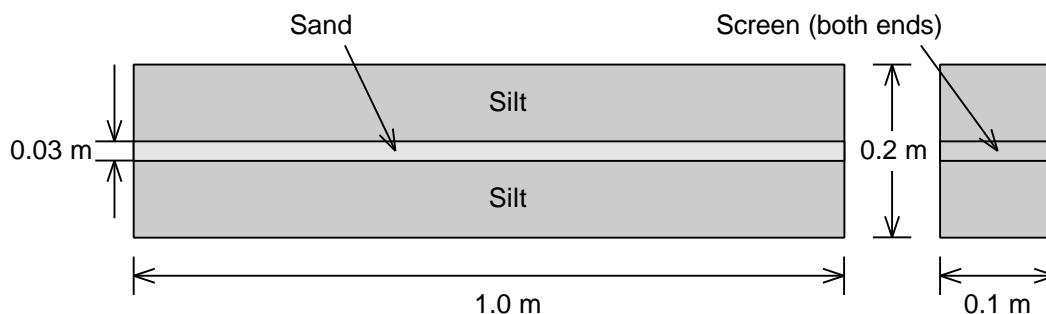


Figure 4.9.1 Laboratory Column.

The dimensions of the column were 1.0 x 0.2 x 0.1 meters. It was packed with two materials: silt and sand. The hydraulic conductivity of the sand was experimentally determined to be 2.3×10^{-4} m/s. The conductivity of the silt was assumed to be 6×10^{-8} m/s. The porosity of the silt was found to be 0.36 by independent experimentation. The porosity of the sand was assumed to be 0.33. The effective diffusion coefficient of 1.21×10^{-9} m²/s was determined by experimentally fitting the “Thick-Layer” model. The dispersivity values α_l and α_t were assumed to be negligible and were set at zero.

The numerical model was tested against the second experiment in the literature. A sodium chloride solution containing 100.0 mg/L Cl⁻ was placed in a constant head reservoir at the inlet end of the column. The pore water velocity used was 0.50 m/d in the sand layer. The initial concentration of Cl⁻ in the column was zero. After seven days of Cl⁻ input, the influent solution was changed to a chloride free solution.

The fundamental equation describing solute transport in the column for the “Thick-Layer” solution is represented in Equation (4.12) below. Equation (4.12) is derived using four assumptions. First, the thickness of the sand layer is much smaller than its length. Second, the hydraulic conductivity of the silt is low and the resulting transport within the silt is by molecular diffusion only. Third, transport in the sand layer is much faster than in the silt. Finally, if local longitudinal dispersion in the sand layer is neglected, the equation describing two-dimensional solute transport of tracer in the sand is:

$$\frac{\partial C}{\partial t} = v_s \frac{\partial C}{\partial x} - D_t \frac{\partial^2 C}{\partial x^2} \quad (4.12)$$

Subject to the boundary conditions

$$C(x, y, 0) = 0 \quad (4.13)$$

$$C(0, y, t) = C_o \quad (4.14)$$

$$C(\infty, y, t) = 0 \quad (4.15)$$

$$\frac{\partial C}{\partial x}(x, 0, t) = 0 \quad (4.16)$$

$$nD_t \frac{\partial C}{\partial x}(x, b, t) = n' D^* \frac{\partial C'}{\partial x}(x, b, t) \quad (4.17)$$

Where: $D_t = a_t v_s + D^*$
 v_s = velocity in the sand layer (L/T)
 a_t = transverse dispersivity coefficient (L)
 D^* = effective diffusion coefficient (L²/T)
 n = porosity in the sand layer
 n' = porosity in the silt layer
 C = concentration in the sand layer
 C' = concentration in the silt layer
 $2b$ = width of the sand layer

In addition, the direction of the solute flux in the sand layer was assumed to be perpendicular to the sand layer axis. The solution to the above system of equations can be found in Sudicky et al. (1985).

The experimental column system described above was entered into the numerical model. The grid spacing in the X and Y directions are 0.0125 m and 0.005 m respectively. The analytical solution assumes $D_l = 0$. However, this is impossible to

represent in the implementation of the numerical model. In the numerical model $D_l = D^*$. Figure 4.9.2 illustrates the results of the test:

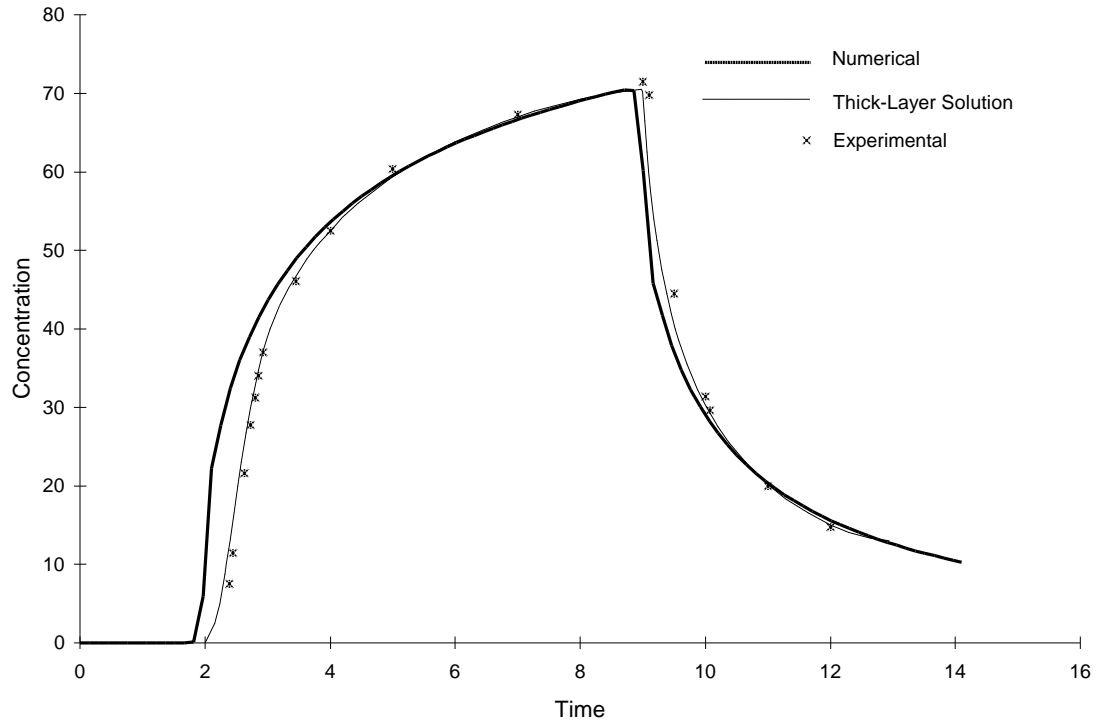


Figure 4.9.2 Concentration at outflow boundary for Stratified System.

It can be seen in Figure 4.9.2, the numerical and analytical values agree quite well, except for the solute front arrival times. The numerical model profile arrives before the analytical solution. As mentioned before, the analytical solution assumes $D_l = 0$. Therefore, it is impossible for the profile to arrive prior to 2 days. It was impossible to set $D_l = 0$ in the model because $D^* = 1.21 \times 10^{-9} \text{ m}^2/\text{s}$. The solute profile undergoes lateral dispersion and arrives sooner than the analytical solution predicts. This should not be interpreted as a problem with the numerical model.

4.10 One-Dimensional Biostimulation Experiment

This section reproduces a modeling effort conducted by Semprini and McCarty (1991) demonstrating biostimulation of indigenous methanotrophic microbes in a saturated aquifer. The purpose of the field and modeling study was to demonstrate in-situ microbial growth due to injection of nutrients. Model simulations included advection and dispersion of two solutes: methane (the electron donor) and oxygen (electron acceptor). The model uses double Monod kinetics to represent biomass growth and nutrient uptake. A single Monod relationship using oxygen as the limiting substrate represents biomass decay.

Figure 4.10.1 illustrates the field experiment design.

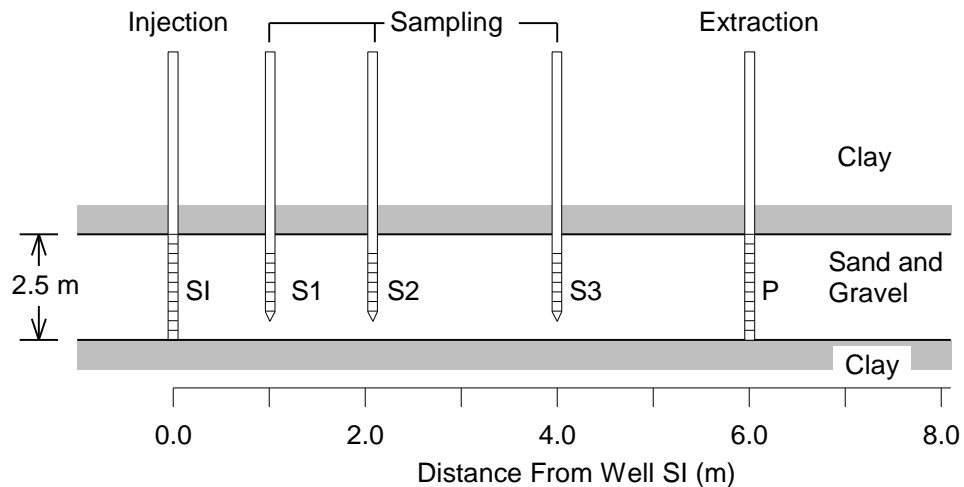


Figure 4.10.1 Schematic representation of the test zone used in biostimulation experiments.

The aquifer was located at a depth of 6.0 m and consisted of fine to course-grained sand. The upper confining layer consisted of clayey sand while the underlying layer consisted of greenish-gray silty clay (Roberts et al., 1990). The experimental well field was designed to inject nutrients into the aquifer at well SI and extract all the injected fluid at well P. Monitoring wells S1, S2 and S3 were located 1.0, 2.2 and 4.0 m from the well SI.

The most difficult part of modeling this experiment is correctly representing boundary conditions. For the purpose of limiting well head clogging, the field study used alternating pulsing of electron donor and acceptor at the injection well. This requires the use of alternating step functions to represent injection concentrations in the model.

Table 4.10.1 presents the input parameters used in this study. The input parameters are identical to those used in the literature except the duration of the first pulsing scheme is shorter by 0.3 of a day.

Table 4.10.1 One-Dimensional Biostimulation Parameters

Parameter Description	Notation	Value
Aquifer Length (m)		24
Number of Nodes		25
Grid Spacing (m)	Δx	0.1
Pore Water Velocity (m/d)	v	2.9
Oxygen Dispersion (m^2/d)	D_{SA}	0.25
Methane Dispersion (m^2/d)	D_{SD}	0.25
Max. Substrate Cons. Rate ($g/g \cdot d$)	k	1.2
Methane Half Saturation (mg/l)	K_{SD}	2.0
Oxygen Half Saturation (mg/l)	K_{SA}	1.0
Yield Coefficient (mg/mg)	Y	0.5
Cell Decay Coefficient (d^{-1})	b	0.15
Stoichiometric Ratio (mg/mg)	F	2.4
Biodegradable Cell Fraction	f_d	0.8
Cell Decay O_2 Demand (mg/mg)	d_c	1.42
Initial Biomass Conc. (mg/l)	X_i	0.18
Oxygen Inject. Conc. (mg/l)	C_{Ao}	26.3
Methane Inject. Conc. (mg/l)	C_{Do}	16.5
O_2 Pulse Interval (d) for (0-18.8d)	t_a	0.02
O_2 Pulse Interval (d) for (18.8-25d)	t_a	0.34
CH_4 Pulse Interval (d) for (0-18.8d)	t_d	0.01
CH_4 Pulse Interval (d) for (18.8-25d)	t_d	0.17

The following figures illustrate the results from this numerical model compared to modeled and field values from Semprini et al. (1991).

Figure 4.10.2 illustrates breakthrough curves for oxygen and methane 2.2 m downstream from the injection point for the first 400 hours of the experiment.

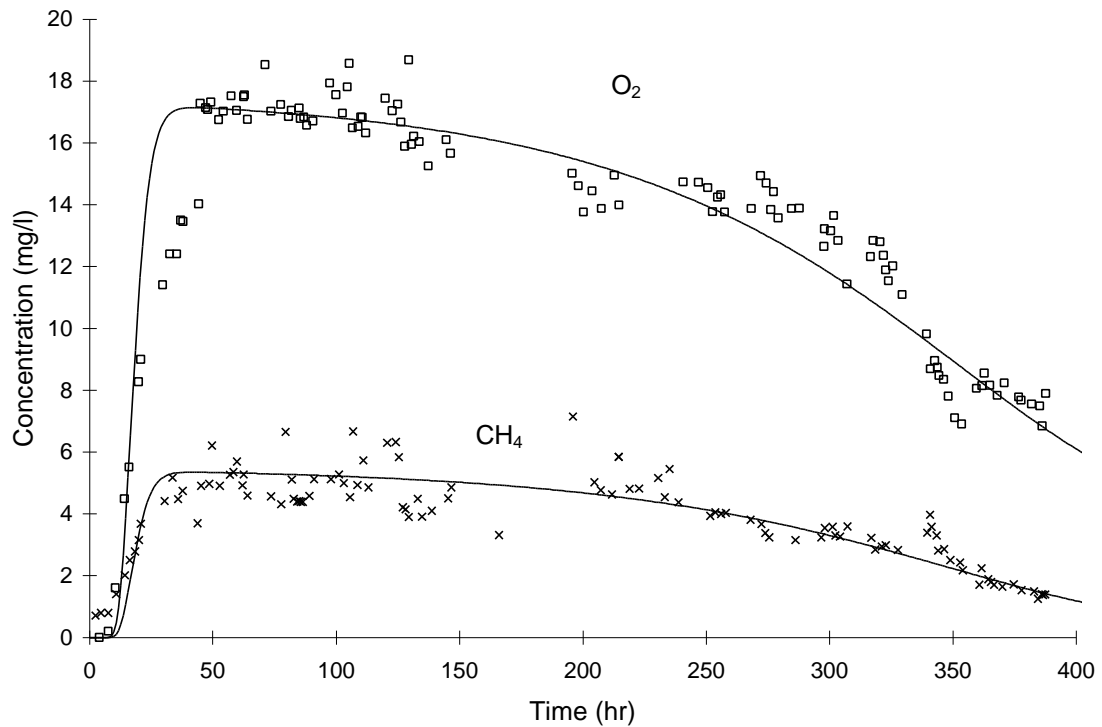


Figure 4.10.2 Experimental (symbols) and modeled (lines, this model) breakthrough curves of methane and oxygen at observation well S2, 2.2 m from injection well SI, (Figure 4 in literature).

Figure 4.10.2 shows that model simulations predict smooth concentration curves while the actual data more prominently show the effects of the nutrient pulsing scheme. Also, Figure 4.10.2 shows that nutrient consumption by biomass growth and decay becomes significant as the experiment proceeds in time. This is due to excessive biomass growth illustrated in Figure 4.10.3.

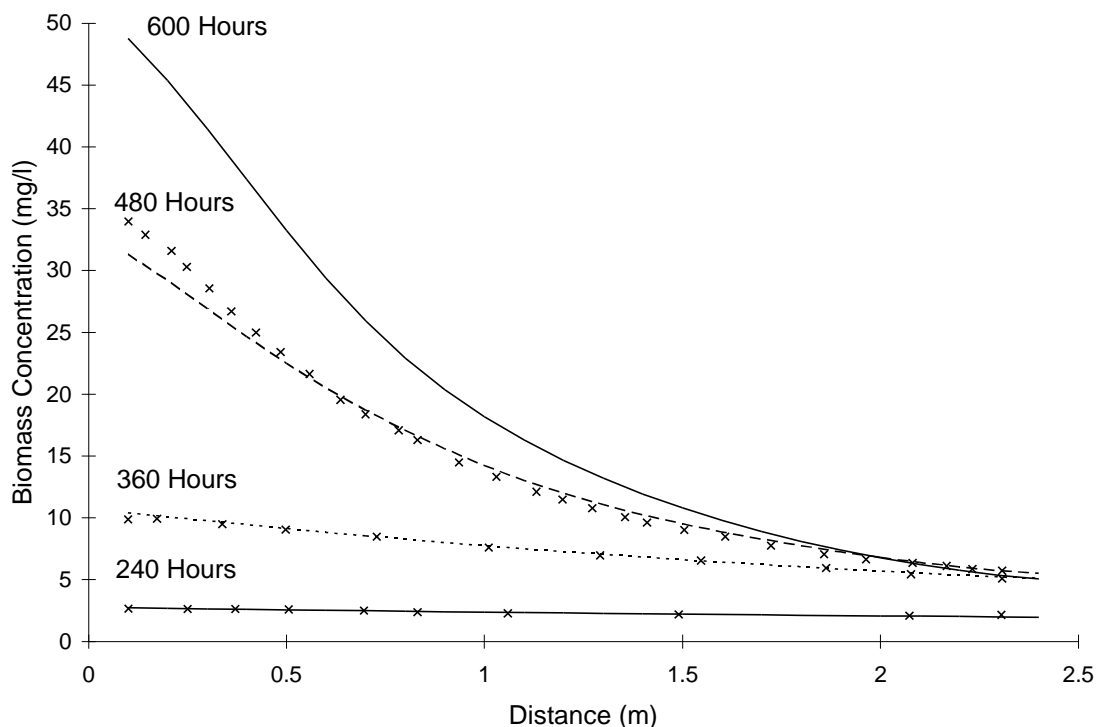


Figure 4.10.3 Modeled biomass profiles computed by Semprini and McCarty (symbols) and this model (lines), (Figure 5 in literature).

Figure 4.10.3 illustrates theoretical biomass concentration profiles for various snapshots in time. The symbols represent data presented by Semprini et al., lines represent values computed by this model. No experimental values were available, obtaining them would have disturbed the subsurface.

Figure 4.10.3 shows that theoretical biomass concentrations continuously grew throughout the entire length of the simulation, especially close to the injection well. One of the points of the alternating pulsing scheme was to eliminate this problem. The results suggest that alternating nutrient pulsing, as implemented in this experiment, was not successful in preventing excessive biomass growth close to the injection well.

Figure 4.10.4 illustrates breakthrough curves for oxygen and methane 2.2 m downstream from the injection point for the last 200 hours of the experiment. Symbols and lines represent experimental and numerical values, respectively.

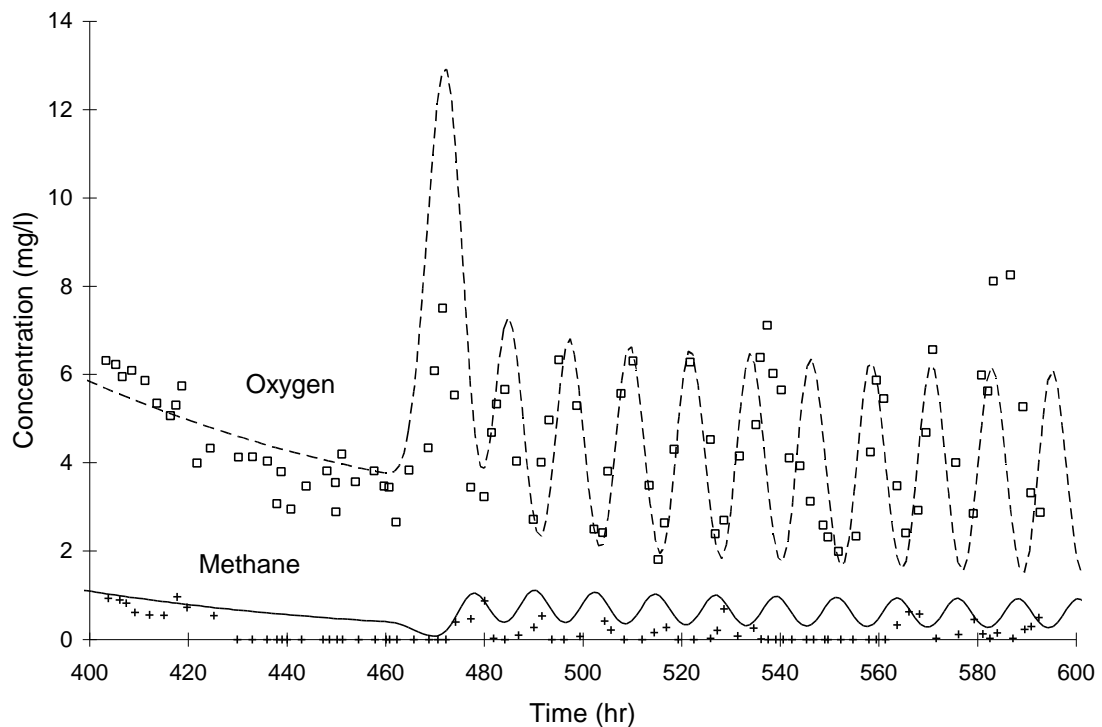


Figure 4.10.4 Experimental (symbols) and modeled (lines, this model) breakthrough curves of methane and oxygen at observation at well S2 under alternative pulsing strategy (Figure 7 in literature).

Figure 4.10.4 shows that model simulation and experimental results agree well, but it appears that the model overpredicts methane concentrations. There may be another process in the aquifer acting as a methane sink that the model does not represent.

Figure 4.10.5 illustrates theoretical biomass concentrations at a point 2.2 m downstream from the injection wells. Symbols and lines represent values reported by Semprini et al. and this study, respectively.

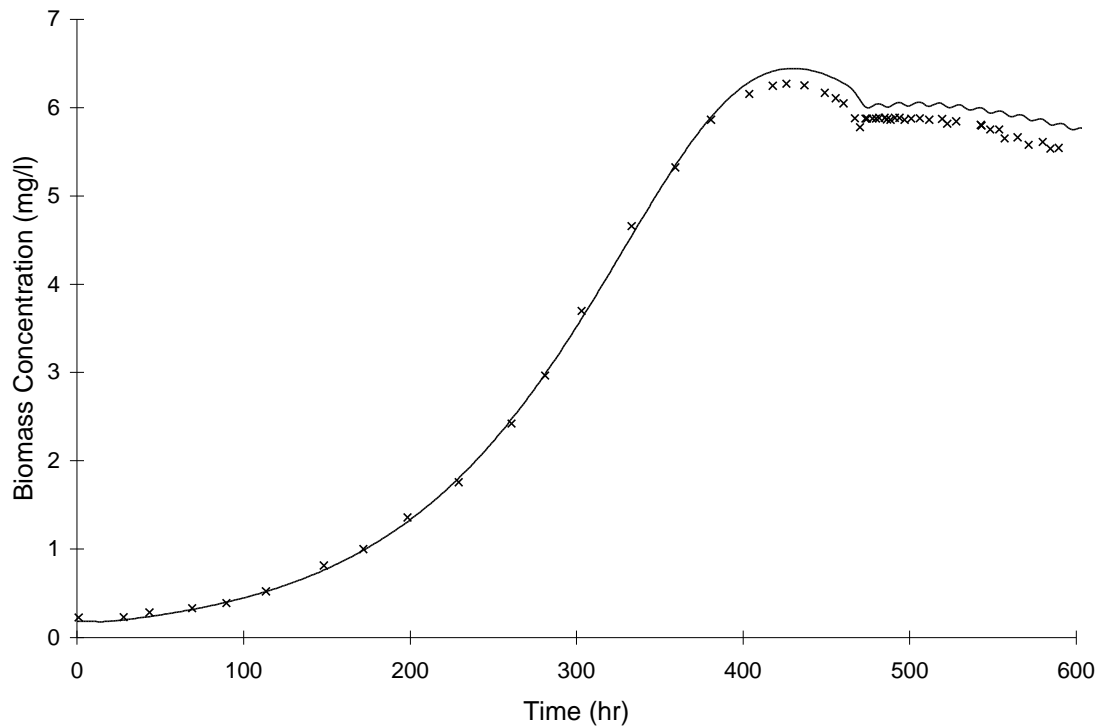


Figure 4.10.5 Modeled biomass concentrations computed by Semprini and McCarty (symbols) and this model (lines) at well S2 (Figure 8 in literature).

There appears to be a small difference between the values reported by Semprini and McCarty and those calculated by this model. One of the potential reasons could be error caused by digitizing of the data from the literature. The trends still appear to be the same.

This section has shown that the model can simulate a real-world in-situ bioremediation scenario. The above figures show that the model appears capable of reproducing the modeling effort conducted by Semprini and McCarty. The modeled and experimental values in figures Figure 4.10.2 and Figure 4.10.4 matched. The predicted biomass concentrations from this model and the literature agreed as well.

5. Example Problem

(Editors Note -- the example problem presented in this chapter is a contrived system that cannot exist in reality. The input parameters, when considered individually, are reasonable; but when combined together, yield an impossible system: namely the dissolved TCE concentration is too high for bioremediation using the chosen kinetic biodegradation parameters, and the dispersivity coefficient is too high for the aquifer size and groundwater velocity. However, this chapter still provides a good example of how to use the model. Please excuse the neglect in parameter selection.)

5.1 Introduction

This chapter illustrates how to present physical systems in mathematical form for the numerical model. This process divides into three major steps: aquifer discretization and flow field boundary conditions; selection of mobile and immobile species; and identification of reaction processes.

This chapter will analyze one-dimensional flow and transport in a saturated confined aquifer contaminated with a TCE spill. Aquifer reactions will include TCE dissolution, sorption, and biodegradation by methanotrophs. The purpose of analyzing the hypothetical aquifer is to illustrate model capabilities. This chapter will not conduct a comprehensive analysis of the problem.

5.2 Problem Description

Figure 5.2.1 illustrates the contaminated aquifer.

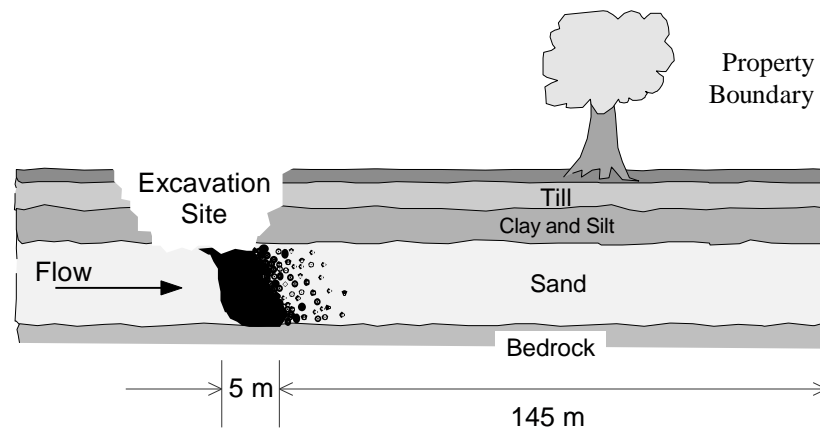


Figure 5.2.1 TCE Spill Site.

A 5 meter long zone in the aquifer is contaminated with a residual TCE saturation (Θ_r) of 0.0625. The spill occurred 145 m from the property boundary. The objective of remediation is to maintain a TCE drinking water standard of 0.005 mg/L at the property boundary.

Table 5.2.1 presents the aquifer properties for this example. They were selected from values reported in the literature for sandy aquifers. Table 5.2.2 presents TCE and biological parameters reported in Semprini et al. (1991b, 1992), Alvarez-Cohen et al., (1993), and Sleep and Sykes (1993).

Table 5.2.1 Aquifer Material Properties

Property	Symbol	Value
Porosity	n	0.25
Solids Density (g/cm^3)	r_s	2.65
Material Bulk Density (g/cm^3)	r_b	1.9875
Hydraulic Conductivity (m/d)	K	8.46
Hydraulic Gradient	dh/dl	2.98×10^{-2}
Linear Specific Discharge ($\text{m}^3/\text{m}^2 \cdot \text{d}$)	q	0.25
Linear Pore Water Velocity (m/d)	V	1.0
Longitudinal Dispersivity (m)	a_l	10
Methanotrophic Bacteria Concentration (mg/L)	X_o	0.1

Table 5.2.2 TCE Sorption and Biodegradation Coefficients

Property	Symbol	Value
Partitioning Coefficient (L/kg)	K_d	2.0
Sorption Rate Coefficient (d^{-1})	a_s	0.2
Maximum Transformation Rate (d^{-1})	k_2	0.01
Half-Saturation Coefficient (mg/L)	K_{S2}	1.0
Aqueous Solubility (mg/L)	C_{sol}	1100
Liquid Density (kg/m^3)	r_{TCE}	1467
Maximum Substrate Utilization Rate (d^{-1})	k	1.2
Methane Half-Saturation (mg/L)	K_{SD}	2.0
Oxygen Half-Saturation (mg/L)	K_{SA}	1.0
Biomass Yield Coefficient (mg biomass/mg CH_4)	Y	0.5
Cell Decay Coefficient (d^{-1})	b	0.15
Oxygen Ratio for Growth (mg O_2 /mg biomass)	F	2.4
Biodegradable Cell Fraction	f_d	0.8
Cell Decay Oxygen Demand (mg O_2 /mg biomass)	d_c	1.42
Intermediate Toxicity Coeff. (mg biomass/mg TCE)	a_{TOX}	20.83

This chapter analyzes three remedial alternatives: no-action, pump and treat, and pump and treat with bioremediation.

5.3 No-action

Figure 5.3.1 illustrates the aquifer representing the no-action scenario.

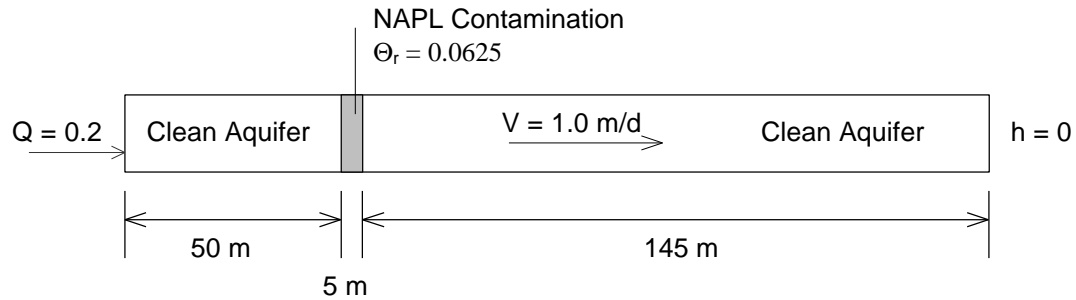


Figure 5.3.1 No Action Aquifer System Layout

The discretized aquifer uses a uniform grid spacing of 5.0 m. A grid spacing of 5.0 m will allow for rapid calculation of solute movement (large Δt) at the expense of grid mesh resolution. Since simulation length is on the order of years, not days, larger time steps are required to reduce computational requirements. The simulation will run for 7 years, printing results every month.

The inflow rate is in terms of pore space fraction per time. It derives from the specific discharge in the aquifer.

$$Q = \frac{q_x}{n\Delta x} = \frac{0.25 \frac{m^3 H_2O}{m^3 Aquifer \times day}}{0.25 \frac{m^3 H_2O}{m^3 Aquifer} \times 5.0 m Aquifer} = 0.2 d^{-1} \quad (5.1)$$

This simulation adds only three parameters; aqueous TCE, sorbed TCE, and NAPL TCE. Table 5.3.1 shows the properties of the parameters.

Table 5.3.1 No-Action Simulation Parameters

Parameter	Type	Initial Value	Comment
TCE (NAPL)	Immobile	46.13 g/kg Dry Wt.	Initial value only in places where TCE was spilled, otherwise value is zero.
TCE (aq)	Mobile	0 mg/L	Aqueous TCE species
TCE (s)	Immobile	0 mg/kg Dry Wt.	Sorbed TCE species

The problem description presented TCE contamination in terms of residual saturation. The following equation calculates the initial concentration presented in Table 5.3.1.

$$TCE_{NAPL} = \Theta_r \frac{\mathbf{r}_{TCE}}{\mathbf{r}_b} = 0.0625 \frac{m^3 TCE}{m^3 H_2O} \times \frac{1467 \frac{kg TCE}{m^3 TCE}}{1987.5 \frac{kg DryWt.}{m^3 DryWt.}} \times \frac{1000g}{kg} = 46.13 \frac{g TCE}{kg DryWt.} \quad (5.2)$$

The simulation neglects any effect of TCE residual saturation on the water saturation.

Two reaction processes occur in the no-action case: TCE dissolution and TCE sorption. This simulation explores both instantaneous and kinetic dissolution and equilibrium linear sorption.

The model uses the following equations to represent TCE dissolution rate:

$$\frac{dCE_{(aq)}}{dt} = a_d (TCE_{sol} - TCE_{(aq)}) \quad (5.3)$$

Where: $TCE_{(aq)}$ = aqueous TCE concentration (mg/L)

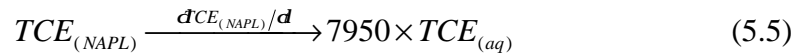
a_d = dissolution rate constant (∞d^{-1})

TCE_{sol} = TCE solubility (1100 mg/L)

For equilibrium dissolution case a_d is infinity, the simulations will use an instantaneous rate equation. The second part of representing TCE dissolution is the mass balance between the two phases. The conversion from TCE NAPL to aqueous phase TCE is.

$$\begin{aligned} TCE_{(aq)} &= \frac{\mathbf{r}_b TCE_{NAPL}}{n} \\ &= TCE_{NAPL} \frac{g TCE}{kg DryWt.} \times 1987.5 \frac{kg DryWt.}{m^3 Aquifer} \times \frac{1}{0.25} \frac{m^3 Aquifer}{m^3 H_2O} \times \frac{1m^3}{1000L} \\ &= \left(7950 \times TCE_{NAPL} \frac{g TCE}{kg DryWt.} \right) \frac{mg TCE}{L H_2O} \end{aligned} \quad (5.4)$$

The resulting stoichiometric equation is:



The equation representing TCE sorption is:

$$\frac{dTCE_{(s)}}{dt} = a_s (K_d TCE_{(aq)} - TCE_{(s)}) \quad (5.6)$$

Where: $TCE_{(s)}$ = sorbed phase TCE concentration (mg/kg Dry Wt.)

a_s = sorption rate coefficient (0.2 d^{-1} or $\infty \text{ d}^{-1}$)

K_d = linear partitioning coefficient (2.0 L/kg Dry Wt.)

$TCE_{(aq)}$ = aqueous phase TCE concentration (mg/L)

In the case where α_s is infinity, the model will use the following equilibrium relationship:

$$TCE_{(s)} = K_d TCE_{(aq)} \quad (5.7)$$

The aqueous and sorbed phase TCE values are in different units. The conversion from sorbed TCE to aqueous TCE is:

$$\begin{aligned} TCE_{(aq)} &= \frac{r_b TCE_{(s)}}{n} \\ &= TCE_{(s)} \frac{\text{mg TCE}}{\text{kg Dry Wt.}} \times 1987.5 \frac{\text{kg Dry Wt.}}{\text{m}^3 \text{ Aquifer}} \times \frac{1}{0.25} \frac{\text{m}^3 \text{ Aquifer}}{\text{m}^3 \text{ H}_2\text{O}} \times \frac{\text{m}^3}{1000 \text{ L}} \\ &= \left(7.95 \times TCE_{(s)} \frac{\text{mg TCE}}{\text{kg Dry Wt.}} \right) \frac{\text{mg TCE}}{\text{L H}_2\text{O}} \end{aligned} \quad (5.8)$$

The resulting stoichiometric equation is:

$$7.95 \times TCE_{(aq)} \xrightarrow{dTCE_{(s)}/dt} TCE_{(s)} \quad (5.9)$$

Figure 5.3.2 illustrates the boundary TCE concentration as a function of time using equilibrium and kinetic sorption isotherms.

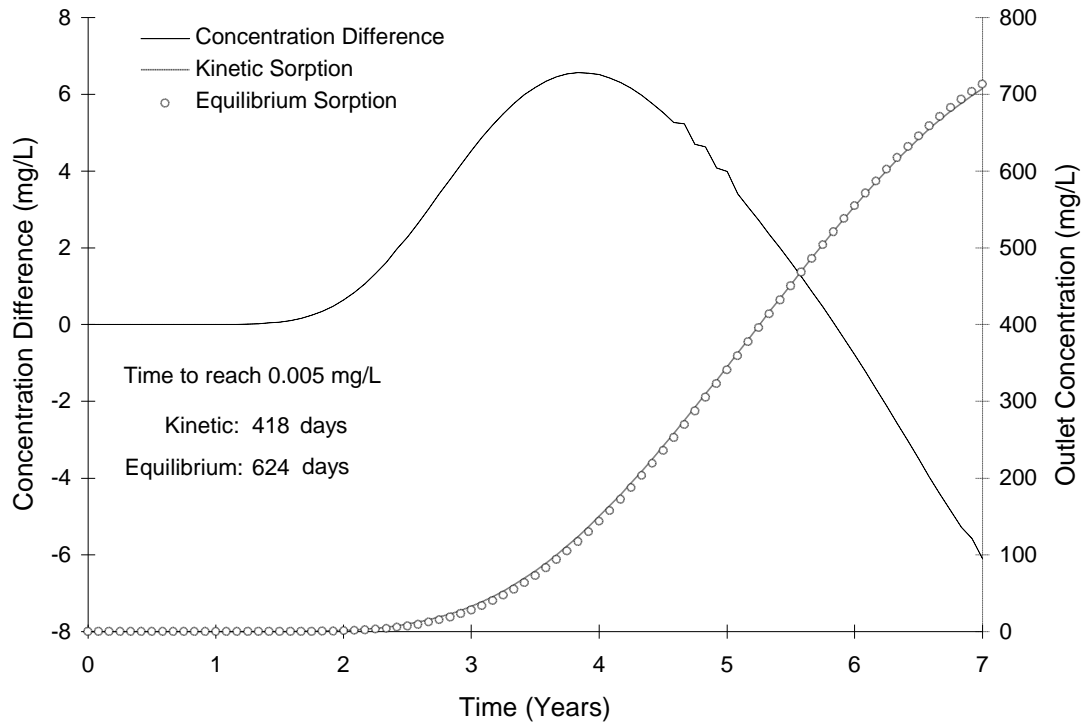


Figure 5.3.2 No Action TCE Border Concentration using Kinetic and Equilibrium Sorption

Figure 5.3.2 shows there is little difference between solutions. Subsequent simulations will use equilibrium sorption because it is computationally faster.

Figure 5.3.3 illustrates boundary concentration sensitivity to different dissolution rates using equilibrium sorption.

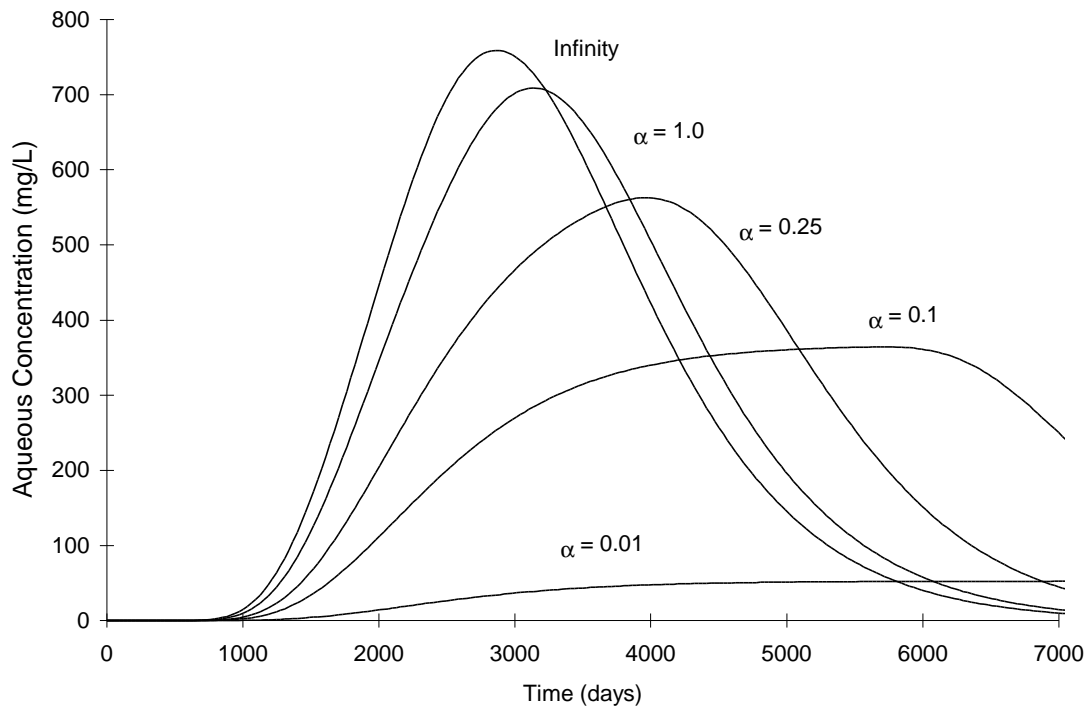


Figure 5.3.3 No Action TCE Border Concentration with different dissolution rates

Figure 5.3.3 shows that the dissolution rate makes a large difference in the results. The problem description did not give a dissolution rate constant. An instantaneous dissolution process will represent dissolution because it provides for the largest peak concentration at the boundary.

Figure 5.3.4 illustrates simulation sensitivity to grid spacing. It compares boundary concentrations using the discretized aquifer described above ($\Delta x = 5.0$ m) and a similar aquifer using a grid spacing of 1.0 m.

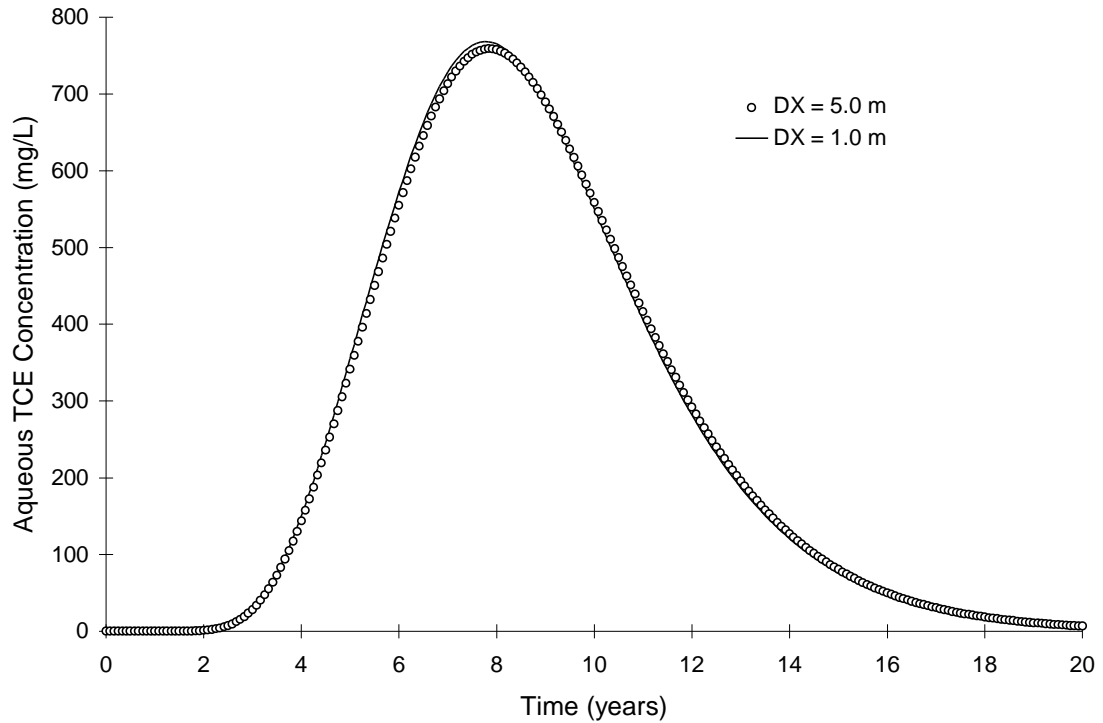


Figure 5.3.4 No Action TCE Border Concentration using different grid spacing

Figure 5.3.4 shows little difference in results. The 5 m aquifer mesh took 14 minutes real time to simulate 20 years while the 1.0 m mesh took 7 hours real time. This is due to a five-fold increase in the number of nodes, a five-fold decrease in the Peclet number causing a ten-fold decrease in the maximum allowable Courant number.

Figure 5.3.5 illustrates the distribution of mass in the first 20 years. “Total mass in System” refers to the sum of NAPL, sorbed TCE, and aqueous TCE inside the aquifer boundary.

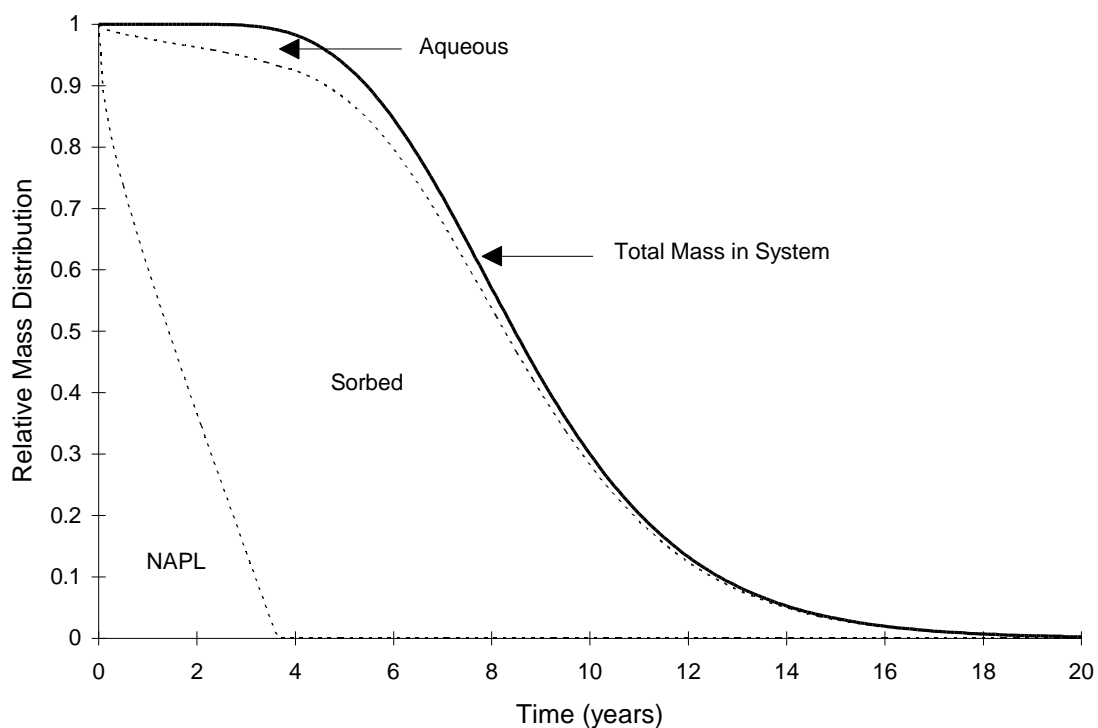


Figure 5.3.5 No Action Distribution of Mass

It appears that it takes more than three years for the TCE NAPL to completely dissolve.

5.4 Pump and Treat

Figure 5.4.1 illustrates the aquifer representing the pump and treat scenario.

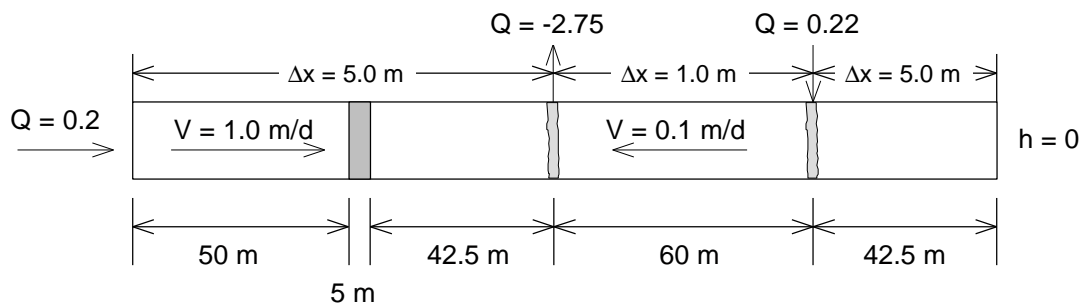


Figure 5.4.1 Pump and Treat Aquifer System Layout

This scenario creates a region in the aquifer consisting of flow in the opposite direction of the natural flow. The induced flow is one-tenth the magnitude of the natural flow. In addition, in the region of backwards flow, the grid spacing changes to 1.0 in order to maintain similar Courant and Peclet numbers throughout the aquifer.

One injection trench and one extraction trench create the region of backwards flow. Node 20 contains the extraction trench. It is 102.5 m from the aquifer boundary. Equation (5.10) illustrates the calculation for the extraction flow rate:

$$\begin{aligned}
 Q &= \frac{(q_{natural} + q_{induced})}{\Delta x \cdot n} \\
 &= (0.25 + 0.025) \frac{m^3 H_2O}{m^2 Aquifer day} \times \frac{1}{4.0m Aquifer} \times \frac{m^3 Aquifer}{0.25m^3 H_2O} \\
 &= 2.75d^{-1}
 \end{aligned} \tag{5.10}$$

The width of the node is 4.0 m due to the change in mesh size between regions. Node 72 represents the injection trench. It is 42.5 m from the aquifer boundary. The calculation of injection flow rate is:

$$\begin{aligned}
 Q &= \frac{(q_{natural} + q_{induced})}{\Delta x \cdot n} \\
 &= (0.25 + 0.025) \frac{m^3 H_2O}{m^2 Aquifer day} \times \frac{1}{5.0m Aquifer} \times \frac{m^3 Aquifer}{0.25m^3 H_2O} \\
 &= 2.2d^{-1}
 \end{aligned} \tag{5.11}$$

In addition this case uses the concentration profiles that exist two months into the no-action simulation. This allows for a two month reaction period from the time of the spill.

Figure 5.4.2 compares aqueous TCE boundary concentration for the no-action and pump-and-treat scenario.

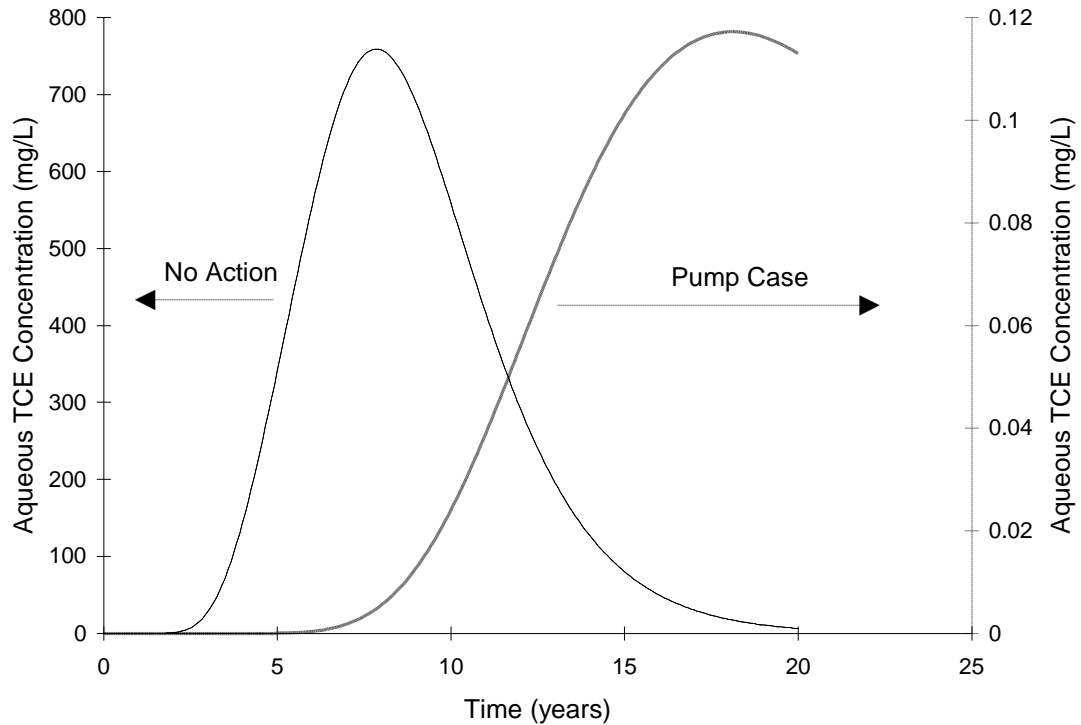


Figure 5.4.2 Pump and Treat vs. No-Action Aqueous TCE Boundary Concentration

Figure 5.4.2 shows that this implementation of pump-and-treat performs much better than the no-action scenario, but still does not meet the drinking water standard. The process of dispersion (in the direction towards the boundary) driven by concentration gradients is still great enough to overcome the advective transport (in the direction away from the boundary) induced by the injection and extraction wells. This results in a net movement of solute in a direction opposite of the fluid flow. This is not a problem with the numerical model. Using equation (2.1) with a large dispersion coefficient and low transport velocity will give net solute movement in a direction counter to the fluid flow direction.

Figure 5.4.3 illustrates the distribution of mass as a function of time.

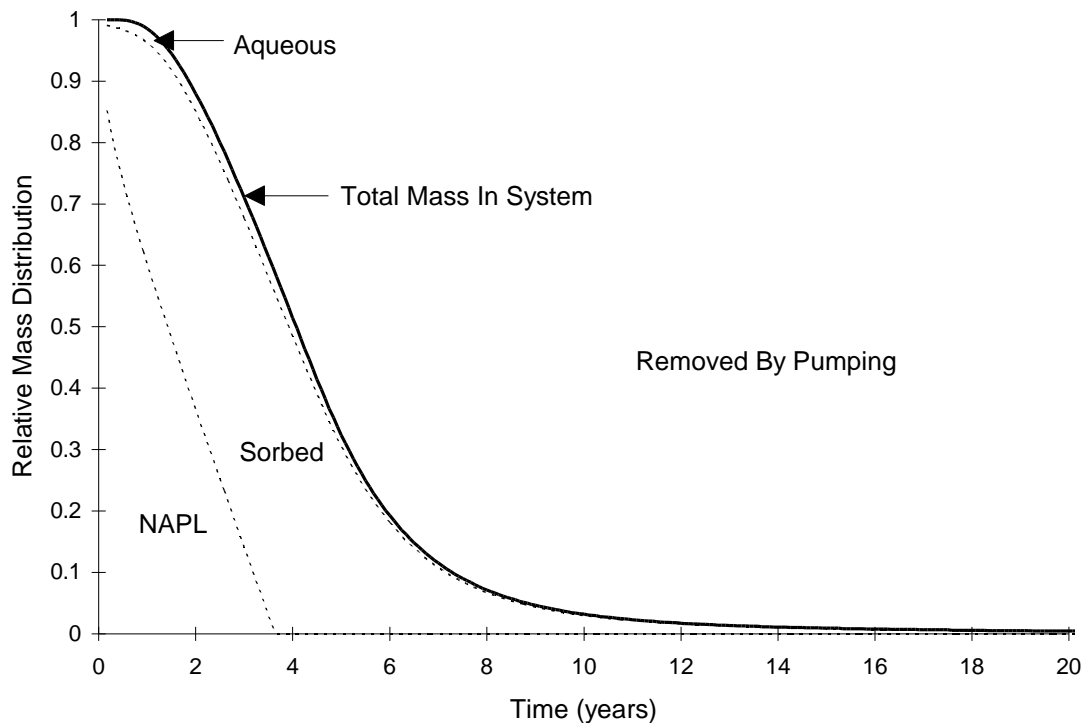


Figure 5.4.3 Pump and Treat Mass Distribution

The cumulative amount of mass exiting at the boundary at 20 years was 0.018% of the total initial mass in the system. Since this fraction was so small, it was not shown in Figure 5.4.3.

5.5 Pump and Treat with Biodegradation

An alternative to higher pumping rates may be addition of methane and oxygen into the aquifer to stimulate methanotrophic degradation of TCE. This simulation takes the previous aquifer and adds biostimulation.

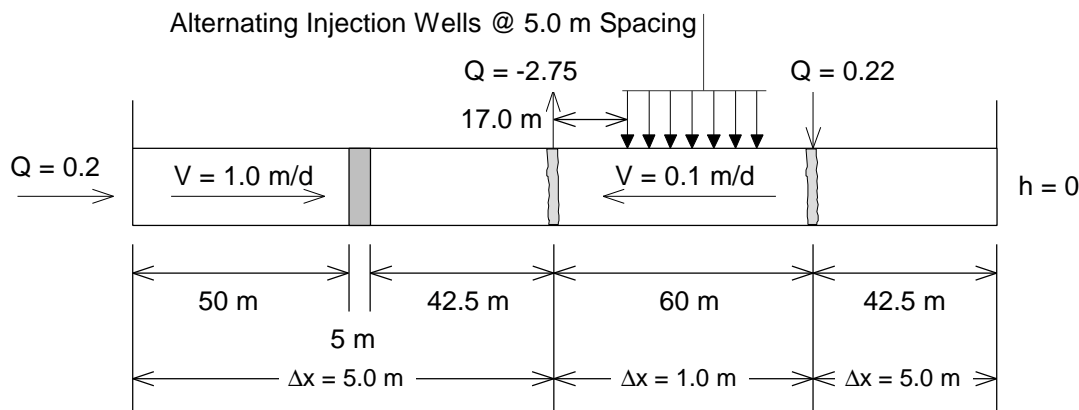


Figure 5.5.1 Pump and Treat with Biodegradation Aquifer System Layout

This scenario adds 4 methane and 3 oxygen injection trenches at a spacing of 5.0 m. It uses prescribed concentrations of oxygen and methane to represent the injection process. The simulation assumes water flux due to nutrient injection is negligible.

This scenario adds four new parameters: oxygen, methane, biomass, and a mass balance tracking parameter “TCE degradation”. Figure 5.5.1 presents the added components.

Table 5.5.1 Pump-and-Treat with Biodegradation parameters

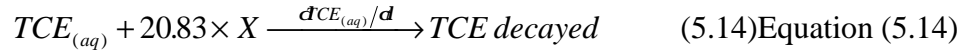
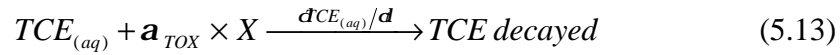
Parameter	Type	Initial Value	Comment
O ₂ (aq)	Mobile	0 mg/L	Parameter representing oxygen.
CH ₄ (aq)	Mobile	0 mg/L	Parameter representing methane.
X	Immobile	0.1 mg/L	Parameter representing biomass.
TCE degraded	Immobile	0 mg/L	Parameter to track degraded TCE for mass balance calculations.

Five additional reactions occur in this scenario; biomass growth, biomass decay, TCE decay, oxygen injection, and methane injection. Aqueous TCE decay is competitive with methane concentration. The equation representing TCE degradation is:

$$\frac{dCE_{(aq)}}{dt} = k_2 X \frac{TCE_{(aq)}}{K_{S,TCE} + TCE_{(aq)} + \frac{K_{S,TCE}}{K_{S,CH_4}} CH_{4(aq)}} \frac{O_{2(aq)}}{K_{S,O_2} + O_{2(aq)}} \quad (5.12)$$

Where: k_2 = maximum TCE degradation coefficient (0.01 mg TCE/mg biomass·day)
 X = biomass concentration (mg/L)
 $TCE_{(aq)}$ = aqueous TCE concentration (mg/L)
 $O_{2(aq)}$ = aqueous oxygen concentration (mg/L)
 $K_{S,TCE}$ = TCE saturation constant (1.0 mg/L)
 K_{S,CH_4} = methane saturation constant (2.0 mg/L)
 K_{S,O_2} = oxygen saturation constant (1.0 mg/L)

Units are consistent for this process. The stoichiometry for the above reaction is:



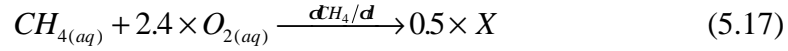
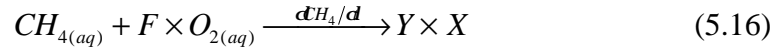
includes the process of intermediate toxicity. The coefficient (20.83 mg biomass/ mg TCE) is from Alvarez-Cohen et al., (1993).

Biomass growth is a competitive process with methane. The rate of methane consumption due to biomass growth is:

$$\frac{dCH_{4(aq)}}{dt} = kX \frac{CH_{4(aq)}}{K_{S,CH_4} + CH_{4(aq)} + \frac{K_{S,CH_4}}{K_{S,TCE}} TCE_{(aq)}} \frac{O_{2(aq)}}{K_{S,O_2} + O_{2(aq)}} \quad (5.15)$$

Where: k = maximum substrate utilization rate (1.2 mg CH_4 /mg biomass·day)
 X = biomass concentration (mg/L)
 $CH_{4(aq)}$ = methane concentration (mg/L)
 $O_{2(aq)}$ = oxygen concentration (mg/L)
 $K_{S,TCE}$ = TCE saturation constant (1.0 mg/L)
 K_{S,CH_4} = methane saturation constant (2.0 mg/L)
 K_{S,O_2} = oxygen saturation constant (1.0 mg/L)

Units are consistent for this reaction. The stoichiometry is:



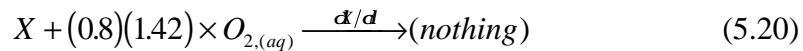
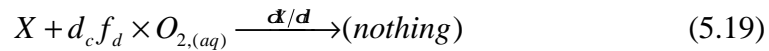
Where: F = stoichiometric ratio of oxygen to methane consumption for biomass growth (mg O_2 /mg CH_4)
 Y = biomass yield coefficient (mg biomass/mg CH_4)

Endogenous biomass decay is a single Monod relationship with oxygen and biomass concentrations.

$$\frac{\alpha}{d} = bX \frac{O_{2(aq)}}{K_{S,O_2} + O_{2(aq)}} \quad (5.18)$$

Where: X = biomass concentration (mg/L)
 b = maximum decay rate (0.15 mg biomass/mg biomass-day)
 $O_{2(aq)}$ = oxygen concentration (mg/L)
 K_{S,O_2} = oxygen saturation constant (1.0 mg/L)

Units are consistent for this reaction. The stoichiometry is:



The simulation uses a prescribed concentration of 10.0 mg/L to represent oxygen injection. It uses a variable methane injection concentration to avoid excessive or insufficient biomass growth.

$$CH_{4(aq)} = 2.933 + 1.5924 \times TCE_{(aq)} - 0.1133 \times X \quad (5.21)$$

Where: $CH_{4(aq)}$ = aqueous methane concentration (mg/L)
 $TCE_{(aq)}$ = aqueous TCE concentration (mg/L)
 X = biomass concentration (mg/L)

The coefficients in equation (5.21) represent a linear combination that results in $\alpha/d = 0$ when $X = 20$ mg/L. The simulation targets maximum biomass concentrations of 20 mg/L. Semprini (1991) modeled in-situ biostimulation with maximum biomass concentrations up to 50 mg/L.

Figure 5.5.2 illustrates the TCE concentration at the outlet boundary as a function of time:

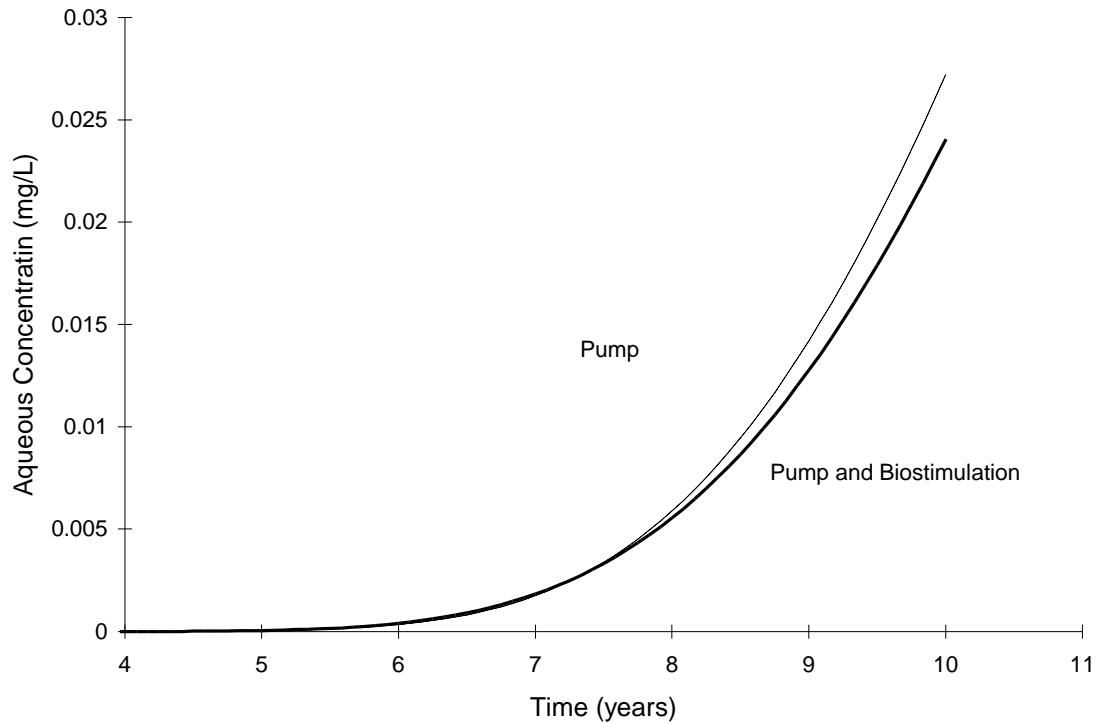


Figure 5.5.2 Pump and Treat boundary TCE concentration with and without Biodegradation

It appears that adding biostimulation to the pump and treat scenario had little success in maintaining the required TCE concentration at the aquifer boundary. This is also illustrated in Figure 5.5.3.

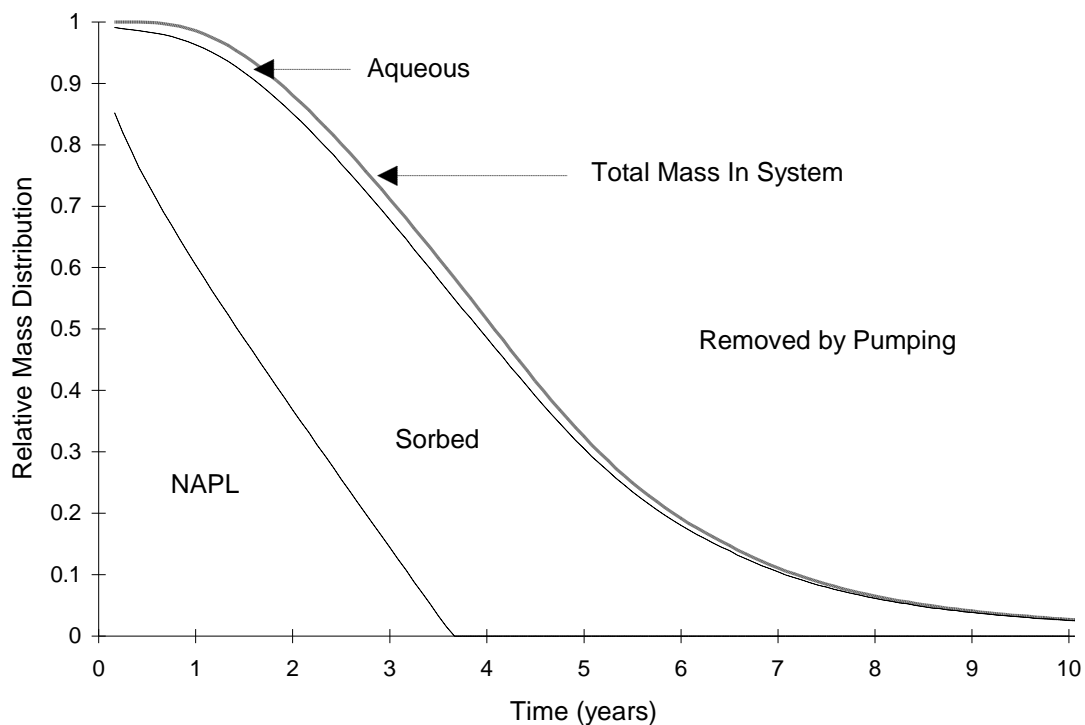


Figure 5.5.3 Pump and Treat with Biodegradation Mass Distribution

At ten years, only 0.0006% of the original TCE contamination exited the system at the boundary; biodegradation accounted for 0.013%. It appears that the zone of biostimulation is having little influence on the TCE concentration in the region of backwards flow. To further study this, consider the distribution of biomass in the aquifer at 7.8 years illustrated in Figure 5.5.4.

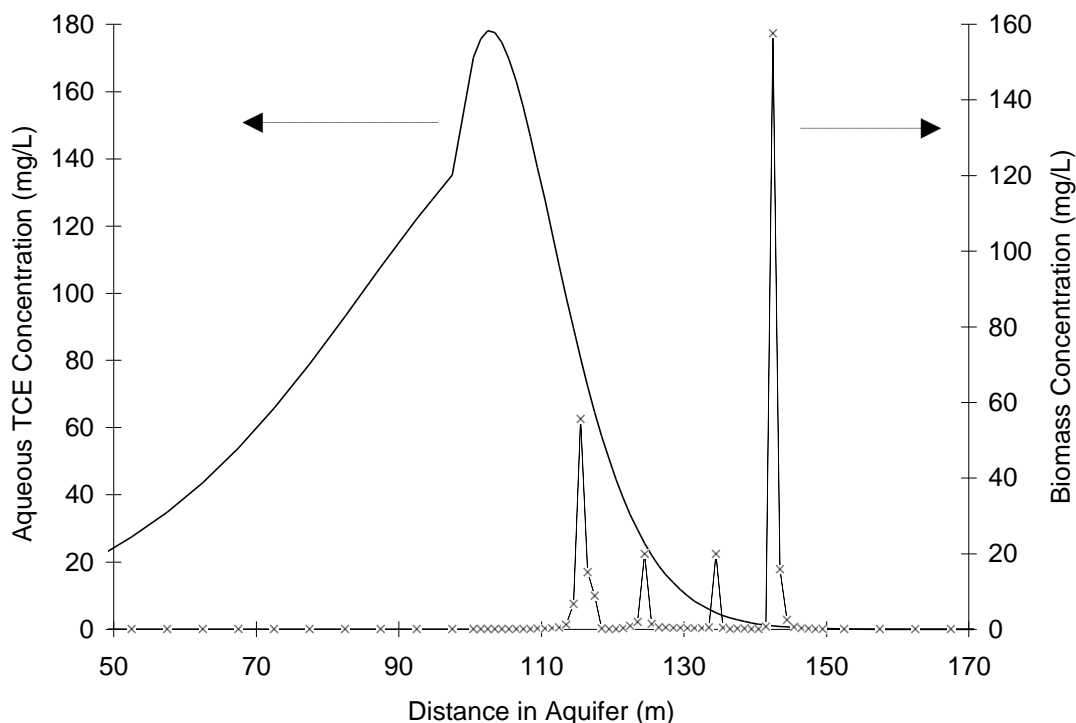


Figure 5.5.4 Distribution of Biomass and TCE_{aq} after 7.8 years.

Figure 5.5.4 shows that biomass growth concentrated in four spikes. In addition, biomass growth exceeds the 20 mg/L target concentration in two places. This occurs because the equation used to regulate methane injection attempts to promote a biomass concentration of 20.0 mg/L at the node itself. Due to lack of oxygen at the injection node, biomass is not growing at this location, causing a higher methane concentration to be injected. The methane travels to a neighboring node where, with a sufficient oxygen supply, excessive growth occurs.

These results suggest that constant injection may not be a suitable method to deliver nutrients to the subsurface. Even when different wells are used to inject the electron acceptor and donor, excessive biomass growth still occurs where the two nutrient fronts meet. It may be necessary to use an alternating injection scheme like the one used by Semprini and McCarty (1991) in their biostimulation experiments.

Figure 5.5.5 illustrates the distribution of nutrients and biomass at 7.8 years.

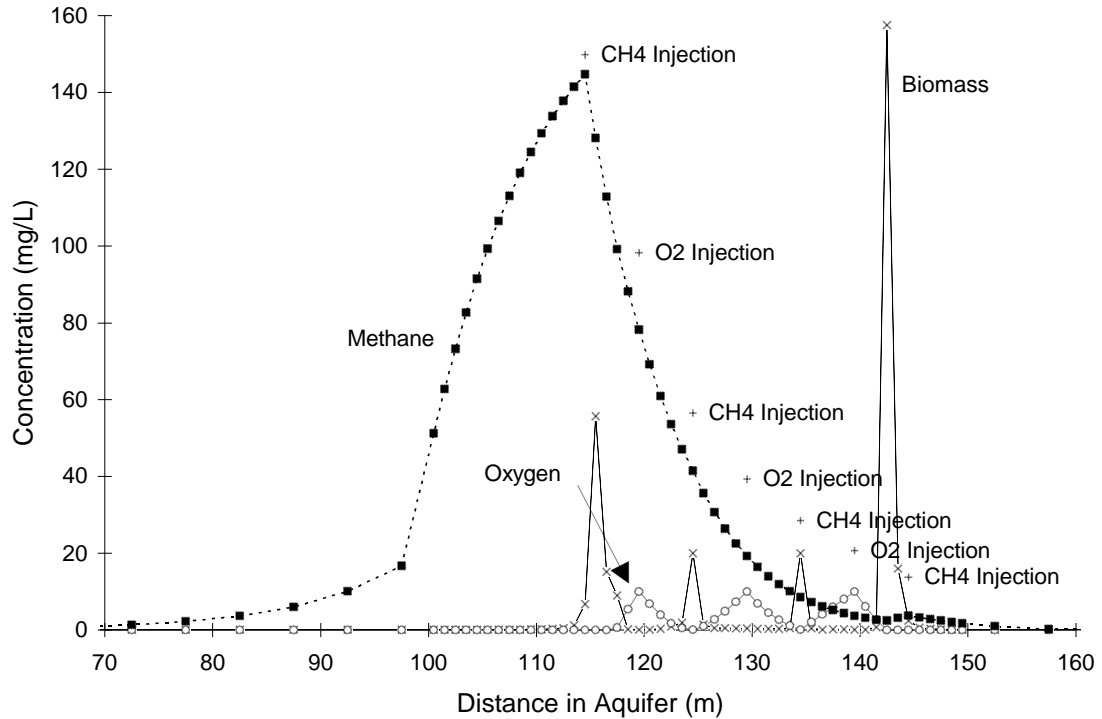


Figure 5.5.5 Distribution of Biomass, Oxygen, and Methane after 7.8 years.

Figure 5.5.5 not only illustrates the peaking of biomass concentrations at places other than injection nodes, it shows that this situation can not occur in the real world. Methane concentrations cannot reach values of 150 mg/L. The maximum solubility of methane in water is approximately 24 mg/L. The model was not programmed to take this into account.

TCE concentrations are too high for bioremediation to work in this case. Equation (5.21) gives the minimum methane concentration to maintain biomass growth. Intermediate toxicity and competitive inhibition by TCE will cause biomass concentrations to drop if methane concentration is less than this value. For example, TCE concentrations greater than 12.1 mg/L will cause biomass to decay when the methane concentration is 20 mg/L (a practical injection concentration limit). Unfortunately, TCE concentrations are much higher than 12.1 mg/L.

5.6 Conclusions

This chapter illustrated how to present physical systems in mathematical form for the numerical model. This chapter analyzed one-dimensional flow and transport in a

saturated confined aquifer contaminated with a TCE spill. Analysis determined that all of the proposed remedial strategies were insufficient. Pumping rates must increase in order for advective transport to overcome dispersive transport in the pump-and-treat scenario. Analysis determined that the bioremediation scenario was unfeasible due to high TCE concentrations.

The example problem presented in this chapter may not be representative of a real world example. The chapter did not address some important factors. First, since the example is one-dimensional, it does not allow for dilution of TCE in the lateral direction. This mixing of neighboring clean groundwater with contaminated groundwater will lower TCE concentrations. Second, the example uses a uniform distribution of TCE at a residual saturation. Real spills can consist of pockets of residual NAPL surrounded by material without residual NAPL. In bioremediation studies, other researchers have used lower aqueous TCE concentrations in the neighborhood of 0.04 mg/L (Semprini, 1993).

Table 5.6.1 presents approximate calculation times required for the simulations using a Gateway computer with a 486DX-33V Intel CPU.

Table 5.6.1 Approximate Computation Times for Various Aquifer Simulations

Simulation	Number of Nodes	Calculation Timestep (days)	Simulation Length	Time required to complete Simulation
No Action ($\Delta x = 5.0$)	20	0.49	20 years	14 min.
No Action ($\Delta x = 1.0$)	200	0.049	20 years	7 hours
Pump Only	80	0.49	20 years	1.5 hours
Pump & Biostimulation	80	0.05	10 years	8 hours

6. Conclusions

This thesis developed a numerical model capable of simulating the processes involved in subsurface remediation. It is a general purpose model, which provides flexibility in input parameters and configurations. It includes the processes of two-dimensional saturated flow; Freundlich and Langmuir sorption isotherms; single, double, and competitive Monod kinetic models; and intermediate toxicity. In addition, it can simultaneously simulate the movement of multiple solutes.

A literature search of existing numerical models discovered that no single existing model provided all of the processes described above. Therefore, this thesis developed a new model. It chose construction of a new model over modifying an existing model for various reasons. The two primary reasons were to avoid programming errors due to unfamiliarity with existing code, and the choice of C++ as the programming language.

Chapter 3 discussed the construction of the model. A finite difference algorithm solved the fluid flow and was easy to integrate with the other numerical method. The Integrated Operator-Splitting method provided easy implementation and flexibility with respect to adding different types of biological and abiotic reactions. The model uses an explicit forward time backwards space finite difference scheme called the Mean Concentration Slope method used by Poulsen (1994). The Linear Integrated method simulated the reaction portion of the IOS method. In addition, the chapter developed maximum and minimum time step criteria for the model.

Chapter 4 evaluated model performance both quantitatively and qualitatively. Due to the lack of simple analytical solutions to advection and dispersion coupled with kinetic reactions, the chapter evaluated advection and dispersion processes independently from reaction processes. The Relative Sum of Squared Error quantified the differences between numerical and analytical solutions. The chapter reported it as a function of Peclet and Courant numbers. The error in advection and dispersion processes was highly dependent on the choice of Courant and Peclet numbers. This has implications on the choice of timestep and grid spacing.

Chapter 5 illustrated the use of the model as an aid in site remediation design. The model investigated different remedial strategies in a fictitious one-dimensional aquifer. The system was highly sensitive to TCE dissolution rate and relatively insensitive to grid mesh size. Model results suggested that pump-and-treat is the only feasible strategy for the spill. Biodegradation appeared to be unfeasible.

Some suggestions for model improvement and expansion surfaced during the use and evaluation of this model. First, execution speed should be increased. The numerical

code needs to be optimized for speed. Secondly, the model is currently limited to two-dimensional simulations, and should be expanded to three. Another improvement is adding transient flow, and multiple fluid flow to the model. These improvements would help increase the utility of this program as a modeling tool.

7. References

1. Alvarez-Cohen, Lisa, McCarty, Perry L., Roberts, Paul V., (1993). *Sorption of Trichloroethylene onto a Zeolite Accompanied by Methanotrophic Biotransformation*, Environmental Science and Technology, 27(10) 2141-2148.
2. Barnes, C. J., (1986). *Equivalent Formulations for Solute and Water Movement in Soils*, Water Resources Research, 22(6) 913-918.
3. Bellin, Alberto, Rinaldo, Andrea, Bosma, Willem Jan P., van der Zee, Sjoerd E. A. T. M., Rubin, Yoram, (1993). *Linear Equilibrium Adsorbing Solute Transport in Physically and Chemically Heterogeneous Porus Formations I. Analytical Solutions*, Water Resources Research 29(12) 4019-4030.
4. Broholm, Kim, Christensen, Thomas H., Jensen, Bjørn K., (1992). *Modeling TCE Degradation by a Mixed Culture of Methane-Oxidizing Bacteria*, Water Resources 26(9) 1177-1185.
5. Celia, Michael A., Kindred, Scott J., Herrera, Ismael, (1989). *Contaminant Transport and Biodegradation: 1. A Numerical Model for Reactive Transport in Porus Media*, Water Resources Research, 25(6) 1141-1148.
6. Chen, Yung-Ming, Abriola, Linda M., Alvarez, Pedro J., Anid, Paul J., Vogel, Timothy M., (1992). *Modeling Transport and Biodegradation of Benzene and Toluene in Sandy Aquifer Material: Comparisons With Experimental Measurements*, Water Resources Research, 28(7) 1833-1847.
7. Chen, Z., McTernan, W. F., (1992). *Multi-substrate, multi-option groundwater transport model*, Journal of Contaminant Hydrology, 11, 215-244.
8. Chiang, C. Y., Salanitro, J. P., Chai, E. Y., Colthart, U. D., Klein C. L., (1989). *Aerobic Biodegradation of Benzene, Toluene, and Zylene in a Sandy Aquifer—Data Analysis and Computer Modeling*, Ground Water, 27(6) 823-834.
9. Cox, Ronald A., Nishikawa, Tracy., (1991). *A new Total Variation Diminishing Scheme for the Solution of Advective-Dominant Solute Transport*, Water Resources Research, 27(10) 2645-2654
10. Demkowicz, L., Oden, J.T., Rachowicz W., (1990). *A New Finite Element Method for Solving Compressible Navier-Stokes equations based on an Operator Splitting Method and h-p Adaptability*, Computer Methods in Applied Mechanics and Engineering, 84(1990) 275-326.
11. Dhawn, S., Erickson, L. E., Fan, L. T., (1993). *Model Development and Simulation of Bioremediation in Soil Beds with Aggregates*, Ground Water 31(2) 271-284
12. Ding, Daoyang, Liu, Philip L-F., (1989). *An Operator-Splitting Algorithm for Two-Dimensional Convection-Dispersion-Reaction Problems*, International Journal for Numerical Methods in Engineering 28, 1023-1040.
13. Ewing, R. F., (1988). *Finite Element Techniques for Convective-Diffusive Transport in Porus media*, Advances in Water Resources, 11, 123-125.
14. Freeze, R. Allan, Cherry, John A., (1979). *Groundwater*, Prentice-Hall, Inc., Englewood Cliffs, N.J.
15. Fetter, C. W., (1993). *Contaminant Hydrogeology*, Macmillan Publishing Company, New York, New York.

16. Frind, Emil O., Duynisveld, W. H. M., Strebel, O., Bottcher J., (1990). *Modeling of Multicomponent Transport with Microbial Transformation in Groundwater: The Fuhrberg Case*, Water Resources Research, 26(8) 1707-1719.
17. Fry, V. A., Istok, J. D., Guenther, R. B., (1993). *An Analytical Solution to the Solute Transport Equation With Rate-Limited Desorption and Decay*, Water Resources Research 29(9) 3201-3208.
18. Fry, V. A., Istok, J. D., (1994). *Effects of rate-limited desorption on the feasibility of in situ bioremediation*, Water Resources Research, 30(8) 2413-2422.
19. Grady, C. P. Leslie. Jr., Lim, Henry C., (1975). *Biological Wastewater Treatment: Theory and Applications*.
20. Grove, David B., Stollenwerk, Kenneth G., (1987). *Chemical Reactions Simulated by Ground-Water-Quality Models*, Water Resources Bulletin 23(4) 601-315.
21. Healy, R. W., Russell, T.F., (1993). *A Finite-Volume Eulerian-Lagrangian Localized Adjoint Method for Solution of the Advection-Dispersion Equation*, Water Resources Research, 29(7) 2399-2413.
22. Hornberger, George M., Mills, Aaron L., Herman, Janet S., (1992). *Bacterial Transport in Porus Media: Evaluation of a Model Using Laboratory Observations*, Water Resources Research, 28(3) 915-938.
23. Istok, Jonathan, (1989). *Groundwater Modeling by the Finite Element Method*, American Geophysical Union, Washington DC.
24. Kindred, Scott J., Celia, Michael A., (1989). *Contaminant Transport and Biodegradation: 2. Conceptual Model and Test Simulations*, Water Resources Research, 25(6) 1149-1159.
25. Kinzelbach, Wolfgang, Schäfer, Wolfgang, (1991). *Numerical Modeling of Natural and Enhanced Denitrification Processes in Aquifers*, Water Resources Research, 27(6) 1123-1135..
26. Klecka, Gary M., Davis, John W., Gray, Doug R., Madison, Steve S., (1990). *Natural Bioremediation of Organic Contaminants in Ground Water: Cliffs-Dow Superfund Site*, Ground Water, 28(4) 534-543.
27. Korom, Scott F., (1991). *Comment on "Modeling of Multicomponent Transport With Microbial Transformation in Groundwater: The Fuhrberg Case" by E. O. Frind et al.*, Water Resources Research, 27(12) 3271-3274.
28. Lindstrom, F. Tom., (1992). *A Mathematical Model for the One-Dimensional Transport and Fate of Oxygen and Substrate in a Water-Saturated Sorbing Homogeneous Porus Medium*, Water Resources Research, 28(9) 2499-2511.
29. Mills, William B., Liu, Sally, Fong, Fred K., (1991). *Literature Review and Model (COMET) for Colloid/Metals Transport in Porus Media*, Ground Water 29(2) 199-207.
30. Miller, Cass T., Rabideau, Alan J., (1993). *Development of Split-Operator, Petrov-Galerkin Methods to Simulate Transport and Diffusion Problems*, Water Resources Research, 29(7) 2227-2240.
31. Mehran, Mohsen, Olsen, Roger L., Rector, Bryan M., (1987). *Distribution Coefficient of Trichloroethylene in Soil-Water Systems*, Ground Water 25(3) 275-282.
32. Moridis, George J., Reddell, Donald L., (1991). *The Laplace Transform Finite Difference Method for Simulation of Flow Through Porous media*, Water Resources Research 27(8) 1873-1884.

33. Odencrantz, (1992). *Modeling the Biodegradation Kinetics of Dissolved Organic Contaminants in a Heterogeneous Two-Dimensional Aquifer*, Ph.D. Thesis, University of Illinois, Urbana-Champaign, Illinois.
34. Poulsen, Tjalfe G., (1991). *Modeling Three Phase, Dynamic Behavior of Organic Pollutants in Unsaturated Soil*, Ms. Thesis, Environmental Engineering Laboratory, University of Aalborg.
35. Poulsen, Tjalfe G., (1994). *An Adaptable Two Dimensional Numerical Model for Simulating Movement of Organic Pollutants in Unsaturated Soils*, Ms. Thesis, The University of Washington, Seattle, Washington.
36. Rao, Bhasker K., Hathaway, Deborah L., (1989). *Three-Dimensional Mixing Cell Solute Transport Model and its Application*, Ground Water, 27(4) 509-516.
37. Rifai, H. S., Bedient, P. B., Wilson, J. W., Miller, K. M., Armstrong, J. M., (1988). *Biodegradation Modeling at Aviation Fuel Spill Site*, Journal of Environmental Engineering, 114(5), 1007-1029.
38. Rittmann, Bruce E., (1993). *The Significance of Biofilms in Porous Media*, Water Resources Research, 29(7) 2195-2202.
39. Roberts, Paul V., Hopkins, Gary D., Mackay, Douglas M., Semprini, Lewis, (1990). *A Field Evaluation of In-Situ Biodegradation of Chlorinated Ethenes: Part 1, Methodology and Field Site Characterization*, Ground Water 28(4) 591-604.
40. Semprini, L., Hopkins, Gary D., Roberts, Paul V., Grbic-Galic, D., McCarty, Perry L., (1991a) *A Field Evaluation of In-Situ Biodegradation of Chlorinated Ethenes: Part 3, Studies of Competitive Inhibition*, Ground Water 29(2) 239-250
41. Semprini, L., McCarty, P. L., (1991). *Comparison Between Model Simulations and Field Results for In-Situ Bioremediation of Chlorinated Aliphatics: Part 1. Biostimulation of Methanotrophic Bacteria*, Ground Water, 29(3) 365-374.
42. Semprini, L., McCarty, P. L., (1993). *Comparison Between Model Simulations and Field Results for In-Situ Bioremediation of Chlorinated Aliphatics: Part 2: Competitive Transformations*, Ground Water, 30(1) 37-44.
43. Semprini, Lewis, Roberts, Paul V., Hopkins, Gary D., McCarty, Perry L., (1990). *A Field Evaluation of In-Situ Biodegradation of Chlorinated Ethenes: Part 2, Results of Biostimulation and Biotransformation Experiments*, Ground Water, 28(5) 715-727.
44. Sleep, Brent E., Sykes, Jonathan F., (1993). *Compositional Simulation of Groundwater Contamination by Organic Compounds, 1. Model Development and Verification*, Water Resources Research, 29(6) 1697-1708.
45. Sleep, Brent E., Sykes, Jonathan F., (1993). *Compositional Simulation of Groundwater Contamination by Organic Compounds, 2. Model Applications*, Water Resources Research, 29(6) 1709-1718.
46. Srinivasan, P., Mercer, W. James., (1988). *Simulation of Biodegradation and Sorption Processes in Ground Water*, Ground Water, 26(4) 475-487.
47. Strand, S.E., Bjelland, M. D., Stensel, H. D., (1989). *Kinetics of Chlorinated Hydrocarbon Degradation by Suspended Cultures of methane-oxidizing bacteria*, Research Journal Water Pollution Control Federation, 26(2) 124-129.
48. Sudicky, E. A., (1984). *The Laplace Transform Galerkin Technique: A Time-Continuous Finite Element Theory and Application to Mass Transport in Ground Water*, Water Resources Research 25(8) 1833-1846.

49. Sudicky, E. A., Gillham, R. W., Frind, E. O., (1985). *Experimental Investigation of Solute Transport in Stratified Porous Media 1. The Nonreactive Case*, Water Resources Research, 21(7) 1035-1041..
50. Taylor, Stewart W., Jaffé, Peter R., (1990a). *Biofilm Growth and the Related Changes in the Physical Properties of a Porus Medium: 1. Experimental Investigation*, Water Resources Research, 26(9) 2153-2159.
51. Taylor, Stewart W., Milly, P.C.D., Jaffé, Peter, (1990). *Biofilm Growth and the Related Changes in the Physical Properties of a Porous Media 2. Permeability*, Water Resources Research, 26(9) 2161-2169.
52. Taylor, Stewart W., Jaffé, Peter R., (1990b). *Biofilm Growth and the Related Changes in the Physical Properties of a Porus Medium: 3. Dispersion and Model Verification*, Water Resources Research, 26(9) 2171-2180.
53. Taylor, Stewart W., Jaffé, Peter R., (1990c). *Substrate and Biomass Transport in a Porus Medium*, Water Resources Research, 26(9) 2181-2194.
54. Tim, Udoyara S., Mostaghimi Saied., (1991). *Model for Predicting Virus Movement Through Soils*, Ground Water 29(2) 251-259.
55. Tim, Udoyara S., Mostaghimi Saied., (1990). *Modeling Transport of a Degradable Chemical and its Metabolites in the Unsaturated Zone*, Ground Water, 27(5) 672-681.
56. Valocchi, Albert J., Malmstead, Michael, (1992). *Accuracy of Operator Splitting for Advection-Dispersion-Reaction Problems*, Water Resources Research, 28(5) 1471-1476.
57. Wind, G.P., Van Doorne, W., (1975). *A Numerical Model for the Simulation of Unsaturated Vertical Flow of Moisture in Soils*, Journal of Hydrology, 24, 1-20.
58. Zheng, C., (1993). *Extension of the Method of Characteristics for Simulation of Solute Transport in Three Dimensions*, Ground Water, 31(3) 456-465.

Appendix A Monod Kinetics and Competitive Inhibition

Before describing the particular implementations of the various types of kinetics, it is necessary to review the theory behind Monod kinetics. Monod kinetics are different from, but still based upon Michaelis-Menten kinetics for enzymes. One can think of Monod Kinetics as describing a chain of enzymatically mediated reactions with a limiting step described by Michaelis-Menten kinetics. This is why the equations for both kinetic models are identical. The following paragraphs describe the development and theory behind Michaelis-Menten kinetics.

The basic assumption behind Michaelis-Menten Enzyme kinetics is that enzymes catalyze reactions by first forming an enzyme-substrate complex (Grady and Lim, 1975). This substrate complex will either decay back to enzyme and substrate (the reverse of the previously mentioned reaction) or irreversibly decay to enzyme and product. These chemical reactions for complex formation and product formation respectively are:



- Where: S = substrate
 E = enzyme
 ES = enzyme-substrate complex
 P = product
 k_1 = rate constant for complex formation
 k_2 = rate constant for reverse complex formation
 k_3 = rate constant for product formation

The rates for the above reactions would be as follows:

$$\left. \frac{d\{ES\}}{dt} \right|_{k_1} = k_1\{S\}\{E\} \quad (\text{A.3})$$

$$-\left. \frac{d\{ES\}}{dt} \right|_{k_2} = k_2\{ES\} \quad (\text{A.4})$$

$$\left. \frac{d\{P\}}{dt} = -\frac{d\{ES\}}{dt} \right|_{k_3} = k_3\{ES\} \quad (\text{A.5})$$

Where: k_1 = rate constant for complex formation
 k_2 = rate constant for complex reverse formation
 k_3 = rate constant for product formation
 $\{S\}$ = concentration of substrate
 $\{E\}$ = concentration of free enzyme
 $\{ES\}$ = concentration of substrate-enzyme complex
 $\{P\}$ = concentration of product concentration

Furthermore, it is assumed the above set of equations are in equilibrium such that:

$$\frac{d\{ES\}}{dt} = 0 \quad (\text{A.6})$$

Therefore:

$$k_1\{E\}\{S\} = k_2\{ES\} + k_3\{ES\} \quad (\text{A.7})$$

A mass balance on the total enzyme is given as:

$$E_T = \{ES\} + \{E\} \quad (\text{A.8})$$

Combining equations (A.7) and (A.8) and substituting into equation (A.5) gives:

$$E_T\{S\} = \left(\frac{k_2 + k_3}{k_1} + \{S\} \right) \{ES\} \quad (\text{A.9})$$

and

$$\frac{d\{P\}}{dt} = \frac{k_3 E_T \{S\}}{\frac{k_2 + k_3}{k_1} + \{S\}} \quad (\text{A.10})$$

so let

$$k_m = \frac{k_2 + k_3}{k_1} \quad (\text{A.11})$$

therefore

$$\frac{d\{P\}}{dt} = \frac{k_3 E_T \{S\}}{k_m + \{S\}} \quad (\text{A.12})$$

- Where: $\{P\}$ = concentration of product
 $\{ES\}$ = concentration of enzyme-substrate complex
 $\{S\}$ = concentration of substrate
 E_T = total complexed and un-complexed enzyme
 k_1 = rate constant for complex formation
 k_2 = rate constant for reverse complex formation
 k_3 = rate constant for product formation
 k_m = “half-saturation” concentration

Which is analogous to Monod kinetics, k_3 is analogous to the maximum specific substrate utilization rate, E_T is analogous to biomass concentration, and k_m is analogous to the half saturation constant. Monod kinetics and its variations, along with other bio-kinetic equations will be presented in the following discussion.

In competitive inhibition an inhibitory complex can combine with the controlling enzyme in addition to the reaction equation (A.1). This additional complex prohibits the enzyme from forming the complex with the substrate of interest.



- Where: I = inhibitor
 E = enzyme
 EI = enzyme-substrate complex
 P = product
 k_4 = rate constant for complex formation
 k_5 = rate constant for reverse complex formation

Equation (A.8) now looks like:

$$E_T = \{ES\} + \{EI\} + \{E\} \quad (\text{A.14})$$

Where: E_T = total complexed and un-complexed enzyme
 $\{E\}$ = concentration of free enzyme
 $\{ES\}$ = concentration of substrate-enzyme complex
 $\{EI\}$ = concentration of inhibitor-enzyme complex

After substitution of equation (A.13) (with the assumption of equilibrium) equation (A.14) becomes:

$$E_T = \{ES\} + \left(\frac{k_4}{k_5} \{I\} + 1 \right) \{E\} \quad (\text{A.15})$$

The same derivation for Michaelis-Menten Kinetics as presented above applies:

$$E_T \{S\} = \left(\left(\frac{k_4}{k_5} \{I\} + 1 \right) \frac{k_2 + k_3}{k_1} + \{S\} \right) \{ES\} \quad (\text{A.16})$$

$$\frac{d\{P\}}{dt} = \frac{k_3 E_T \{S\}}{\left(\frac{k_4}{k_5} \{I\} + 1 \right) \frac{k_2 + k_3}{k_1} + \{S\}} \quad (\text{A.17})$$

so let

$$k_I = \frac{k_4}{k_5} \quad (\text{A.18})$$

therefore

$$\frac{d\{P\}}{dt} = \frac{k_3 E_T \{S\}}{k_m (1 + \{I\}/k_I) + \{S\}} \quad (\text{A.19})$$

Where: $\{P\}$ = concentration of product
 $\{ES\}$ = concentration of enzyme-substrate complex
 $\{S\}$ = concentration of substrate
 $\{I\}$ = concentration of inhibitor
 E_T = total complexed and un-complexed enzyme
 k_1 = rate constant for complex formation
 k_2 = rate constant for reverse complex formation
 k_3 = rate constant for product formation
 k_m = “half-saturation” concentration
 k_I = “saturation” constant for inhibitor

There are other types of inhibition, such as un-competitive, and substrate inhibition which are not presented here.

Semprini (1991) studied the competitive inhibition of TCE degradation by methane. A double Monod form of inhibition kinetics was used:

$$\frac{dC_c}{dt} = -Xk_c \frac{C_2}{K_{Sc} + C_c + C_i/K_i} \frac{C_A}{K_A + C_A} \quad (\text{A.20})$$

Where: C_c = concentration of contaminant
 C_i = concentration of the inhibitor
 C_A = concentration of the electron acceptor
 K_{Sc} = saturation constant for contaminant
 K_A = saturation constant for the electron acceptor
 k_c = maximum transformation rate
 K_i = inhibition constant

It should be noted equation (A.20) is in the form of double Monod kinetics, however, the first term in the equation is the same form as equation (A.19). The second order electron acceptor term was included since the presence of an electron acceptor was required for the contaminant transformation.

Appendix B Integrated Operator-Splitting Method

In 1992, Valocchi and Malmstead (V&M below) explored a mass balance error inherent in the standard operator-splitting method. In their analysis, they proposed an “alternating” operator-splitting method to reduce mass balance errors at a constant concentration boundary. This thesis proposes a second alternative, integrated operator-splitting.

This appendix will describe the integrated operator-splitting method (IOS) and conduct the error analysis of V&M. The results of the IOS error analysis will be compared to those of standard OS.

Before conducting the error analysis it is necessary to describe IOS and how it differs from OS. In OS the advection-dispersion processes are de-coupled from the reaction processes. The advection-dispersion problem is solved first, resulting in an intermediate concentration. This intermediate concentration is used as the initial concentration for the reaction problem. The reaction problem is solved over the same timestep resulting in the final concentration at the end of the timestep. IOS eliminates the use of the intermediate solution. Instead, it uses the change in concentration calculated in the advection-dispersion step as a source/sink term in the system of reaction equations. It was speculated that using the initial concentration at a timestep and accounting advection and dispersion implicitly in the reaction equations would reduce the error in the final solution. It will be shown later, for the case of a one-dimensional aquifer with a continuous source of a non-conservative solute, the error in IOS is lower than OS.

The discrete form of equation (3.1) is used to calculate the change in concentration at a node over a given timestep is:

$$\Delta C = C_f - C_i = \Delta C_F + \Delta C_{\text{rxn}} \quad (\text{B.1})$$

Where: ΔC = change in concentration over a time interval
 C_f = concentration at end of time interval
 C_i = concentration at beginning of time interval
 ΔC_F = change in concentration due to advective-dispersive flux
 ΔC_{rxn} = change in reaction due to kinetic reactions

It should be noted the solution to the kinetic reaction equation uses the linear integrated method described in Appendix D. Table B.1 describes the steps used to solve equation (B.1).

Table B.1 IOS Order of Calculation

Step	Compute	Comment
1	$\Delta C_F = f(C_i, \Delta t)$	Compute the change in concentration at a node due to conservative advective-dispersive flux
2	$C_f = C_{i_o} + \mathbf{D}C_F$	Compute a trial final concentration, it is needed for the calculation of kinetic reactions.
3	$\Delta C_{\text{rxn}} = f(C_i, C_f, \Delta t)$	Compute the change in concentration due to kinetic reactions, which is a function of initial and final concentrations, and the length of time period.
4	$\Delta C = \mathbf{D}C_F + \Delta C_{\text{rxn}}$	Compute the trial change in concentration at the node
5	$C_f = C_i + \Delta C$	Compute new trial final concentration. If the change in C_f from the last iteration is not sufficiently small, go back to step 3 and continue iteration.

Having described the IOS method, the error analysis used by V&M can be conducted. First consider a one-dimensional aquifer with a constant source of solute undergoing first order decay. The boundary and initial conditions are:

$$C(x = 0, t > 0) = C_o \quad (\text{B.2})$$

$$C(x, t = 0) = 0 \quad (\text{B.3})$$

and the equation of first order decay is:

$$\frac{\mathbf{d}C}{\mathbf{d}t} = -kC \quad (\text{B.4})$$

To determine the change in concentration due to first order decay over the timestep, $\mathbf{D}t$, using the LI method, the following integration is performed:

$$\Delta C_{\text{rxn}} = -k \int_0^{\Delta t} \left[\frac{C_f - C_i}{\Delta t} t + C_i \right] dt \quad (\text{B.5})$$

$$\Delta C_{\text{rxn}} = -k \left[\frac{C_f - C_i}{2\Delta t} t^2 + C_i t \right]_0^{\Delta t} \quad (\text{B.6})$$

$$\Delta C_{\text{rxn}} = \frac{-k\Delta t}{2} [C_f + C_i] \quad (\text{B.7})$$

Since first order decay is a relatively simple reaction, the final concentration, C_f , can be determined directly, it will not be necessary to perform the iterative procedure outlined in Table B.1. Since $C_f = C_i + \Delta C_F + \Delta C_{\text{rxn}}$ equation (B.7) becomes:

$$\Delta C_{\text{rxn}} = \frac{-k\Delta t}{2} [(C_i + \Delta C_K + \Delta C_{\text{rxn}}) + C_i] \quad (\text{B.8})$$

$$\Delta C_{\text{rxn}} \left[1 + \frac{k\Delta t}{2} \right] = \frac{-k\Delta t}{2} [2C_i + \Delta C_F] \quad (\text{B.9})$$

$$\Delta C_{\text{rxn}} = \frac{-k\Delta t}{2} \left[\frac{2C_i + \Delta C_F}{1 + \frac{k\Delta t}{2}} \right] \quad (\text{B.10})$$

$$\Delta C_{\text{rxn}} = -k\Delta t \left[\frac{2C_i + \Delta C_F}{2 + k\Delta t} \right] \quad (\text{B.11})$$

At the end of the first timestep the simulation equation (B.1).becomes:

$$\Delta C = \Delta C_F - k\Delta t \left[\frac{2C_i + \Delta C_F}{2 + k\Delta t} \right] \quad (\text{B.12})$$

Solving for the final concentration:

$$C_f = C_i + \Delta C_F - k\Delta t \left[\frac{2C_i + \Delta C_F}{2 + k\Delta t} \right] \quad (\text{B.13})$$

Now substituting $C^*(X, Dt)$ for $C_i + \Delta C_F$ to change (B.13) into a form similar to equation (12) in V&M yields:

$$C_{\text{IOS}}(x, \Delta t) = C_f = C^*(x, \Delta t) - k\Delta t \left[\frac{C^*(x, \Delta t) + C_i}{2 + k\Delta t} \right] \quad (\text{B.14})$$

Since in the first time step, $C_i = 0$, equation (B.14) becomes:

$$C_{\text{IOS}}(x, \Delta t) = C^*(x, \Delta t) \left[1 - \frac{k\Delta t}{2 + k\Delta t} \right] \quad (\text{B.15})$$

$C^*(x, \Delta t)$ is the “perfect” solution to the advective-dispersive equation at the end of timestep Δt at location x . Now continuing with the IOS form of equation (15) of V&M:

$$e(x, \Delta t) = C_{\text{exact}}(x, \Delta t) - C_{\text{IOS}}(x, \Delta t) \quad (\text{B.16})$$

$$e(x, \Delta t) = \frac{C_o v}{A} \int_0^{\Delta t} e^{-k(\Delta t-t)} G^{\text{NR}}(x, \Delta t-t) dt - \frac{C_o v}{A} \int_0^{\Delta t} \left[1 + \frac{k\Delta t}{2 + k\Delta t} \right] G^{\text{NR}}(x, \Delta t-t) dt \quad (\text{B.17})$$

Simplifying:

$$e(x, \Delta t) = \frac{C_o v}{A} \int_0^{\Delta t} G^{\text{NR}}(x, \Delta t+t) \left[e^{-k\Delta t} e^{kt} - \left(1 - \frac{k\Delta t}{2 + k\Delta t} \right) \right] dt \quad (\text{B.18})$$

Integrating the above equation over an infinite aquifer;

$$\int_0^{\infty} e(x, \Delta t) dx = \frac{C_o v}{A} \int_0^{\Delta t} \left[e^{-k\Delta t} e^{kt} - \left(1 - \frac{k\Delta t}{2 + k\Delta t} \right) \right] \int_0^{\infty} G^{\text{NR}}(x, \Delta t+t) dx dt \quad (\text{B.19})$$

leads to the mass balance error over the entire aquifer at the first timestep, Δt :

$$\bar{e}(\Delta t) = C_o v \int_0^{\Delta t} \left[e^{-k\Delta t} e^{kt} - \left(1 - \frac{k\Delta t}{2 + k\Delta t} \right) \right] dt \quad (\text{B.20})$$

$$\bar{e}(\Delta t) = C_o v \left[e^{-k\Delta t} \int_0^{\Delta t} e^{kt} dt - \left(1 - \frac{k\Delta t}{2 + k\Delta t} \right) \int_0^{\Delta t} dt \right] \quad (\text{B.21})$$

$$\bar{e}(\Delta t) = C_o v \left[\frac{1}{k} e^{-k\Delta t} (e^{k\Delta t} - 1) - \Delta t \left(1 - \frac{k\Delta t}{2 + k\Delta t} \right) \right] \quad (\text{B.22})$$

To find the relative mass error, it is necessary to divide by total mass in the system:

$$E_{\text{IOS}}(\Delta t) = \frac{C_o v \left[\frac{1}{k} e^{-k\Delta t} (e^{k\Delta t} - 1) - \Delta t \left(1 - \frac{k\Delta t}{2 + k\Delta t} \right) \right]}{C_o v \left[\frac{1}{k} (1 - e^{-k\Delta t}) \right]} \quad (\text{B.23})$$

Which reduces to the relative cumulative mass balance error at the first timestep, Δt .

$$E_{\text{IOS}}(\Delta t) = 1 - \frac{k\Delta t \left(1 - \frac{k\Delta t}{2 + k\Delta t} \right)}{1 - e^{-k\Delta t}} \quad (\text{B.24})$$

Which is a function of kDt , the same as the error term derived by V&M for standard OS. Figure B.1 illustrates the differences in error between these two methods. It should be noted, the IOS error is reported as an absolute value. The IOS error is negative in value but less in magnitude than OS.

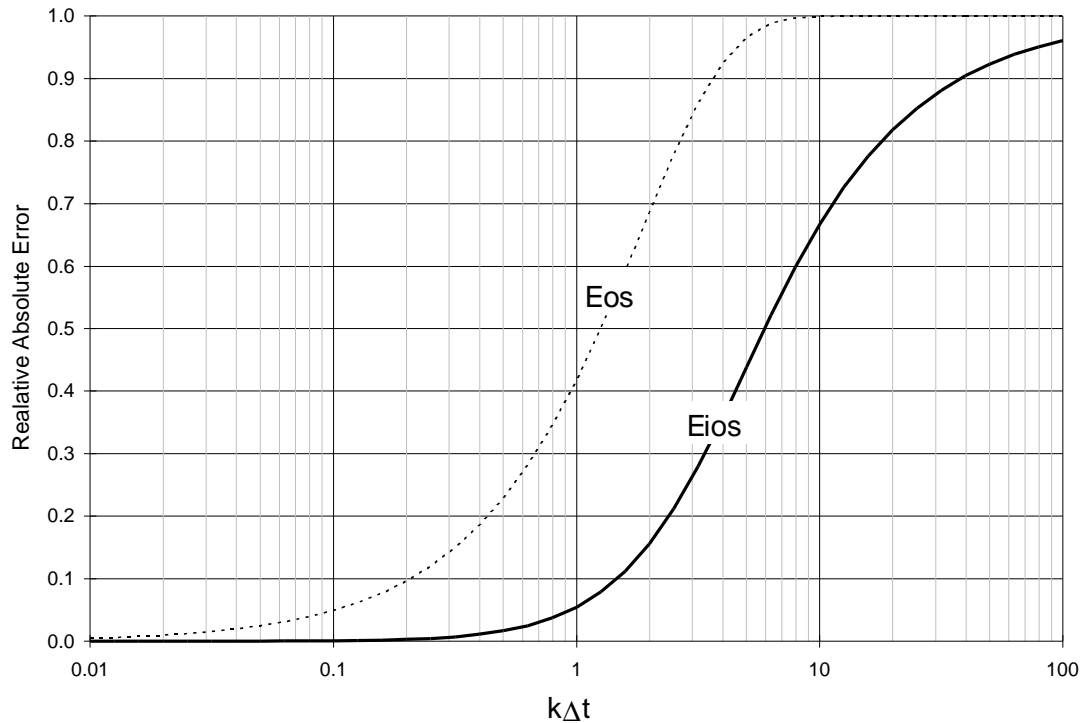


Figure B.1 Comparison of IOS and OS Error as a Function of kDt .

Appendix C Solute Transport Equation

This work uses the MCS solution scheme developed by Wind and van Doorne (1975), and Poulsen (1994) to solve the advection-dispersion portion of the system of equations. This appendix is a quick overview of the calculations used to derive the equations.

First, consider advection and dispersion in a one dimensional aquifer. The fundamental equation for the change in concentration of a solute in time in one-dimensional space is:

$$n \frac{dC}{dt} = \frac{d}{dx} \left[nD \frac{dC}{dx} - qC \right] + R(C,t) \quad (C.1)$$

Where: dC/dt = time rate of change in concentration
 C = concentration
 D = dispersion coefficient
 q = darcy flux
 n = material porosity
 R = net rate of reaction (sink/source term)

For this discussion we are only interested in the advection-dispersion part of equation (C.1), the reactive portion will be ignored. Equation (C.1) can therefore be rewritten in the form:

$$\frac{dC}{dt} = - \frac{d}{dx} \left[nD \frac{dC}{dx} - qC \right] \quad (C.2)$$

Where J is the equation of solute flux in the x direction. The solute flux equation is defined as:

$$J = -D \frac{dC}{dx} + \frac{q}{n} C \quad (C.3)$$

The above equation is the one of interest. Next, it will be necessary to convert equation (C.3) into a discretized form. This will be done by setting boundary conditions and integrating equation (C.3) with respect to space at a given time instant. Rewriting equation (C.3) in standard form for the solution of the first order linear differential equation yields:

$$\frac{dC}{dx} - \frac{q}{nD}C = -\frac{J}{D} \quad (C.4)$$

The next step is to solve the homogeneous equation. D and q are assumed to be constant and uniform over the area of integration.

$$\frac{dC}{dx} - \frac{q}{nD}C = 0 \quad (C.5)$$

$$C = Ke^{\left(\frac{q}{nD}x\right)} \quad (C.6)$$

Next, the solution of the non-homogeneous equation is computed. $K'(x)$ refers to the derivative of the constant of integration, K , with respect to x .

$$K'(x)e^{\left(\frac{q}{nD}x\right)} = -\frac{J}{D} \quad (C.7)$$

$$K'(x) = -\frac{J}{D}e^{\left(-\frac{q}{nD}x\right)} \quad (C.8)$$

$$K(x) = -\frac{J}{D}\left(-\frac{nD}{q}e^{-\frac{q}{nD}x}\right) + K \quad (C.9)$$

$$K(x) = -\frac{Jn}{q}e^{-\frac{q}{nD}x} + K \quad (C.10)$$

Therefore:

$$C = \left[\frac{Jn}{q}e^{-\frac{q}{nD}x} + K \right] e^{\frac{q}{nD}x} \quad (C.11)$$

$$C = \frac{Jn}{q} + Ke^{\frac{q}{nD}x} \quad (C.12)$$

To eliminate the constant of integration “ K ”, the boundary conditions ($C=C_1, x=x_1$) and ($C=C_2, x=x_2$) are substituted into equation (C.12):

$$\frac{qC_1 - Jn}{qe^{\frac{q}{nD}x_1}} = \frac{qC_2 - Jn}{qe^{\frac{q}{nD}x_2}} \quad (C.13)$$

With rearrangement yields:

$$J = \frac{qC_2 - qC_1}{n \left(1 - e^{\left(\frac{q}{nD} [x_2 - x_1] \right)} \right)} + \frac{q}{n} C_1 \quad (\text{C.14})$$

J is the flux from boundary (1) to boundary (2). Equation (C.14) is prone to artificial numerical dispersion. It is necessary to define a term to correct the actual dispersion coefficient for this artificial numerical dispersion.

First, it is necessary to explain some nomenclature. t refers to the current time period, or the beginning of the current time interval. $t + \mathbf{Dt}$ refers to the next time period, or the ending of the current time interval. x refers to the current index in the aquifer. $x - \mathbf{Dx}$ refers to the previous index and $x + \mathbf{Dx}$ to the next index. Δt refers to the time interval. Δx refers to the grid spacing.

The equation for change in concentration as a function of time can be written:

$$\frac{dC}{dt} = -\frac{dJ}{dx} \quad (\text{C.15})$$

In discrete terms, it is written:

$$\frac{C_{t+\Delta t, x} - C_{t, x}}{\Delta t} = -\frac{J_{t, x} - J_{t, x-\Delta x}}{\Delta x} \quad (\text{C.16})$$

Expanding yields:

$$\frac{C_{t+\Delta t, x} - C_{t, x}}{\Delta t} = \frac{q}{n \left(e^{\left(\frac{q}{nD} \Delta x \right)} - 1 \right)} \frac{C_{t, x+\Delta x} - 2C_{t, x} + C_{t, x-\Delta x}}{\Delta x} - \frac{q}{n} \frac{C_{t, x} - C_{t, x-\Delta x}}{\Delta x} \quad (\text{C.17})$$

Equation (C.17) can be considered a finite-difference approximation to the advection-dispersion equation (Poulsen 1991). A Taylor expansion based method was used to find and correct for second order numerical errors. If the following Taylor expansion series are used (neglecting terms of fourth order and higher):

$$C_{t,x} = C_{t,x} \quad (\text{C.18})$$

$$C_{t+\Delta t,x} = C_{t,x} + \Delta t \frac{dC}{dt} + \frac{(\Delta t)^2}{2} \frac{d^2C}{dt^2} + \frac{(\Delta t)^3}{6} \frac{d^3C}{dt^3} \quad (\text{C.19})$$

$$C_{t,x+\Delta x} = C_{t,x} + \Delta x \frac{dC}{dx} + \frac{(\Delta x)^2}{2} \frac{d^2C}{dx^2} + \frac{(\Delta x)^3}{6} \frac{d^3C}{dx^3} \quad (\text{C.20})$$

$$C_{t,x-\Delta x} = C_{t,x} - \Delta x \frac{dC}{dx} + \frac{(\Delta x)^2}{2} \frac{d^2C}{dx^2} - \frac{(\Delta x)^3}{6} \frac{d^3C}{dx^3} \quad (\text{C.21})$$

Rewriting equation (C.1) to solve for the change in concentration in time, then differentiating twice with respect to time:

$$\frac{dC}{dt} = D \frac{d^2C}{dx^2} - \frac{q}{n} \frac{dC}{dx} \quad (\text{C.22})$$

$$\frac{d^2C}{dt^2} = \frac{q^2}{n^2} \frac{d^2C}{dx^2} - 2 \frac{q}{n} D \frac{d^3C}{dx^3} + D^2 \frac{d^4C}{dx^4} \quad (\text{C.23})$$

$$\frac{d^3C}{dt^3} = \left(\frac{q}{n}\right)^3 \frac{d^3C}{dx^3} \quad (\text{C.24})$$

If equations (C.18) through (C.24) are substituted into equation (C.17) and simplified, the following equation will result:

$$n \frac{dC}{dt} + \frac{q}{n} \frac{dC}{dx} = \left(\frac{q}{n} \frac{\Delta x}{2} - \frac{q^2}{n^2} \frac{\Delta t}{2} + \frac{q \Delta x}{n \left(e^{\frac{q}{nD} \Delta x} - 1 \right)} \right) \frac{d^2C}{dx^2} + \left(\frac{q^3}{n^3} \frac{(\Delta t)^2}{6} - \frac{q^2}{n^2} \frac{(\Delta x)^2}{6} + \frac{q D \Delta t}{n} \right) \frac{d^3C}{dx^3} \quad (\text{C.25})$$

When comparing equation (C.25) with equation (C.22), one can see the numerical correction. The second order term approximates the artificial numerical dispersion created by the numerical method. The numerical dispersion coefficient would be the difference between the second order term in equation (C.25) and the actual dispersion coefficient, or:

$$D_{num} = \frac{q}{n} \frac{\Delta x}{2} - \frac{q^2}{n^2} \frac{\Delta t}{2} + \frac{q\Delta x}{n \left(e^{\frac{q}{nD}\Delta x} - 1 \right)} - D \quad (C.26)$$

The next step is to determine how the correction for numerical dispersion fits into equation (C.14). First compare equation (C.14), which is the finite difference equation for flux between two nodes, with equation (C.3). Comparison of the terms in these equations which involve dispersion;

$$-D \frac{dC}{dx} \leftrightarrow \frac{\Delta x}{n} \frac{q}{1 - e^{\left(\frac{q}{nD}\Delta x\right)}} \frac{C_2 - C_1}{\Delta x} \quad (C.27)$$

show that the “equivalent” dispersion term for the finite difference equation of solute flux is:

$$D^* = \frac{-\Delta x}{n} \frac{q}{1 - e^{\left(\frac{q}{nD}\Delta x\right)}} \quad (C.28)$$

Equation (C.14) now becomes:

$$J = \left[\frac{-n}{\Delta x} (D^* - D_{num}) \right] (C_2 - C_1) + qC_1 \quad (C.29)$$

After inserting equations (C.26) and (C.28) into equation (C.29) and simplifying, the one dimensional equation for flux between two nodes in a one dimensional aquifer becomes:

$$J = \left(\frac{q}{2} - \frac{q^2 \Delta t}{2n\Delta x} - \frac{nD}{\Delta x} \right) (C_2 - C_1) + qC_1 \quad (C.30)$$

It should be noted Equation (C.30) is also equivalent to the implementation of the FTBS mixing cell model used by Rao and Hathaway (1989) which cited the use of a numerical dispersion coefficient in the x direction to be:

$$D_x = \frac{q_x}{n} \frac{\Delta x}{2} - \left(\frac{q_x}{n} \right)^2 \frac{\Delta t}{2} \quad (C.31)$$

Which is the same as calculated here, accounting for the difference in the conventions and placement of the porosity, n , and grid spacing, Δx .

Equation (C.30) is only for one dimension. It is necessary to have an equation of flux which corresponds to a two dimensional aquifer. The fundamental equation for the change in conservative solute concentration as a function of time in two dimensions is:

$$n \frac{\mathcal{C}}{\mathcal{t}} - \frac{\mathcal{d}}{\mathcal{t}} \left(q_x C - n D_{xx} \frac{\mathcal{C}}{\mathcal{t}} - n D_{xy} \frac{\mathcal{C}}{\mathcal{t}} \right) - \frac{\mathcal{d}}{\mathcal{t}} \left(q_y C - n D_{yy} \frac{\mathcal{C}}{\mathcal{t}} - n D_{xy} \frac{\mathcal{C}}{\mathcal{t}} \right) \quad (\text{C.32})$$

Where: $D_{xx} = (\mathbf{a}_t v_y^2 + \mathbf{a}_l v_x^2) / \sqrt{v_x^2 + v_y^2}$
 $D_{yy} = (\mathbf{a}_t v_x^2 + \mathbf{a}_l v_y^2) / \sqrt{v_x^2 + v_y^2}$
 $D_{xy} = (\mathbf{a}_l - \mathbf{a}_t) v_x v_y / \sqrt{v_x^2 + v_y^2}$
 $v_x =$ pore water velocity in x direction, q_x/n
 $v_y =$ pore water velocity in y direction, q_y/n
 $\mathbf{a}_l =$ longitudinal dispersivity
 $\mathbf{a}_t =$ transverse dispersivity
 $q_x =$ darcy flux in x direction
 $q_y =$ darcy flux in y direction
 $n =$ material porosity

Once again, from equation (C.32) the flux components in both the x and y directions respectively can be defined as:

$$J_x = -D_{xx} \frac{\mathcal{C}}{\mathcal{t}} - D_{xy} \frac{\mathcal{C}}{\mathcal{t}} + \frac{q_x}{n} C \quad (\text{C.33})$$

$$J_y = -D_{yy} \frac{\mathcal{C}}{\mathcal{t}} - D_{xy} \frac{\mathcal{C}}{\mathcal{t}} + \frac{q_y}{n} C \quad (\text{C.34})$$

It can be seen, there is an extra term, D_{xy} , included in the two dimensional flux equations. It is necessary to include this term in the FTBS solution scheme. For this discussion consider only the flux in the X direction (equation (C.33)), the equations for the Y direction will be similar.

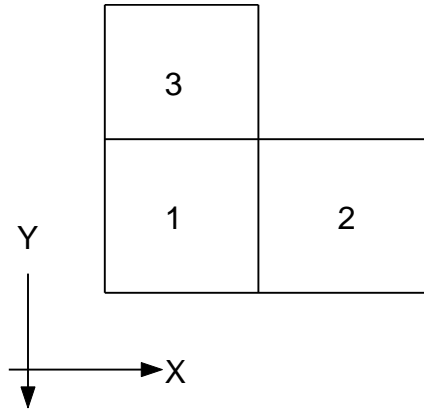
Equation (C.33) can be re-written in the form:

$$J_x = -\left(D_{xx} + D_{xy} \frac{\mathbf{d}}{\mathbf{d}} \frac{\mathbf{d}}{\mathbf{d}}\right) \frac{\mathbf{d}}{\mathbf{d}} + \frac{q_x}{n} C \quad (\text{C.35})$$

Which is in the same form as the one dimensional flux equation. So, if the “effective” dispersion coefficient were to be defined as:

$$D_e = D_{xx} + D_{xy} \frac{\mathbf{d}}{\mathbf{d}} \frac{\mathbf{d}}{\mathbf{d}} \quad (\text{C.36})$$

and using the following grid layout;



the discretized form would be:

$$D_e = D_{xx} + D_{xy} \frac{C_1 - C_3}{\Delta y} \frac{\Delta x}{C_2 - C_1} \quad (\text{C.37})$$

Inserting equation (C.36) into (C.30) yields:

$$J_x = \left(\frac{q_x}{2} - \frac{q_x^2 \Delta t}{2n\Delta x} - \frac{n}{\Delta x} \left(D_{xx} + D_{xy} \frac{C_1 - C_3}{\Delta y} \frac{\Delta x}{C_2 - C_1} \right) \right) (C_2 - C_1) + qC_1 \quad (\text{C.38})$$

And when simplified:

$$J_x = \left(\frac{q_x}{2} - \frac{q_x^2 \Delta t}{2n\Delta x} - \frac{nD_{xx}}{\Delta x} \right) (C_2 - C_1) + \frac{nD_{xy}}{\Delta y} (C_1 - C_3) + qC_1 \quad (\text{C.39})$$

Which is the equation for flux in the X direction between two nodes in a two dimensional aquifer. This is reasonable, since the numerical dispersion term is second order, not third. If one were to expect a correction for D_{xy} , it would have to be third order, which, in this implementation, was neglected.

Appendix D Linear Integrated Method

There are many methods that could have been chosen to solve the reaction portion of the advection-dispersion-reaction equation in the operator-splitting scheme. Finite difference schemes could have been used. Odencrantz (1992) used a fourth order Runge-Kutta method using 5 to 100 sub-time steps for every advection-dispersion timestep. For this work, the linear integrated (LI) method was chosen. It is assumed this method is not new, however it is not known what it is otherwise called. The basic premise that underlies the LI method is that concentrations are assumed to only vary linearly over the given time step, Δt . Equation (D.1) depicts the formula used to represent concentration as a function of time.

$$C = \frac{C_f - C_o}{\Delta t} t + C_o \quad (\text{D.1})$$

Where: C = concentration as a function of time (t)
 C_f = final concentration
 C_o = initial concentration
 Δt = time step
 t = time

The final concentrations at the end of a time step are determined by substituting the linearized equation (D.1) into the reaction equations and then integrating over the time step. Δt . An initial guess for the final concentration is used to determine the change in concentration due to each reaction in the system. Then, the individual integrated reaction rates are summed up to determine the net change in concentration due to reaction. The final concentration is then calculated as the initial concentration plus the net concentration change. The process is then repeated using this new final concentration. Iterations continue until the change in the final concentration between iterations is sufficiently small. This particular iterative method of the solution of the LI system of equations may not be the most efficient, but it is easy to code, and should return the same value as another method would.

In most cases the LI method will converge quickly. However, there are cases where reaction rates are large, they may cause concentrations to fall in the negative range. With certain reactions, this can cause an oscillatory effect in the calculations. A solution will not be found. To fix this problem, one only needs to decrease the size of the time step used in the calculation until a timestep small enough is found. This will break the effect.

For an example of the implementation of the LI method, consider a first order decay reaction:

$$\frac{dC}{dt} = -kC \quad (\text{D.2})$$

Substituting equation (D.1) into equation (D.2) yields:

$$\frac{dC}{dt} = -k \left(\frac{C_f - C_o}{\Delta t} t + C_o \right) \quad (\text{D.3})$$

The LI method then requires integration over the time period, Δt .

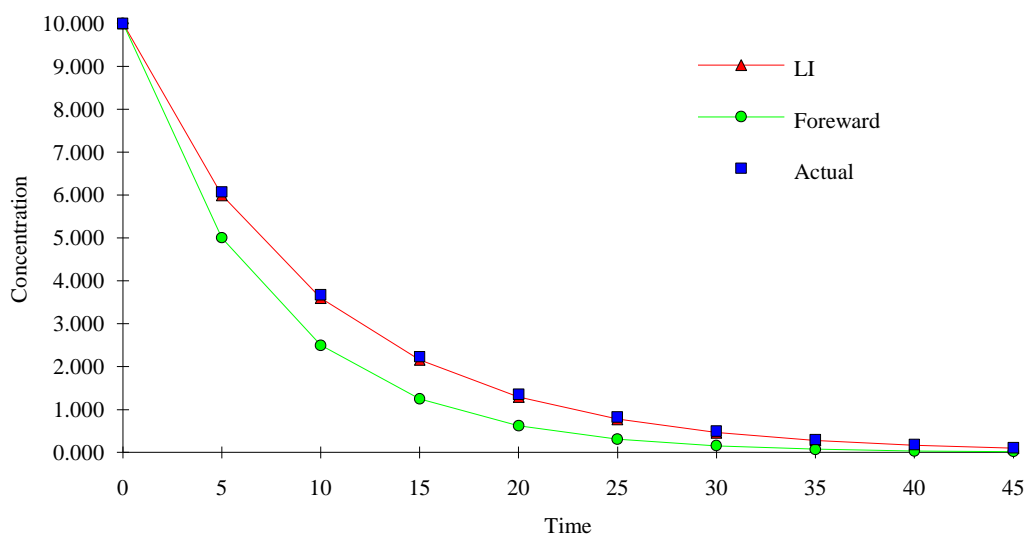
$$\int_{C_o}^{C_f} dC = - \int_0^{\Delta t} k \left(\frac{C_f - C_o}{\Delta t} t + C_o \right) dt \quad (\text{D.4})$$

which yields:

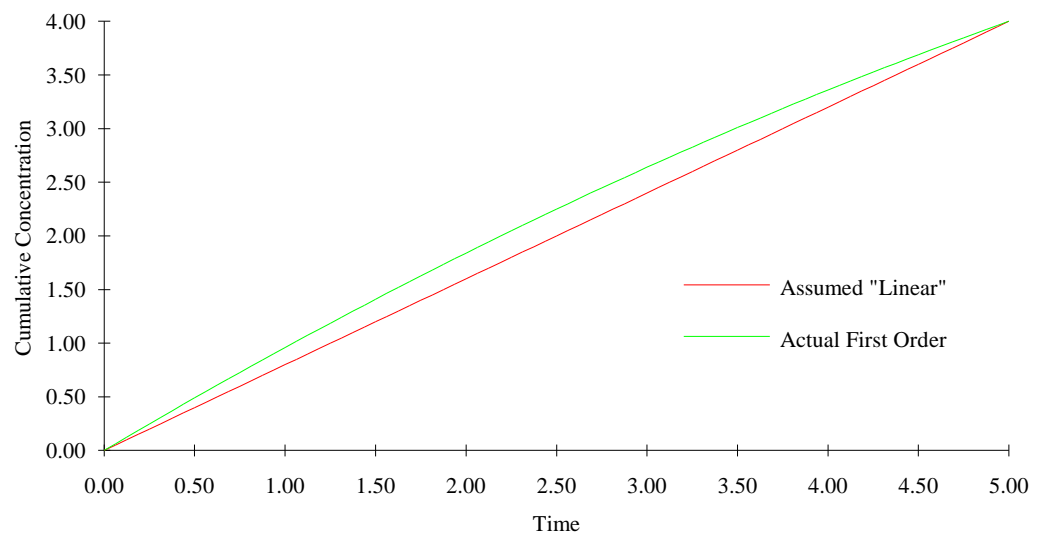
$$\Delta C = -k\Delta t \frac{C_o + C_f}{2} \quad (\text{D.5})$$

Due to the simplicity of the first order equation, the change in concentration is a function of the average of the initial and final concentration of the time step. Most equations however, are not this simple.

The following figure depicts the a comparison of a first order decay reaction using the LI method and a forward finite difference method. Both methods use $k = -0.1$ and $\Delta t = 5.0$.



It may be necessary to analyze each reaction separately, and develop criteria for the maximum allowable time step in order to minimize errors. For example consider the first order reaction mentioned above. The following figure illustrates the difference in cumulative concentration change due to reaction between the assumed “linear” relationship and the actual first order relationship (assuming the only reaction occurring is the first order decay reaction). If the relationship varies too much from the linear line, it may be necessary to decrease the time step. The maximum allowable time step may be a function of how much deviation from linearity is allowed, and the magnitude of the reaction coefficients. However, analysis such as this were not included here, they were considered to be out of the scope of this work.



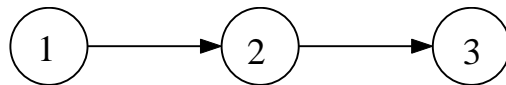
Appendix E Global Timestep Calculation

This appendix describes how the equation for the optimal timestep was developed. It describes the theory behind the criteria, as well as the calculations made to arrive at the equations. Calculations for one and two dimensions are included.

The method used to determine the maximum allowable timestep was first used by Wind and van Doorne (1975) to calculate criteria used in solving the variably saturated flow problem using the MCS method. The equations used in the study were quite similar in structure to the governing equations here. The method is repeated here.

The timestep criteria sought in this appendix is based on the theory of “amplification” of roundoff errors. Due to machine precision, there will always be some small error in the calculations. It is desired to determine the timestep at which these errors will not “amplify” or cause larger errors in subsequent time intervals. If the timestep is too large, the error, originally introduced by roundoff, will be a factor larger in the subsequent time step. The same error will then be another factor larger in the following time step and so on. This will lead to oscillations in space as iterations progress, and may even cause the method to fail.

Since it is far easier to explain the mathematics for a one dimensional aquifer, the one dimensional case is presented first. Consider the case of the following node segments in one dimension:



From the MCS method, the fluxes into node 2 and out of node 2 respectively are:

$$J_{12} = \left(\frac{q}{2} - \frac{q^2}{2\Delta x} - \frac{nD}{\Delta x} \right) (C_2 - C_1) + qC_1 \quad (\text{E.1})$$

$$J_{23} = \left(\frac{q}{2} - \frac{q^2}{2\Delta x} - \frac{nD}{\Delta x} \right) (C_3 - C_2) + qC_2 \quad (\text{E.2})$$

Where: q = darcy flux in the x direction (a positive value)
 Dx = distance between nodes
 n = material porosity
 D = dispersion coefficient
 C_1 = solute concentration in node 1
 C_2 = solute concentration in node 2
 C_3 = solute concentration in node 3

Now, over a timestep, Dt , the change in concentration at node two can be given as:

$$\Delta C_2 = \frac{J_{12} - J_{23}}{n\Delta x} \Delta t \quad (\text{E.3})$$

or when combined with equations (E.1) and (E.2) can be given as:

$$\Delta C_2 = \frac{\Delta t}{n\Delta x} \left(\begin{array}{l} \left[\left(\frac{q}{2} - \frac{q^2 \Delta t}{2n\Delta x} - \frac{nD}{\Delta x} \right) (C_2 - C_1) + qC_1 \right] \\ - \left[\left(\frac{q}{2} - \frac{q^2 \Delta t}{2n\Delta x} - \frac{nD}{\Delta x} \right) (C_3 - C_2) + qC_2 \right] \end{array} \right) \quad (\text{E.4})$$

$$\Delta C_2 = \frac{\Delta t}{n\Delta x} \left(\left[\left(\frac{q}{2} - \frac{q^2 \Delta t}{2n\Delta x} - \frac{nD}{\Delta x} \right) (2C_2 - C_3 - C_1) + q(C_1 - C_2) \right] \right) \quad (\text{E.5})$$

Equation (E.5) is the “correct” change in concentration at node two over the time interval Dt . Now introduce a small error, e_2 , such that the calculation of C_2 at the beginning of the timestep is in error:

$$C_2^* = C_2 + e_2 \quad (\text{E.6})$$

Denoting the change in concentration using the “incorrect” value for C_2 as DC_2^* , the error in the change of concentration over Dt can be computed:

$$\mathbf{\Delta}C_2 = \Delta C_2^* - \Delta C_2 = \frac{\Delta t}{n\Delta x} \left(\left(\frac{q}{2} - \frac{q^2 \Delta t}{2n\Delta x} - \frac{nD}{\Delta x} \right) (2C_2^* - 2C_2) + q(C_2 - C_2^*) \right) \quad (\text{E.7})$$

or:

$$\mathbf{\Delta}C_2 = \frac{\Delta t}{n\Delta x} \left(\left(q - \frac{q^2 \Delta t}{n\Delta x} - \frac{2nD}{\Delta x} \right) e_2 - qe_2 \right) \quad (\text{E.8})$$

Simplifying:

$$\mathbf{\Delta}C_2 = \left[-\left(\frac{q\Delta t}{n\Delta x} \right)^2 - \frac{2\Delta t D}{\Delta x^2} \right] e_2 \quad (\text{E.9})$$

Dividing by the error:

$$\frac{\mathbf{\Delta}C_2}{e_2} = -\left(\frac{q\Delta t}{n\Delta x} \right)^2 - \frac{2\Delta t D}{\Delta x^2} = Co^2 - \frac{2Co}{Pe} \quad (\text{E.10})$$

Where Co is the courant number and Pe is the peclet number.

In order to keep errors from “amplifying”, the magnitude of the error produced by Equation (E.5) must be less than the *original* error. In mathematical terms this can be stated:

$$\left| \frac{\mathbf{\Delta}C_2}{e_2} \right| \leq 1 \quad (\text{E.11})$$

Which translates into:

$$Co^2 + \frac{2Co}{Pe} + 1 \geq 0 \quad (\text{E.12})$$

and

$$Co^2 + \frac{2Co}{Pe} - 1 \leq 0 \quad (\text{E.13})$$

Equation (E.12) is satisfied for all $Pe > 0$ and $Co > 0$. However Equation (E.13) is not. The solution is:

$$Co \leq \sqrt{\frac{1}{Pe^2} + 1} - \frac{1}{Pe} \quad (\text{E.14})$$

Equation (E.14) must be satisfied at all nodes in the simulation in order to prevent errors from amplifying. The easiest way to satisfy (E.14) is to adjust the global timestep. The equation used to calculate the maximum timestep can be derived from Equation (E.14) to be:

$$\Delta t \leq \sqrt{\left(\frac{n^2 D}{q^2}\right)^2 + \left(\frac{n \Delta x}{q}\right)^2} - \frac{n^2 D}{q^2} \quad (\text{E.15})$$

In addition to the maximum allowable timestep, numerical analysis showed there exists a minimum allowable timestep as well. The error caused by too small of a timestep is only a fraction of the error caused by too large of a timestep. However, the error is too large to ignore.

Consider a special case of the one dimensional example above. In the case of a retreating solute front, $\mathbf{d}/\mathbf{d} \geq 0$, $\mathbf{d}/\mathbf{d} \leq 0$, $q \geq 0$, the flux out of a node over a timestep must not be greater than the solute concentration in that node. Or in other words, the flux cannot be so great that it will cause the concentration at the end of the timestep to become negative. In mathematical terms this can be stated.

$$J = \left(\frac{q}{2} - \frac{q^2 \Delta t}{2n\Delta x} - \frac{nD}{\Delta x}\right)(C_2 - C_1) + qC_1 \leq qC_1 \quad (\text{E.16})$$

Since in this case, $(C_2 - C_1)$ is positive, it can be demonstrated the following equation must be satisfied:

$$\frac{q}{2} - \frac{q^2 \Delta t}{2n\Delta x} - \frac{nD}{\Delta x} \leq 0 \quad (\text{E.17})$$

Rearranging yields:

$$\frac{q^2 \Delta t}{2n\Delta x} \geq \frac{q}{2} - \frac{nD}{\Delta x} \quad (\text{E.18})$$

$$\frac{q\Delta t}{n\Delta x} \geq 1 - \frac{2nD}{q\Delta x} \quad (\text{E.19})$$

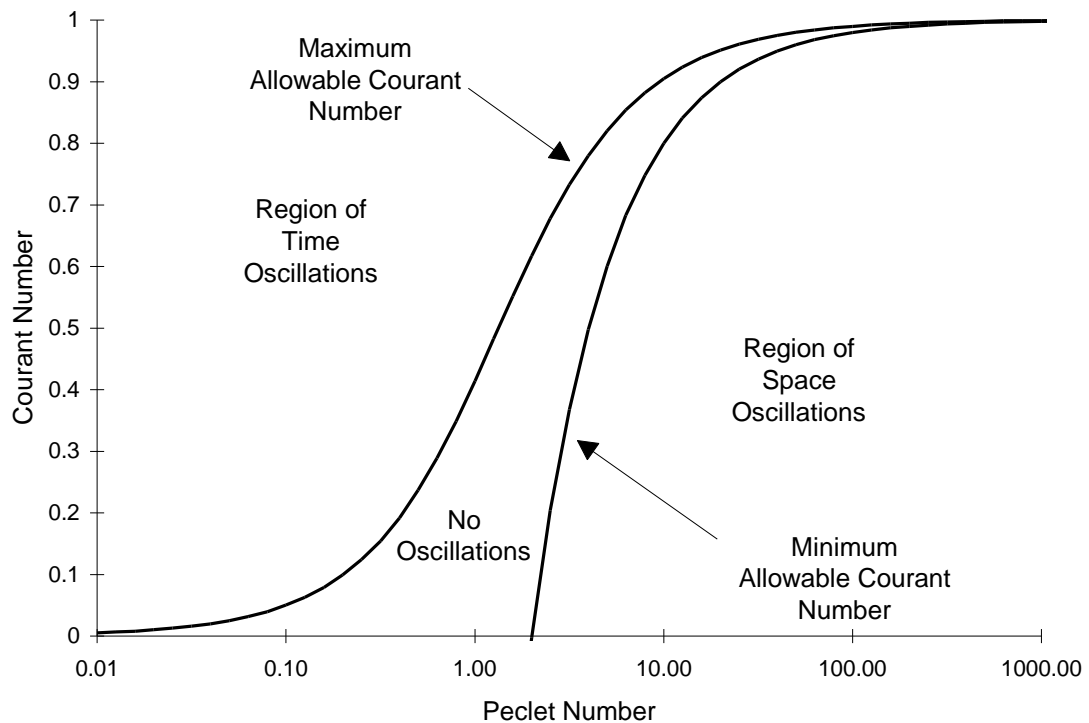
Which translates into a minimum timestep criteria:

$$\Delta t \geq \frac{n\Delta x}{q} - \frac{2n^2 D}{q^2} \quad (\text{E.20})$$

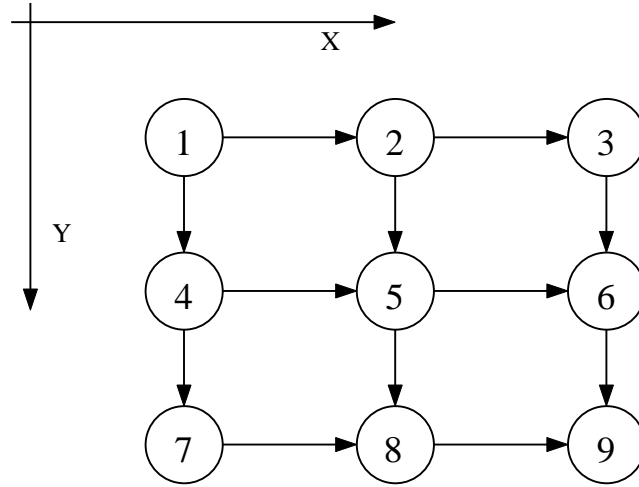
or a courant number criteria:

$$Co \geq 1 - \frac{2}{Pe} \quad (\text{E.21})$$

The following graph illustrates the different timestep criteria equations for a one dimensional aquifer as a function of pecelet and courant numbers superimposed with contour lines of the RSSE. For a detailed discussion of the RSSE, see the main text.



Equations (E.18) and (E.21) are only for one dimension. It is necessary to repeat the analysis for two dimensions. Consider the case of the following node segments in two dimensions:



From the MCS method, the fluxes into and out of node 5 are:

$$J_{45} = \left(\frac{q_x}{2} - \frac{q_x^2}{2\Delta x} - \frac{nD_{xx}}{\Delta x} \right) (C_5 - C_4) - \frac{nD_{xy}}{\Delta x \Delta y} (C_4 - C_1) + q_x C_4 \quad (\text{E.22})$$

$$J_{56} = \left(\frac{q_x}{2} - \frac{q_x^2}{2\Delta x} - \frac{nD_{xx}}{\Delta x} \right) (C_6 - C_5) - \frac{nD_{xy}}{\Delta x \Delta y} (C_5 - C_2) + q_x C_5 \quad (\text{E.23})$$

$$J_{25} = \left(\frac{q_y}{2} - \frac{q_y^2}{2\Delta y} - \frac{nD_{yy}}{\Delta y} \right) (C_5 - C_2) - \frac{nD_{xy}}{\Delta x \Delta y} (C_2 - C_1) + q_y C_2 \quad (\text{E.24})$$

$$J_{58} = \left(\frac{q_y}{2} - \frac{q_y^2}{2\Delta y} - \frac{nD_{yy}}{\Delta y} \right) (C_8 - C_5) - \frac{nD_{xy}}{\Delta x \Delta y} (C_5 - C_4) + q_y C_5 \quad (\text{E.25})$$

Over the timestep, \mathbf{Dt} , the change in concentration at node five can be given as:

$$\Delta C_5 = \frac{J_{45} - J_{56}}{n\Delta x} \Delta t + \frac{J_{25} - J_{58}}{n\Delta y} \Delta t \quad (\text{E.26})$$

Simplifying Equations (E.22) to (E.26) yields:

$$\begin{aligned}
\Delta C_5 = & \left(\frac{q_x \Delta t}{2n\Delta x} - \frac{1}{2} \left(\frac{q_x \Delta t}{n\Delta x} \right)^2 - \frac{nD_{xx}}{\Delta x^2} \right) (2C_5 - C_4 - C_6) \\
& + \left(\frac{q_y \Delta t}{2n\Delta y} - \frac{1}{2} \left(\frac{q_y \Delta t}{n\Delta y} \right)^2 - \frac{nD_{yy}}{\Delta y^2} \right) (2C_5 - C_2 - C_8) \\
& - 2 \frac{D_{xy} \Delta t}{\Delta x \Delta y} (C_4 + C_2 - C_1 - C_5) \\
& + \frac{q_x \Delta t}{n\Delta x} (C_4 - C_5) + \frac{q_x \Delta t}{n\Delta x} (C_2 - C_5)
\end{aligned} \tag{E.27}$$

The associated error in the change in concentration is:

$$\begin{aligned}
\mathbf{\Delta} C_5 = & \left(\frac{q_x \Delta t}{n\Delta x} - \left(\frac{q_x \Delta t}{n\Delta x} \right)^2 - \frac{2nD_{xx}}{\Delta x^2} \right) e_5 \\
& + \left(\frac{q_y \Delta t}{n\Delta y} - \left(\frac{q_y \Delta t}{n\Delta y} \right)^2 - \frac{2nD_{yy}}{\Delta y^2} \right) e_5 \\
& + 2 \frac{D_{xy} \Delta t}{\Delta x \Delta y} e_5 \\
& - \frac{q_x \Delta t}{n\Delta x} e_5 - \frac{q_x \Delta t}{n\Delta x} e_5
\end{aligned} \tag{E.28}$$

And the relative error becomes:

$$\frac{\mathbf{\Delta} C_5}{e_5} = -\Delta t^2 \left(\left(\frac{q_x}{n\Delta x} \right)^2 + \left(\frac{q_y}{n\Delta y} \right)^2 \right) - 2\Delta t \left(\frac{D_{xx}}{\Delta x^2} + \frac{D_{yy}}{\Delta y^2} - \frac{D_{xy}}{\Delta x \Delta y} \right) \tag{E.29}$$

The associated inequality is:

$$\Delta t^2 \left(\left(\frac{q_x}{n\Delta x} \right)^2 + \left(\frac{q_y}{n\Delta y} \right)^2 \right) + 2\Delta t \left(\frac{D_{xx}}{\Delta x^2} + \frac{D_{yy}}{\Delta y^2} - \frac{D_{xy}}{\Delta x \Delta y} \right) - 1 \leq 0 \tag{E.30}$$

Therefore the maximum timestep for a two-dimensional simulation that allows stability is:

$$\Delta t \leq \frac{-B + \sqrt{B^2 + A}}{A} \quad (\text{E.31})$$

Where: $A = \left(\frac{q_x}{n\Delta x}\right)^2 + \left(\frac{q_y}{n\Delta y}\right)^2$

$$B = \frac{D_{xx}}{\Delta x^2} + \frac{D_{yy}}{\Delta y^2} - \frac{D_{xy}}{\Delta x\Delta y}$$

In addition, the corresponding minimum timestep criteria in two dimensions was developed using the similarity of the other one and two-dimensional criteria equations:

$$\Delta t \geq \frac{\sqrt{A} - 2B}{A} \quad (\text{E.32})$$

It can be shown, in the case of one-dimension, the above two dimensional equations reduce to the one dimensional equations calculated above.

Appendix F Additional Kinetic Reaction Verification Tests

This appendix continues the verification analysis of kinetic reactions from the Model Performance chapter. Refer to this chapter for details on the analysis.

Single Monod

The equation for single Monod decay is:

$$\frac{dC}{dt} = \frac{kC}{K_s + C} \quad (7.33)$$

Where: dC/dt = time rate of change of concentration (M/L³·T)
 C = concentration of solute species (M/L³)
 k = maximum rate constant (T⁻¹)
 K_s = half saturation constant (M/L³)

Figure F.1 compares model solutions with the true solutions using a global calculation timestep of 2.0 and varying coefficients. Circles and lines denote numerical and true solutions respectively.

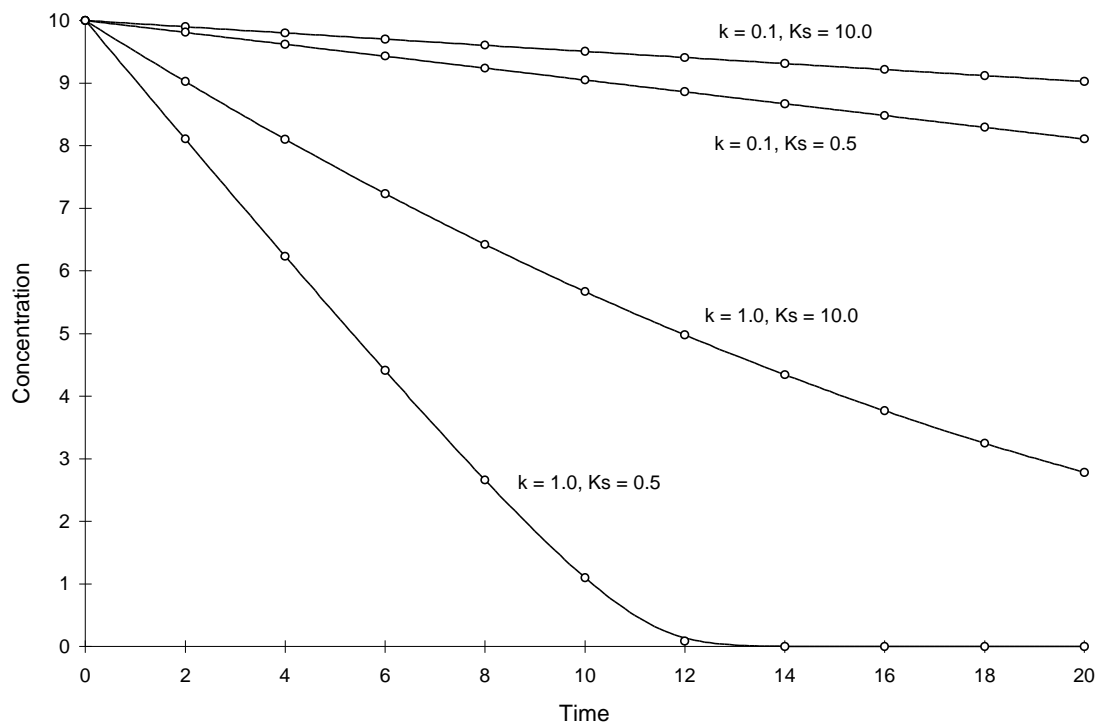


Figure F.1 Single Monod Decay with Varying k , and K_s .

The numerical and true values appear to agree well. The squared relative residual was computed at time 20.0 for the coefficients above. Figure F.2 illustrates the results.

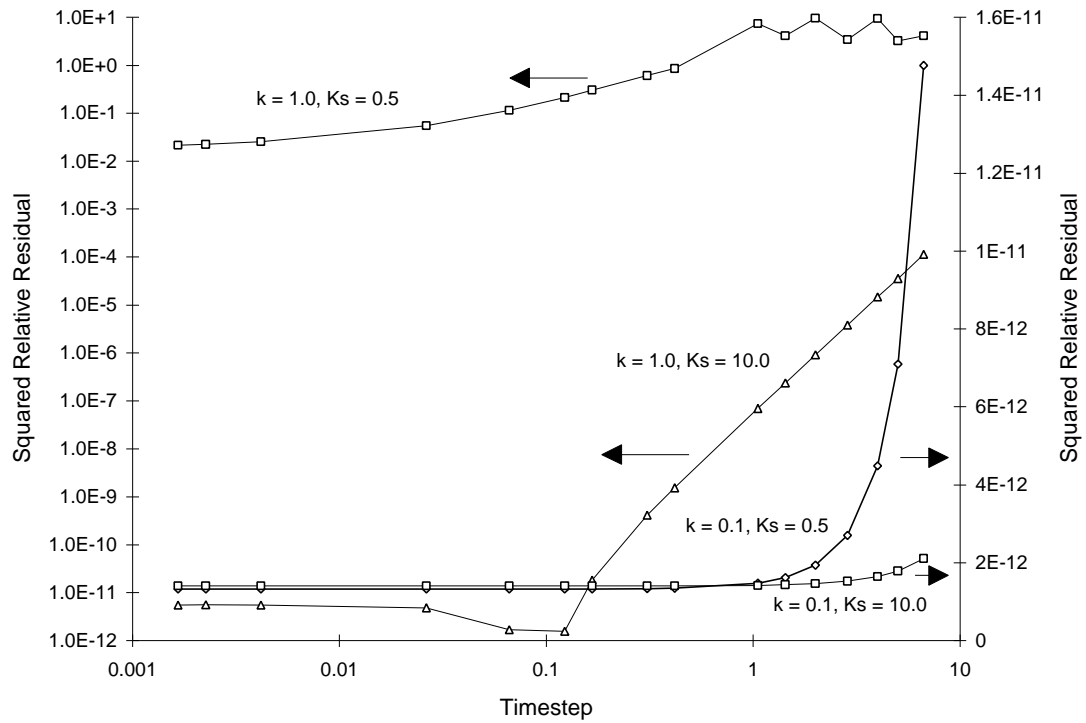


Figure F.2 Squared Relative Residual as a Function of Single Monod Decay Coefficients and Global Timestep.

Once again, Figure F.2 shows the residual calculation is higher for higher time steps. The highest relative residual was found for the case of $k = 1.0$ and $K_s = 0.5$, where the concentration was allowed to fall to values less than 10^{-8} .

Double Monod

The double Monod reaction is:



$$\text{rate} = \frac{k X C_a C_d}{(K_{sa} + C_a)(K_{sd} + C_d)} \quad (7.35)$$

- Where: C_a = concentration of electron acceptor (M/L^{-3})
 C_d = concentration of electron donor (M/L^{-3})
 X = biomass concentration (M/L^{-3})
 k = maximum rate constant ($\text{L}^{-6}/\text{M}^2 \cdot \text{T}$)
 K_{sa} = half saturation constant for electron acceptor (M/L^{-3})
 K_{sd} = half saturation constant for electron donor (M/L^{-3})
 Y_a = stoichiometry coefficient for electron acceptor
 Y_d = stoichiometry coefficient for electron donor
 Y_x = stoichiometry coefficient for biomass

The results are:

Figure F.3 compares model and true solutions using a global calculation timestep of 2.0. For this test $k = 0.2$, $K_{sa} = 5.0$, $K_{sd} = 10.0$, $Y_x = 0.5$, $Y_A = 1.0$, $Y_D = 2.5$. Circles and lines denote numerical and true values respectively.

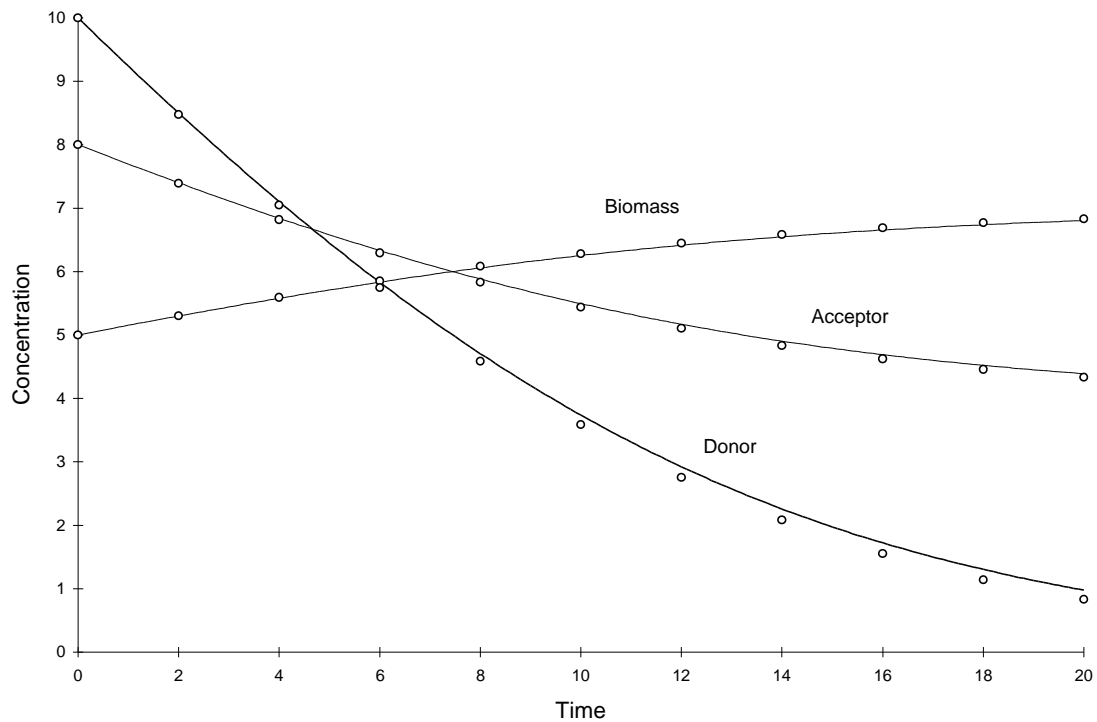


Figure F.3 Double Monod Decay.

$$k = 0.2, K_{sa} = 5.0, K_{sd} = 10.0, Y_x = 0.5, Y_A = 1.0, Y_D = 2.5.$$

It can be seen there is a small discrepancy between numerical and true values in the solution to the electron donor. The decay rate of this chemical was the largest. The squared relative residual was calculated at timestep 20.0. Figure F.4 shows the results as a function of global timestep:

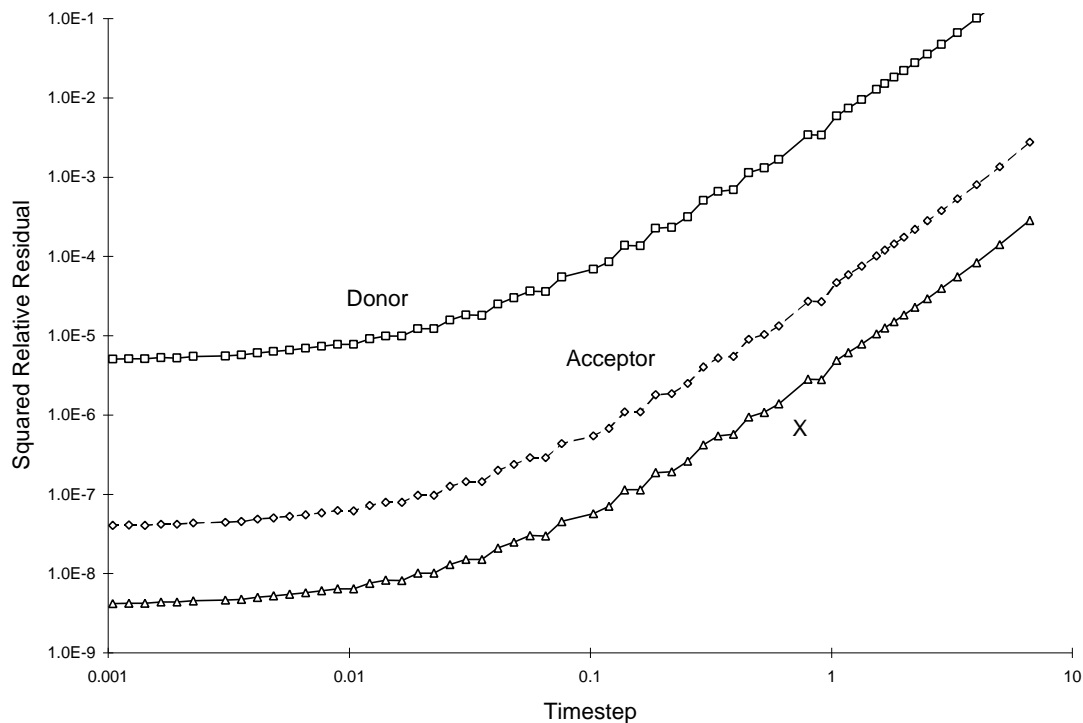


Figure F.4 Squared Relative Residual as a Function Global Timestep for Double Monod Reaction.

Kinetic Linear Sorption

The kinetic implementation of the linear sorption isotherm is as follows:

$$-\frac{dC}{dt} = \frac{dS}{dt} = a(K_d C - S) \quad (7.36)$$

Where: C = concentration of solute species (M/L^3)
 S = concentration of sorbed species (M/L^3)
 a = rate coefficient (T^{-1})
 K_d = sorption coefficient

Figure F.5 compares model and true solutions using a global calculation timestep of 2.0. For this test $a = 0.1$ and $K_d = 2.0$. Circles and lines denote numerical and true values respectively.

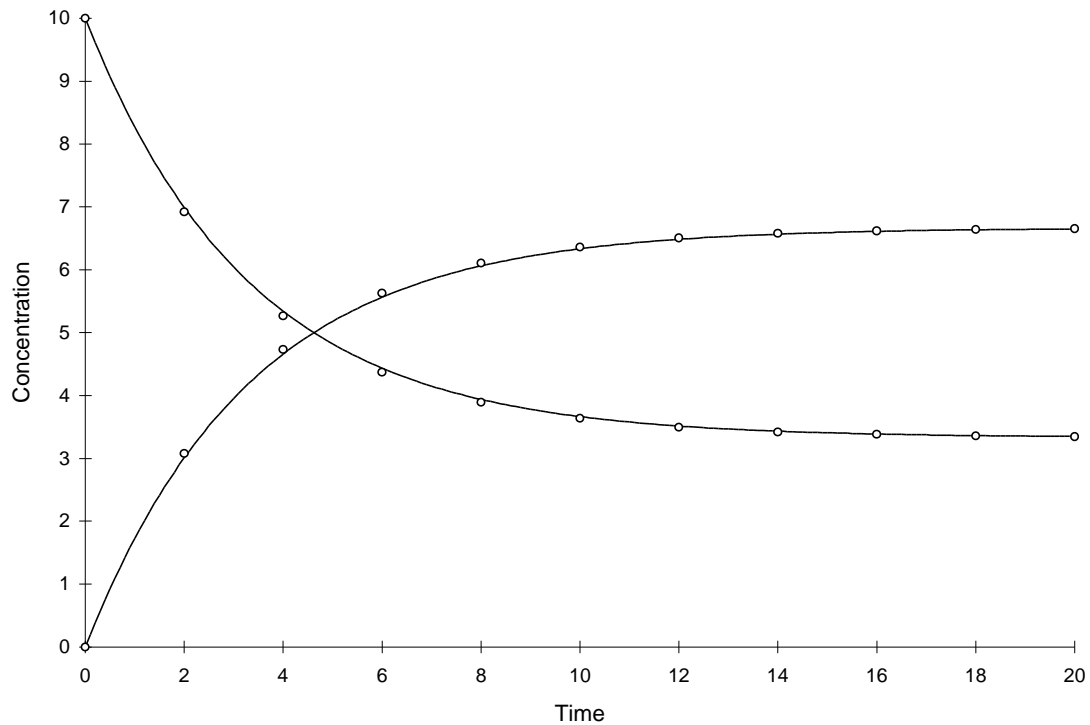


Figure F.5 Kinetic Linear Sorption, $a = 0.1$, $K_d = 2.0$.

The numerical and true values visually match quite well. The squared relative residual was calculated at timestep 10.0. Figure F.6 shows the results as a function of global timestep:

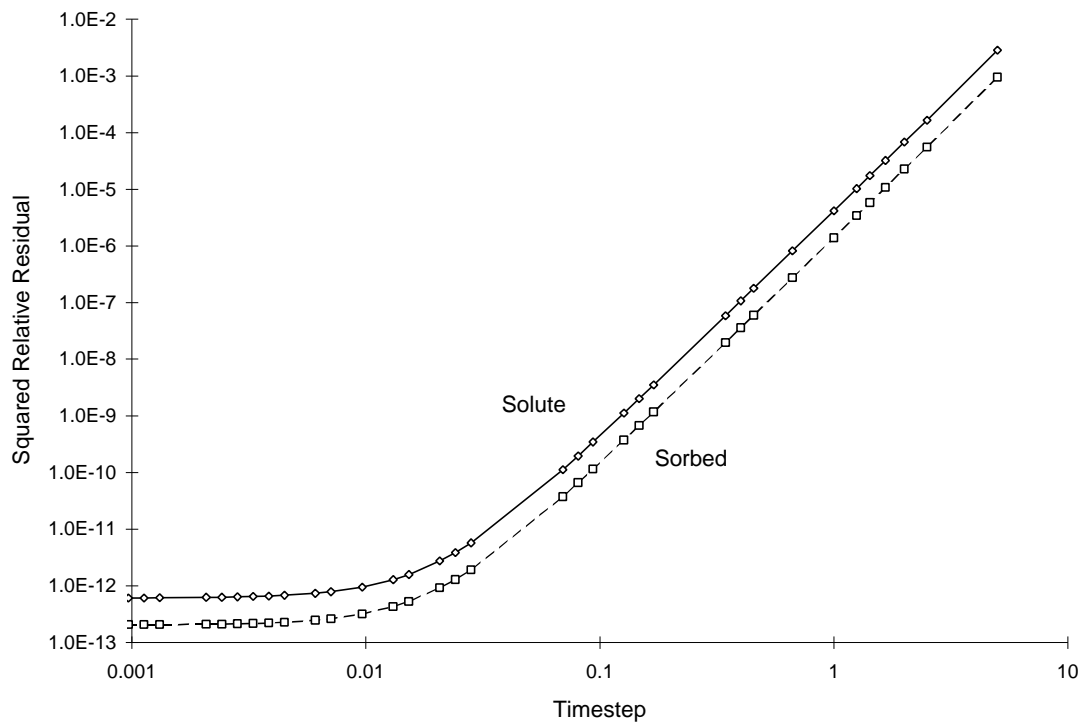


Figure F.6 Squared Relative Residual as a Function of Global Timestep for Kinetic Linear Sorption.

Kinetic Langmuir Sorption

The kinetic implementation of the Langmuir sorption isotherm is:

$$-\frac{\mathbf{d}C}{\mathbf{d}t} = \frac{\mathbf{d}S}{\mathbf{d}t} = \mathbf{a} \left(\frac{k_1 C}{k_2 + C} - S \right) \quad (7.37)$$

- Where: C = concentration of solute species (M/L^3)
 S = concentration of sorbed species (M/L^3)
 \mathbf{a} = rate coefficient (T^{-1})
 k_1 = sorption coefficient
 k_2 = sorption coefficient (M/L^3)

Figure F.7 compares model and true solutions using a global calculation timestep of 2.0. For this test $\mathbf{a} = 0.1$, $k_1 = 8.0$, and $k_2 = 1.0$. Circles and lines denote numerical and true values respectively.

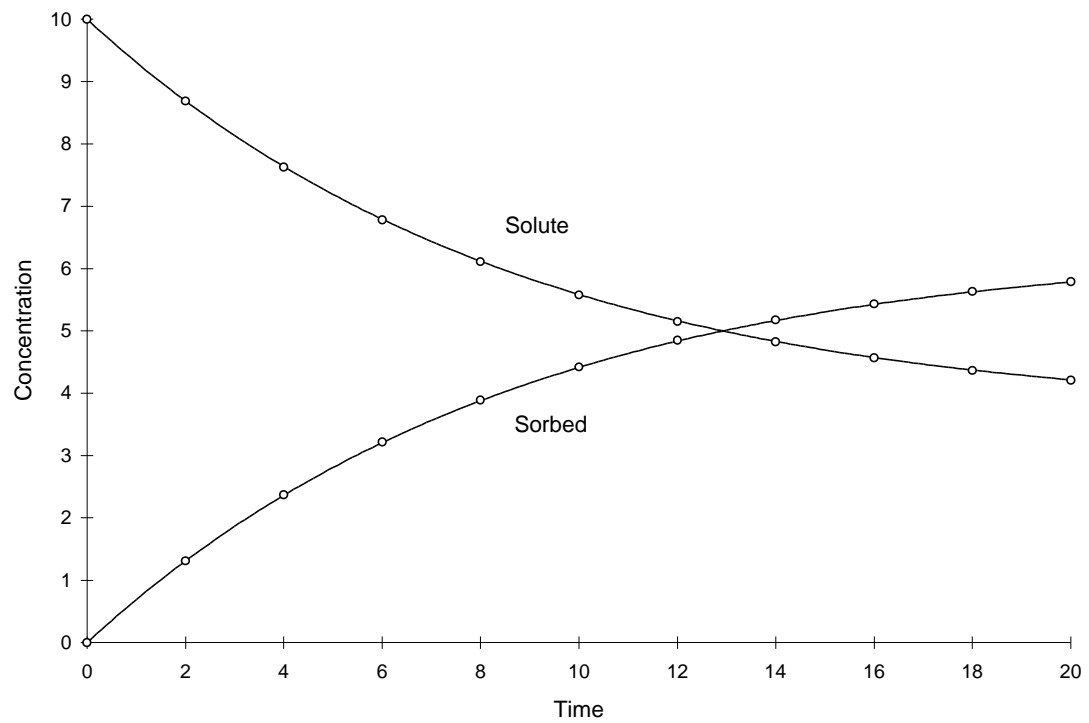


Figure F.7 Kinetic Langmuir Sorption, $a = 0.1$, $k_1 = 8.0$, $k_2 = 1.0$.

It can be seen the numerical and true values visually match quite well. The squared relative residual was calculated at timestep 20.0. Figure F.8 shows the results as a function of global timestep:

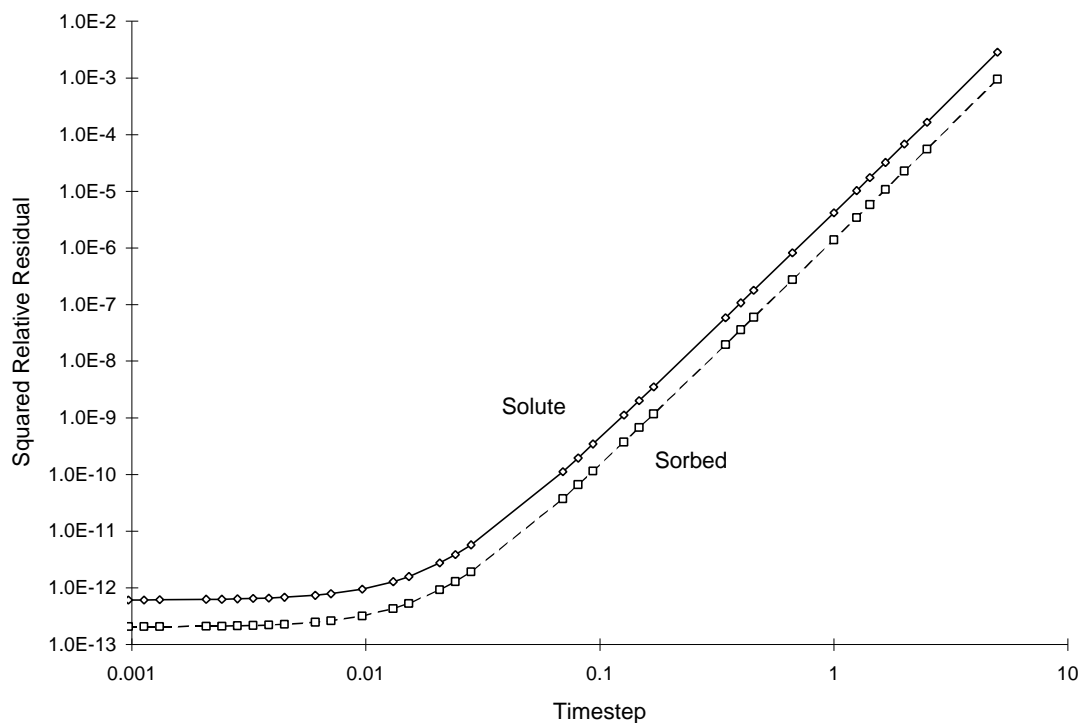


Figure F.8 Squared Relative Residual as a Function of Global Timestep for Kinetic Langmuir Sorption.

Kinetic Freundlich Sorption

The kinetic implementation of the Freundlich sorption isotherm is as follows:

$$-\frac{dC}{dt} = \frac{dS}{dt} = a(kC^n - S) \quad (7.38)$$

- Where: C = concentration of solute species (M/L^3)
 S = concentration of sorbed species (M/L^3)
 a = rate coefficient (T^{-1})
 k = sorption coefficient
 n = sorption coefficient

Figure F.9 compares model true solutions using a global calculation timestep of 2.0. For this test $a = 0.2$, $k = 2.0$, and $n = 0.8$. Circles and lines denote numerical and true values respectively.

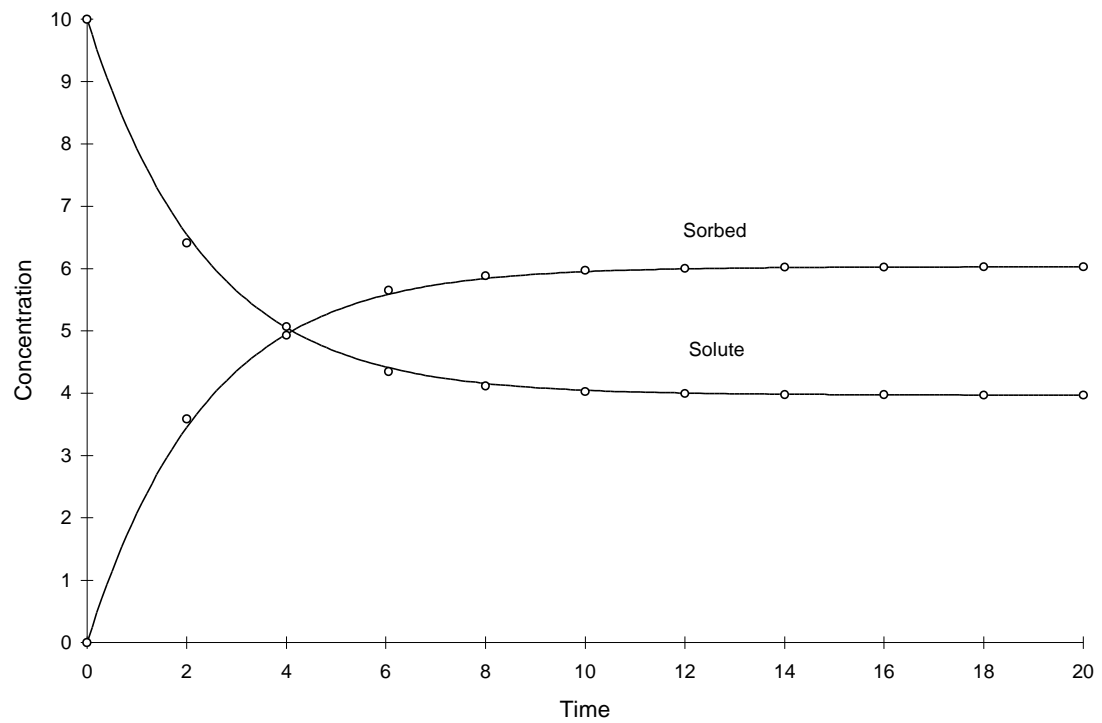


Figure F.9 Kinetic Freundlich Sorption, $a = 0.2$, $k = 2.0$, $n = 0.8$.

It can be seen the numerical and true values visually match quite well. The squared relative residual was calculated at timestep 6.0. Figure F.10 shows the results as a function of global timestep:

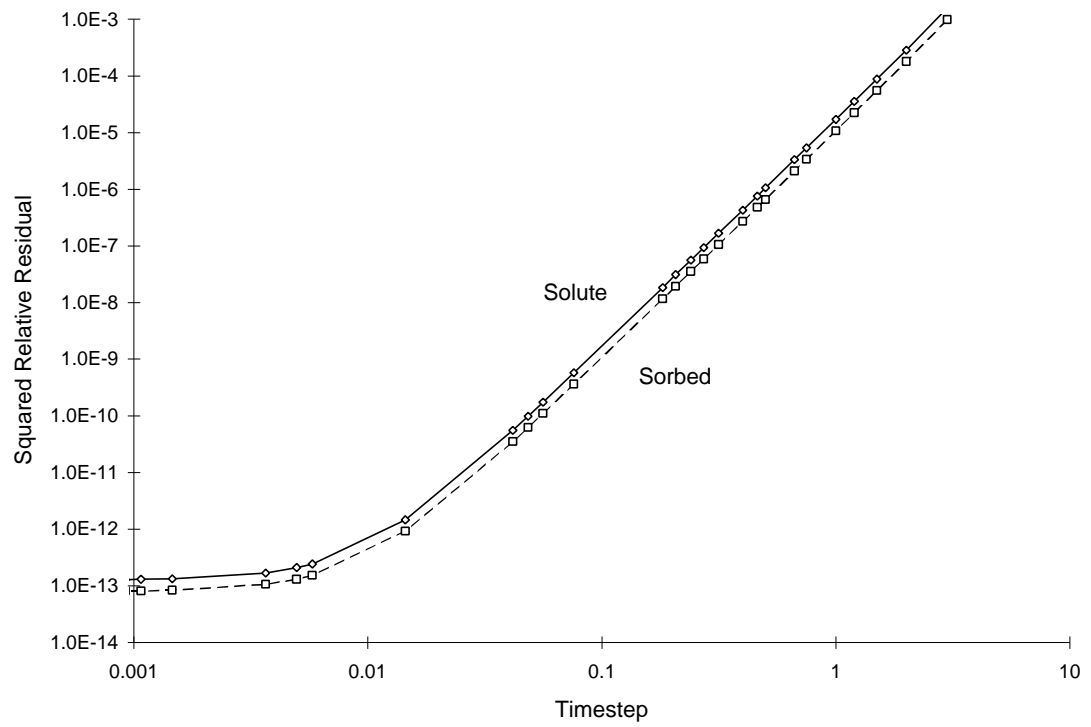


Figure F.10 Squared Relative Residual as a Function of Global Timestep for Kinetic Freundlich Sorption.

Appendix G Bugs User's Manual

The BUGS (SCRATCHPAD) User's Manual is available from BUGBYTES, INC., please visit <http://www.bugbytes.com> for more details.